NASA Technical Paper 1004

Evaluation of Approximate Methods for the Prediction of Noise Shielding by Airframe Components

Warren F. Ahtye and Geraldine McCulley

JANUARY 1980

NASA

NASA Technical Paper 1004

Evaluation of Approximate Methods for the Prediction of Noise Shielding by Airframe Components

Warren F. Ahtye
Ames Research Center
Moffett Field, California
and
Geraldine McCulley
Informatics, Inc.
Palo Alto, California

National Aeronautics
and Space Administration

**Scientific and Technical
Information Office**

1980

A

EVALUATION OF APPROXIMATE METHODS FOR THE PREDICTION OF NOISE SHIELDING BY AIRFRAME COMPONENTS

Warren F. Ahtye and Geraldine McCulley

Ames Research Center
and
Informatics, Inc.

The present investigation was conducted to evaluate some approximate methods for the prediction of shielding of monochromatic sound and broadband noise by aircraft components. The approach was to make anechoic-chamber measurements of the shielding of a point source by various simple geometric shapes, and to then compare the measured values with those calculated by the superposition of asymptotic closed-form solutions for the shielding by a semi-infinite plane barrier.

The shields used in the measurements consisted of rectangular plates, a circular cylinder, and a rectangular plate attached to the cylinder to simulate a wing-body combination. The normalized frequency, defined as a product of the acoustic wave number and either the plate width or cylinder diameter, ranged from 4.6 to 114.

Microphone traverses in front of the rectangular plates and cylinders generally showed a series of diffraction bands that matched those predicted by the approximate methods, except for differences in the magnitudes of the attenuation maxima which can be attributed to experimental inaccuracies.

The shielding of wing-body combinations was predicted by modifications of the approximations used for rectangular and cylindrical shielding. Although the approximations failed to predict diffraction patterns in certain regions, they did predict the average level of wing-body shielding with an average deviation of less than 3 dB.

Restrictions on allowable levels of propulsive noise reaching the surrounding community from a STOL aircraft can result in serious design constraints. Some current designs for propulsive lift aircraft, such as the Boeing YC-14 transport (ref. 1) and the NASA Quiet Short-Haul Research Aircraft (ref. 2), take advantage of the shielding capabilities of the wing by mounting the engines above the wing. A key element needed to determine the optimum engine and wing-body configuration is the accurate prediction of the acoustic shielding. The predictive technique must also be sufficiently simple for the designer to use and shorten the computation time of the monochromatic solutions so that the superposition of these solutions for the prediction of broadband noise and distributed sources can be made within a reasonable time.

Obviously, these simple approximations must be based on rigorous calculations (as opposed to empirical correlations), otherwise their accuracy over a wide range of applications would be decreased. Calculations of shielding of monochromatic sound by finite two-dimensional barriers have been made with varying degrees of accuracy. Exact solutions exist for only a few cases with high degrees of symmetry. For example, Primakoff et al. (ref. 3) showed the results of an exact solution for the shielding of a point source by a circular disk, where the point source was located on the axis of symmetry, and the field points were restricted to regions near the axis of symmetry. Leitner (ref. 4) presented a corresponding calculation for plane acoustic waves with normal incidence. The next level of approximation is to use the Kirchoff approximation which assumes the free-field values of the incident wave as boundary values. Primakoff et al. and Leitner also used the Kirchoff approximation for shielding calculations to compare with their exact solutions. Subsequently, Davis and Gabrielsen (ref. 5) applied the Kirchoff approximation to the calculation of shielding of a point source by a rectangular barrier.

In contrast to the numerical integration required for the Kirchoff approximation, Bowman, Senior, and Uslenghi (ref. 6) present an approximate closed-form solution for the shielding by a semi-infinite barrier of monochromatic sound waves emanating from a point source with no restrictions on source location. This solution has its origin in an exact integral expression containing Bessel functions. The approximation arises from the use of an asymptotic expansion for the Bessel functions. This approximate closed-form solution forms the basis for the approximate calculations used in this paper.

The method of approximating shielding by a quadrilateral by the superposition of semi-infinite barrier solutions was suggested by Conticelli, Di Blasi, and O'Keefe (ref. 7). Their procedure was to take a given edge of the quadrilateral (e.g., the leading edge of the wing), extend it to plus and minus infinity, thereby

forming a semi-infinite barrier, and to then calculate the shielding for that edge using the closed-form solution of reference 6. The resultant shielding, at a given field point, from all sides of the plate was then found by simple addition of the pressure magnitudes from each of the corresponding semi-infinite barriers. Conticelli, Di Blasi, and O'Keefe (ref. 7) mentioned a series of measurements in an anechoic chamber to determine the accuracy of this approximation. The results of these measurements were presented in reference 7, but were not discussed. Dunn et al. presented some of the results for a wing-flap configuration in reference 8; the accuracy of the results varied.

The main objective of the investigation reported herein was to determine the accuracy of approximation for the shielding of monochromatic and broadband sound by a wing. For convenience, a series of rectangles was used as shields rather than arbitrary trapezia. It appears, however, that the accuracy of the approximations, as determined from measurements using rectangles, should be representative of the accuracy for trapezia; at least, there are no apparent indications to the contrary. To complete the study of wing shielding, the effect of edge radius for these rectangular plates was also determined.

Approximations for fuselage shielding were evaluated by making a series of measurements with a circular cylinder of finite length. The measured shielding by the cylinder was compared with that by a rectangular plate whose width was approximately the same as the diameter of the cylinder; it was thus hoped that the approximations for the rectangle could somehow be extended to the cylinder.

Finally, the shielding by a wing-body combination was measured. A rectangular plate was attached to the cylinder to simulate a high-wing configuration. The point source was positioned under the wing to simulate under-the-wing mounting of engines. Although this shielding configuration is too complex for accurate prediction, it was possible to modify the predicted shielding for a wing alone or for a body alone, such that wing-body shielding was adequately approximated.

SYMBOLS

c speed of sound

D distance from plate (or cylinder) to traverse line

d diameter of cylinder

f acoustic frequency

k acoustic wave number

L length of plate (or cylinder)

LVE left visual edge

p acoustic pressure

R distance from source to field point

R' distance from image source to field point

R_1 characteristic distance

RVE right visual edge

SPL sound-pressure level

V_D velocity potential for diffracted field

V_G velocity potential for geometric optics field

V_s shielded velocity potential

V_u unshielded velocity potential

W width of plate

x,y,z rectangular Cartesian coordinates

θ traverse angle

ρ projected radius

ρ_a density of ambient air

ρ,ϕ,z circular cylindrical coordinates

ω acoustic angular frequency

Subscripts:

o source

s shielded

s source

u unshielded

Special symbol:

ΔSPL shielding

SOUND SOURCE AND SHIELDS

The sound source is composed of a high-frequency driver loudspeaker installed in an enclosure with the sound from the throat of the loudspeaker coupled to an inverse-taper horn. The components are shown in figure 1. The inverse-taper horn was used to reduce the size of the aperture in order to approximate a point source,[1] since the shielding predictions evaluated in this paper are based on sound emitted by a point source.

The high-frequency driver loudspeaker has a usable response from 500 Hz to 20 kHz. An anechoic chamber calibration of this loudspeaker without the horn showed that, for any given frequency within the usable range, its output is linear over a range of 26 dB (corresponding to a range of voltage inputs from 0.5 V to 10 V). A comparison of the oscilloscope waveforms from the output of the sine-wave generator and the output of the speaker as monitored by a condenser microphone from 1 kHz to 20 kHz, showed virtually no difference in the far field.

The loudspeaker enclosure is a box with outer dimensions of 29 cm X 25 cm X 25 cm, constructed of 2.5-cm-thick plywood, with the outer surfaces covered with 0.32-cm-thick lead sheets tc increase the acoustical transmission loss. The interior of the box was filled with acoustical foam. An inverse-taper horn was constructed of two layers of 0.32-cm sheets of lead sandwiched between several layers of fiberglass. The opening at the large end is the same diameter as the throat diameter of the loudspeaker (2.54 cm). The opening at the small end has a diameter of 0.63 cm. The transmission loss through the surfaces of the enclosure and the sides of the inverse-taper horns was estimated to be at least 30 dB, thereby insuring that virtually all the noise emanated from the small opening at the end of the horn.

In spite of these precautions, there were perceptible deviations from the idealized point source behavior in the far field. When sine waves were fed into the sound source, the resulting oscilloscope traces for the signals from a far-field microphone showed varying degrees of anharmonicity. The anharmonicity was fairly large at 1 kHz, peaked at 2 kHz, and decreased with increasing frequency. At 4 kHz the anharmonicity was very small. Fortunately, the omnidirectionality of the source was unaffected by this waveform distortion. A plausible explanation for this waveform distortion is the formation of partial standing waves inside the horn. The superposition of incident waves and reflected waves with their phase differences would account for the large waveform distortion. There should be no perceptible effect of this type of waveform distortion for broadband noise.

At the high end of the frequency spectrum, there was a different type of deviation from the idealized point source behavior which affected both sine-wave and broadband sound inputs. This effect resulted in a departure from omnidirectionality at large angles from the axis of the horn. This deviation is shown in figure 2. The deviation can be attributed to the finite size of the opening at the end of the horn. This finite size results in various portions of the opening contributing with differing phase at a given field point, with differences in the propagation distances comparable to an acoustical wavelength. For example, at 20 kHz the ratio of the acoustic wavelength to the diameter of the opening at the tip of the horn is 2.6. A calculation by Olson (ref. 9) showed approximately the same directionality pattern for a circular piston source, where the ratio of wavelength to diameter was 2.0. The anechoic-chamber measurements showed that this deviation decreased with decreasing frequency, and was barely perceptible at 10 kHz.

The shields used in these measurements have simple shapes – rectangular plates and a circular cylinder of finite length. Two of the rectangular plates, used in most of the measurements, were constructed from 0.32-cm-thick sheets of aluminum, with a profile 50 cm X 200 cm (equivalent to a wing of aspect ratio 8). The edges on the first shield were square, whereas the edges on the second shield were sharp, as shown in figure 3. A third shield, with laminated wood construction, had semicircular edges of relatively large radius. A half-size rectangular shield

[1] A source is considered a point source if the magnitude of its far-field pressure varies inversely with the distance from the source to the field point, independent of the orientation of the field point (i.e., the point source is omnidirectional). For a point source emitting simple harmonic sound waves, the pressure variation is $p = \exp(ikR)/kR$ where k is the acoustic wave number and R is the radial distance from the point source to the far-field point.

(25 X 100 cm) with square edges was also constructed from 0.32-cm-thick sheet aluminum.

The circular cylinder consisted of a length of commercially available concrete form made of polyethylene-cardboard laminate. The cylinder was made more rigid by plywood disks installed at both ends. The diameter of the concrete form was chosen to be as close as possible to the width of the large rectangular plate. The diameter of the cylinder was 47 cm and the length was 300 cm.

The shields were suspended from the ceiling of the anechoic chamber by 0.05-cm steel wire. The orientation of the shield was maintained by guying the bottom edge to several points on the floor grid with 0.07-cm linen twine.

INSTRUMENTATION AND TEST PROCEDURE

Two functional groups of instrumentation were required – one to generate a reproducible level of sound at the tip of the inverse-taper horn, and another to record the sound-pressure level as monitored by a far-field microphone. A schematic of these two groups of instruments is shown in figure 4.

The loudspeaker was driven by a generator emitting either monochromatic sound or pink noise. (Pink noise is defined as broadband noise containing equal energy per octave band.) If pink noise was required, the broadband signal was initially processed by a filter that passed third-octave band noise centered on the desired frequency. If monochromatic sound was required, its frequency was carefully monitored by a frequency counter. In either case, the amplifier gain setting was determined by the voltage across the loudspeaker terminals. This is the key to the accuracy of the experiment, since the source output for a given shielded run should be the same as that for the corresponding unshielded run.

The variation of sound-pressure level (SPL) with traverse distance was monitored by a traversing microphone. The measured SPL was then processed through the bandpass filter set for a bandwidth of one-third octave for the harmonic runs as well as the pink-noise runs. The microphone stand was mounted on a moving carriage which was driven by an electric motor via a pulley system. The traverse length was 5.07 m and the traverse time was 4.7 min. In most of the measurements, the microphone height was adjusted so that it was the same as the source height. The graphic level recorder continuously recorded SPL versus traverse distance. For a given source-shield configuration, the usual procedure was to make a series of traverses to measure the harmonic noise, with frequencies of 1, 2, 4, 8, 12, 16, and 20 kHz, and to then follow with a series of one-third-octave pink-noise traverses with the same center frequencies, with one exception – the 12.0 kHz case is replaced by the standard 12.5 kHz for broadband noise.

ANECHOIC CHAMBER EFFECTS

All tests were made in an anechoic chamber (fig. 5(a)) having free working dimensions of 7.6 m by 5.5 m by 3.4 m (height). The room interior is lined with approximately 1720 polyurethane-polyesther wedges, designed to provide free-field conditions down to 150 Hz for normal incident sound waves. Several floor grids were installed at one end of the chamber beneath the source and shield. These grids were covered by at least 15 cm of acoustical foam during the measurements. At the other end of the chamber, a row of floor grids was installed across the width of the chamber to support the track for the traversing microphone. The track was shielded from the sound source by two rows of acoustical wedges (fig. 5(b)).

Several different configurations of source and microphone track locations were used in the anechoic chamber; they are shown in figure 6. For use in subsequent discussion, each configuration is given the designation shown in table 1.

Because the lowest frequencies used in these measurements were considerably above 150 Hz, it was initially assumed that there would be no reflections from the acoustical wedges, even at glancing angles of incidence, and that any location of source or microphone track was permissible. The resulting base runs (i.e., shield removed) were analyzed by comparing the

TABLE 1.– SOURCE-TRACK CONFIGURATION DESIGNATIONS

Source-track configuration	Source location	Track position
A	Corner	Far
B	Corner	Intermediate
C	Center	Far
D	Center	Intermediate

measured variation of SPL versus traverse distance with the expected variation for a point source. The agreement was excellent (±0.5 dB) at frequencies below 12 kHz for Configurations B, C, and D (table 1). Unfortunately, the base runs showed perceptible deviations for the source-track location of Configuration A at frequencies as high as 2 kHz. The effect was most pronounced for monochromatic sound at 1 kHz where the measured variation of SPL deviated by as much as 6.5 dB from the predicted variation, as shown in figure 7. Note that the deviations occurred when the microphone and source were close to the same wall. This behavior can only be attributed to glancing reflections from the acoustical wedges. This was further substantiated by the disappearance of the deviation when the source was shifted to the center location (Configuration C), or when the track was shifted to the intermediate position (Configuration B). As a result of the large deviation, all monochromatic sound and pink-noise shielding runs at 1 kHz with the source-track location of Configuration A were discarded.

At frequencies near 2 kHz, the base-run deviations for Configuration A were smaller. In this case, the maximum deviation occurred when the microphone and source were on opposite sides of the anechoic chamber, as shown in figure 7. However, comparisons of runs with a given source-shield arrangement for Configurations A and C, and dimensionally similar source-shield configurations for Configurations A and D, showed that these deviations in the base run at 2 kHz had only a small effect on the shielding (~1 dB). Consequently, all monochromatic sound and pink-noise shielding runs at 2 kHz with the source-track location of Configuration A were used in the analysis.

DATA REDUCTION

The data from the graphic level recorder is simply a representation of the sound-pressure level (SPL) versus traverse distance, and in this form does not give a measure of the effectiveness of the shielding for dimensionally similar source-shield configurations. However, the shielding, ΔSPL, versus the traverse angle, θ, does give an unambiguous measure. Consequently, this is the form used in this report. Since over 500 traverses were measured, many with extremely complex diffraction patterns, it would have been infeasible to manually convert the graphic level recorder data into the desired ΔSPL-versus-θ form. Consequently, it was decided to first convert the traces on the strip charts into digital data, use a computer to calculate ΔSPL versus traverse angle, and to then plot and display these quantities.

The electronic components used in this conversion are shown in the schematic diagram of figure 8. The strip chart data including the coordinate system was converted to digital data through the use of a sonic tablet and pen. The processed trace and coordinate axes were sent to the remote display station where they were digitized, then displayed for a visual check with the strip chart. All the processed traverses were recorded on tape, ready for computational purposes. The program for the calculation of ΔSPL and the conversion of traverse distance to traverse angle was loaded into the computer. For a given traverse, the proper shielded and unshielded data were recalled from tape storage. The calculated ΔSPL-versus-θ were displayed at the remote station, and the display copied by a hard-copy unit.

APPROXIMATIONS USED IN SHIELDING PREDICTIONS

The shielding predictions used in this report are based on the solution for the shielding of a monochromatic point source by a semi-infinite barrier as described in reference 6. The half-plane solution is given in terms of the acoustic velocity potential V, whereas measured shielding is given in terms of the rms value of the acoustical pressure p. Note that both p and V are complex quantities. In the far field the two quantities are related by the expression

$$p = i\omega\rho_a V \tag{1}$$

where ρ_a is the density of the ambient air, and ω is the angular frequency of the monochromatic sound. As a result of equation (1), the shielding can be expressed as

$$\Delta\text{SPL} = \text{SPL}_s - \text{SPL}_u = 20 \log_{10} \frac{|p_s|}{|p_u|} = 20 \log_{10} \frac{|V_s|}{|V_u|} \tag{2}$$

where the subscript s denotes the field-point quantities for the shielded case and the subscript u denotes field-point quantities for the unshielded case. Normally, ΔSPL is a negative quantity. For a

monochromatic point source separated from the field point by distance R, the unshielded velocity potential is given by

$$V_u = \frac{\exp(ikR)}{kR} \tag{3}$$

where k is the acoustic wave number. The expression for V_s is given in terms of the cylindrical coordinates shown in figure 9. The z-axis is located along the edge of the half-plane, and the projected radius ρ is measured in the $z = 0$ plane. The half-plane barrier is in the $\phi = 0$ plane. The source coordinates are (ρ_o, ϕ_o, z_o), the mirror image coordinates are $(\rho_o, 2\pi - \phi_o, z_o)$, and the field-point coordinates are (ρ, ϕ, z). The velocity potentials are expressed in terms of three distances, R, R', and R_1. The distance from the source to the field point, R, is given by

$$R = [\rho^2 + \rho_o^2 - 2\rho\rho_o \cos(\phi - \phi_o) + (z - z_o)^2]^{1/2} \tag{4}$$

The distance from the image source to the field point R' is given by

$$R' = [\rho^2 + \rho_o^2 - 2\rho\rho_o \cos(\phi + \phi_o) + (z - z_o)^2]^{1/2} \tag{5}$$

A characteristic diffraction distance is given by

$$R_1 = [(\rho + \rho_o)^2 + (z - z_o)^2]^{1/2} \tag{6}$$

In addition, the velocity potentials are expressed in terms of the Fresnel integral $F(\tau)$, the Heaviside step function $\eta(\psi)$, and the sign function $\mathrm{sgn}(x)$, where

$$F(\tau) = \int_{\tau}^{\infty} \exp(i\mu^2)\,d\mu \tag{7}$$

$$\eta(\psi) = \begin{cases} 1 & \psi > 0 \\ 0 & \psi < 0 \end{cases} \tag{8}$$

and

$$\mathrm{sgn}(x) = \begin{cases} 1 & x > 0 \\ -1 & x < 0 \end{cases} \tag{9}$$

The expression for the shielded velocity potential is expressed in terms of the definitions in equations (3) through (8). With the restrictions that $k(R_1 - R) \gg 1$, $k(R_1 - R') \gg 1$, and $kR_1 \gg 1$, V_s can be expressed (ref. 6, pp. 334–335) as the sum of a geometrical optics field V_G, and a diffracted field V_D.

$$V_s = V_G + V_D \tag{10}$$

where

$$V_G = \eta(\pi + \phi_o - \phi)\frac{\exp(ikR)}{kR} + \eta(\pi - \phi_o - \phi)\frac{\exp(ikR')}{kR'} \tag{11}$$

and

$$V_D = -\sqrt{\frac{2}{\pi k R_1}}\exp\left(-\frac{1}{4}i\pi\right)\left\{\mathrm{sgn}(\pi + \phi_o - \phi) \times \frac{\exp(ikR)}{\sqrt{k(R_1 + R)}} F[\sqrt{k(R_1 - R)}] + \mathrm{sgn}(\pi - \phi_o - \phi)\frac{\exp(ikR')}{\sqrt{k(R_1 + R')}} F[\sqrt{k(R_1 - R')}]\right\} \tag{12}$$

The shielding of a monochromatic point source by a semi-infinite hard barrier is completely described by equations (10) through (12). Conticelli, Di Biasi, and O'Keefe (ref. 7) suggested that semi-infinite barrier shielding could be combined in such a way so as to approximate the shielding by a quadrilateral. Their recommended procedure was to take a given edge of the quadrilateral (e.g., the leading edge of the wing), extend it to plus and minus infinity,[2] thereby forming a semi-infinite barier, and to then calculate the shielding, $|V_s/V_u|$, for that particular edge using

[2]It will be shown in the following sections that the agreement between measured and predicted values of noise shielding for rectangular plates is surprisingly good considering the grossness of the approximation. There is a plausible explanation for this agreement. Assume that the diffracted waves leaving a given semi-infinite plane behave as if the sound were being emitted from a line of distributed sources located along the edge of the semi-infinite plane. Due to spherical spreading of the primary point source, the line-source amplitudes should have a Gaussian-type distribution with the peak of the distribution at a point on the edge directly opposite the point source ($y_{edge} = y_{source}$). If the amplitude decay is rapid enough, and if the phases of the distributed sources change rapidly enough with increasing distance away from y_{source} so that phase cancellation results, then the portions of the semi-infinite edge far enough from y_{source} should contribute very little to the shielding.

equations (10) through (12). The resultant shielding at a given field point from all four sides of the quadrilateral was then found by simple addition of the shielding, $|V_{s_i}/V_u|$, from each of the corresponding semi-infinite barriers so that the resultant ΔSPL was given as

$$\Delta SPL = 20 \log_{10}\left(\frac{\sum_{i=1}^{4} |V_{s_i}|}{|V_u|}\right) \qquad (13)$$

This particular superposition of semi-infinite barrier solutions for a point source is not a good approximation as it neglects the phase relationship between the diffracted waves from the four edges on their arrival at a given field point. The phase relationship can be preserved by adding the complex expressions for V_{s_i} for each side before the absolute value is taken. This superposition is given by

$$\Delta SPL = 20 \log_{10}\left(\frac{\left|\sum_{i=1}^{4} V_{s_i}\right|}{|V_u|}\right) \qquad (14)$$

Comparisons of the predicted shielding for the two methods are shown in figure 10. A rectangular shield 50 cm X 200 cm was assumed for these calculations with the monochromatic point source located either in a symmetric or asymmetric position behind the plate. It can be seen that the summation of absolute values of V_{s_i} (eq. (13)) shows no diffraction patterns due to the destruction of the phase relationship between the diffracted waves from the four edges. In contrast, the summation of complex values of V_{s_i} (eq. (14)) shows diffraction patterns. In addition, equation (13) consistently gives smaller values of ΔSPL, especially at the lower frequencies. These comparisons clearly show why equation (14) is preferred to equation (13), especially for the prediction of the details of the shielded sound field. As a result, equation (14) is used in this report to predict shielding of monochromatic sound waves.

For the predicted shielding of broadband noise, such as the pink noise used in these measurements, the assumed point-source model consisted of a superposition of an ensemble of monochromatic point sources, each emitting with random phase relationship but with the prescribed distribution of amplitudes for pink noise. This model had a physical basis, being based on observations of oscilloscope traces generated by the output of a commercial pink-noise generator.

The following procedure was used. A given third-octave frequency band was divided into 100 equally spaced increments, each increment to be represented by a monochromatic point source. The emitted spherical wave from this incremental point source diffracts around the edges of the shield, and the resultant waves from each edge were assumed to arrive at a given field point with the phases specified by equations (10) through (12). Therefore, the acoustical pressure due to the jth frequency increment is given by $\sum_i p_{s_{ij}}$, where subscript i denotes a given edge of the shield. It should be pointed out that $p_{s_{ij}}$ is a complex quantity. This assumption is in line with the reasoning for equation (14). Because pink noise[3] is defined as random-frequency noise containing equal energy in each octave of the audio spectrum, its power amplitude must be attenuated at a rate of 3-dB per octave. Consequently, the weighting function for each frequency interval within the given third-octave band, A_j, can be related to the center frequency by

$$\frac{\log_{10} A_j - \log_{10} A_{ref}}{\log_{10} f_j - \log_{10} f_{ref}} = -\frac{1}{2} \qquad (15)$$

The reference amplitude and corresponding frequency can be taken at any convenient point. Finally, the absolute value of $A_j \sum_i p_{s_{ij}}$ must be taken prior to the summation over all frequency increments in order to preserve phase independency between each frequency increment. The expression for broadband shielding in terms of the acoustical pressure is then

$$\Delta SPL = 20 \log_{10}\left(\frac{\sum_{j=1}^{n} \left|A_j \sum_{i=1}^{4} p_{s_{ij}}\right|}{\sum_{j=1}^{n} |A_j p_{u_j}|}\right) \qquad (16)$$

To express ΔSPL in terms of the velocity potential, the relationship in equation (1) must be used. The

[3] If white noise (equal energy per frequency interval) were used, no weighting function would be required.

expression for broadband shielding in terms of the velocity potential is then

$$\Delta SPL = 20 \log_{10} \left(\frac{\sum_{j=1}^{n} \left| A_j f_j \sum_{i=1}^{4} V_{s_{ij}} \right|}{\sum_{j=1}^{n} |A_j f_j V_{u_j}|} \right) \quad (17)$$

The accuracy of this broadband approximation is dependent on the number of divisions taken for a given third-octave frequency band. To determine this dependency, a series of calculations was made with the number of divisions, n, varied from 2 to 100. Figure 11 shows some typical variations of n versus ΔSPL as calculated from equation (17). Note that ΔSPL approaches an asymptotic limit above an n of 50. Consequently, 100 divisions were used for all the pink-noise calculations.

The computer program for the calculation of ΔSPL from rectangular shields for monochromatic sound and broadband noise is described in the appendix.

RESULTS AND DISCUSSION

Rectangular Plates

This section describes the comparisons of predicted and measured shielding of a point source by rectangular plates. A typical source-shield arrangement is shown in figure 12. The location of the point source with reference to the center of the plate is given in terms of rectangular coordinates normalized by the width of the plate. The orientation of this coordinate system is also shown in figure 12. The various source-shield combinations that were tested are shown in figure 13. Each configuration is described by a two-view drawing with the location of the point source indicated by a filled circle in the top view, and by a dotted circle in the front view. The arrow in the front view indicates the microphone traverse direction which is always parallel to the plane of the plates.

Each configuration is identified by a series designation. For example, the letters LR denote the use of the large rectangular shield (0.5 m × 2.0 m) and the letters SR denote the use of the small rectangular shield (0.25 m × 1.0 m). Sine-wave and pink-noise measurements and calculations were made for 19 series in the LR set and for 5 series in the SR set. The data for these two sets represent over 300 traverses. In the interest of brevity, less than half of the data will be described; however, data will be presented for the more demanding situations to indicate the accuracy of the prediction scheme over the entire range of the measurements. The agreement between predicted and measured shielding for the omitted data is at least as good as that for the presented data, and is much better for most of the omitted configurations.

The predicted and measured ΔSPL's are plotted as functions of the traverse angle θ, as shown in figure 12. The angle $\theta = 0°$ is defined as that point where the microphone is directly opposite the point source. Note that the point source and traverse line were contained in the same horizontal plane for the LR and SR sets. The angles for the left and right visual edges (LVE and RVE) define the demarcations between the geometric shadow zone and the left and right light zones in keeping with optical terminology.

The value of the acoustic frequency will be given in two forms. The first is the conventional cycles per unit time, f, given in kilohertz. This form will usually be used when frequency-dependent experimental errors affect the data. The second is the dimensionless frequency, kW, where k is the wave number ($2\pi f/c$) and W is the width of the plate. This form will be used to generalize the results for their use in dimensionally similar situations.

Series LR1– The comparisons of predicted and measured shielding for this series will be discussed in detail, including the discussions of experimental inaccuracies (e.g., wall reflections and imprecise shield alignment) which will have a direct bearing on the interpretation of the results for other series. The LR1 series is a fairly demanding test of the prediction methodology because of the configuration symmetry. The left and right edges should each contribute comparable acoustic radiation at small θ's, and because of the interference of the waves from these two edges, should determine the characteristics of the diffraction patterns over the entire range of θ's. The top and bottom edges should not contribute significantly to the diffraction because of their large distances from the point source. The predicted shielding is compared with the measured shielding for both monochromatic and pink noise in figure 14 for kW (products of wave number, k, and plate width, W) from 9 to 183 (frequencies from 1 kHz to 20 kHz).

Monochromatic shielding in the shadow zone will be discussed first. With one exception, the agreement between predicted and measured shielding in figure 14 was fairly good up to a kW of 110. The accuracy for the prediction of the locations of the peaks and valleys[4] was excellent. The accuracy for the prediction of magnitudes of these peaks was variable but in most of the cases the agreement was within 1 dB. The one exception in this range, where the prediction of peak magnitudes was poor, occurred at a frequency of 2 kHz (kW = 18). This discrepancy can be attributed to the anharmonicity from the sound source which reached a maximum in the neighborhood of 2 kHz. If it is assumed that the anharmonicity is in the form of nonlinear distortion (ref. 10), then a comparison of the measured shielding with the shielding predicted at a slightly higher frequency might show better agreement. This comparison is shown in figure 15, where the prediction frequency was assumed to be 2.05 kHz. The agreement was better in the shadow zone.

At frequencies above a kW of 110, the predicted and measured values begin to deviate deep in the shadow zone and near the visual edges. As the frequency was increased beyond a kW of 110, the shielding deep in the shadow zone was increasingly underpredicted, with the difference reaching a value of 5 dB at the highest frequency measured (f = 20 kHz, kW = 183). It should be pointed out that the size of this disparity may not be crucial since it occurs in a region where large shielding (22 dB) exists. This underprediction probably arises from some deficiency in the predictive method. The predictions of Davis and Gabrielsen (ref. 5) using the Kirchoff approximation showed better agreement with these measurements at these higher frequencies.

The other deviation between predicted and measured shielding values at high frequencies occurred near the visual edges. The discrepancy was not manifested by any large differences in the magnitudes of the peaks, but in a considerable change in the diffraction patterns. This discrepancy can be attributed to the inaccuracy in positioning the point source with respect to the rectangular plate. It was estimated that the positioning was only accurate to ±0.1 cm with the measuring devices used. This accuracy corresponds to a displacement along the traverse equivalent to one-quarter of a wavelength on the traverse line for an 8-kHz tone. Hence, perceptible discrepancies in the diffraction patterns near the visual edges at frequencies above 8 kHz may be attributed to positioning errors as was substantiated experimentally by displacing the source horizontally by 0.2 cm. This resulted in virtually no change in the envelope drawn along the peaks of the shielding for frequencies greater than 8 kHz, but resulted in large changes in the pattern itself, such as the shifting of peaks to different θ's and coalescence of peaks or valleys.

Monochromatic shielding in the light zone is also shown in figure 14. The agreement is fairly good except for the lowest frequency where wall reflections may have had an effect.

Figure 14 also presents the comparisons of predicted and measured shielding of broadband noise. The advantage in using broadband noise for the comparison is that many of the experimentally induced errors were reduced or eliminated. For example, the effects of inaccurate positioning of the source and anechoic chamber wall reflections were reduced because of phase cancellation, and the source anharmonicity effects were eliminated. The only error that could not be reduced was the high-frequency departure from omnidirectionality at large angles from the axis of the horn (fig. 2).

A comparison of the measured shielding for monochromatic sound and one-third-octave band pink noise (fig. 16) shows that the levels of shielding are comparable and the locations of the diffraction peaks and valleys were the same deep in the shadow zone. Consequently, if the monochromatic approximation contains any inadequacies, they should become apparent in the prediction of broadband shielding which is based on the monochromatic approximation. For the above reasons, the contention is made that the comparisons between the predictions and measurements of broadband noise are better indications of the accuracy of the predictive techniques for monochromatic sound than the actual comparisons for the monochromatic case.

The predicted broadband shielding in figure 14 in the light zone as well as the shadow zone were calculated by the use of the four-sided solution of equation (17). At most frequencies the agreement between predicted and measured values was fairly good. The agreement for the broadband traverses was definitely superior to that for the monochromatic traverses. It should be pointed out that at 2 kHz (kW = 18), where a large discrepancy existed for the monochromatic comparison, the agreement was excellent due to the absence of source anharmonicity

[4]The terms peak and valley refer to the attenuation minimum and maximum, respectively, in the diffraction pattern for ΔSPL.

effects on broadband measurements. At high frequencies ($kW \geq 37$) there were 2 to 4 dB underpredictions of the shielding deep in the shadow zone, slightly better than the monochromatic comparison.

Series LR2– The configuration for this series is asymmetric with the source located directly behind the right edge of the plate at $\theta = 0°$. Comparisons of predicted and measured shielding for monochromatic sound and broadband noise are shown in figure 17.

The main features of the predicted monochromatic shielding for this configuration are similar to those for Series LR1. Predicted shielding is a good approximation for both monochromatic sound and broadband noise. Especially noteworthy was the agreement between the measured diffraction pattern deep in the light zone. The agreement at the lower frequencies was better than those for Series LR1, as the asymmetry is less sensitive to any small inaccuracies in the predictive method.

Series LR3 and LR4– These two series are characterized by substantial contributions to the diffraction patterns from three edges rather than two as in Series LR1 and LR2. Because of this additional complication, they should be more difficult to predict than the LR1 and LR2 series. The comparisons between predicted and measured values of shielding for these series are shown in figures 18 and 19. With one exception, the agreement between predicted and measured shielding was approximately the same as those in Series LR1 and LR2, with relatively poor agreement for the monochromatic traverses at 2kHz ($kW = 18$) due to the combined effects of wall reflections and source anharmonicity.

The exception was the high frequency ($kW \geq 73$) comparisons for Series LR3 in the center of the shadow zone ($|\theta| < 10°$), where there were large discrepancies. In this region there are equal contributions from the three edges since the source is equidistant from the three edges at $\theta = 0°$, resulting in the prediction of an alternating series of high and low peaks. The measurements showed the alternating peaks at $kW = 73$ and 110 but to a lesser degree. As the frequency was increased, the measurements showed smaller differences between the amplitudes of the high and low peaks. It is not known how much of this disparity between predicted and measured values for this unique condition was caused by source positioning error and how much of it was the result of an inadequacy of predictive method. The answer can only be resolved by the use of a more accurate prediction technique.

The appearance of a series of peaks with large variations is unique to that particular source-shield geometry of the LR3 series. Any lateral shift of the source which reduces the symmetry, such as in the LR4 series (fig. 19), or vertical shift of the source, such as in the LR13 series (fig. 20), also removed the alternations.

Series SRH– This series differs from the previous ones in that the traverse line is parallel to the long axis of the rectangle. The agreement between the predicted and measured shielding shown in figure 21 is fairly good. The shape of the diffraction patterns was accurately predicted; however, the level of shielding was underpredicted at the higher frequencies. This discrepancy was similar to those found deep in the shadow zone for the series previously described.

Low-frequency comparisons– The comparisons of predicted and measured shielding in series LR1 and LR2 did not conclusively establish the accuracy of the predictive method at very low frequencies. Consequently, additional comparisons for a number of traverses from different series (SR1, SR2, SR4, and LR7) are shown in figure 22 for the two lowest kW of 4.5 and 9. The agreement was good at a kW of 9. At the lowest frequency measured ($kW = 4.5$) the prediction and measurement showed the same shape for ΔSPL versus θ. However, the magnitude of the shielding was consistently underpredicted by 2 dB. It is believed that the low-frequency limitation on equations (10) and (11) have been exceeded. For this reason, it is recommended that this particular predictive method for rectangular plates be limited to values of kW no smaller than 4.5.

Effect of edge shape– The shape of the edges may affect the shielding when the dimensions of the edge (e.g., shield thickness or edge diameter) are comparable to one-quarter of the acoustical wavelength. To determine this effect, measured shielding from a large rectangular plate with sharp edges of 0.04-cm thickness (Series LR11) was compared with that from a plate with semicircular edges of 5.1-cm diameter (series LR12).[5] The comparisons (fig. 23) show that edge shape has little effect in the center of the shadow zone ($|\theta| < 15°$) for monochromatic sound and broadband noise. At larger θ's for both monochromatic sound and broadband noise, the shielding from the rounded edge was 2 dB less than the shielding from the sharp edge at higher frequencies ($kW \geq 110$).

[5]These dimensions correspond to one-quarter wavelengths for frequencies of 207 kHz and 1.63 kHz, respectively.

In addition, there were large differences between the diffraction patterns for the two types of edges.

Cylinders

Exact solutions for the shielding of a point source by infinitely long circular cylinders are given in reference 6. The general solution, valid for near- and far-field points, is in the form of an infinite sum of integrals containing Bessel and Hankel functions, where the variable of integration ranges from minus to plus infinity. When the field point is infinitely far away the solution reduces to an infinite sum of algebraic terms containing the same functions. Because of the complexity of these solutions, they do not lend themselves to rapid calculations.

An alternative approach is to use the calculations for rectangular shielding described in previous sections to approximate cylindrical shielding. This section evaluates this approach by comparing measured cylindrical shielding with measured and predicted rectangular shielding. The various source-shield combinations that were tested are shown in figure 13. The orientation of the coordinate system is the same as that for the rectangular plate (fig. 12), with the origin of the coordinate system located at the geometric center of the cylinder. The coordinates of the point source are normalized by the diameter of the cylinder.

Only two source positions were used, the near position (z_s/d = 1.02) and the far position (z_s/d = 2.07). The series designation C denotes the cylinder positioned so that its axis of revolution was vertical, and the designation CH denotes the cylinder positioned so that its axis was horizontal.

Relationship between cylindrical and planar shielding– Comparisons of measured diffraction patterns resulting from the shielding by the cylinder with those from the shielding by a rectangular plate showed some significant similarities. The diffraction patterns from both types of shields peaked at the same values of θ providing two conditions were met: First, the width of the plate had to be about the same as the diameter of the cylinder, and second, the source had to be symmetrically located behind the cylinder (e.g., Series C1) and the plate (e.g., Series LR1).

The shielding from all the LR series with these qualifications (Series LR1, LR5–LR9, LR11, and LR12) were compared with the shielding from Series C1. Of these, only the comparisons with Series LR5 (fig. 24) showed that the magnitude of shielding was essentially the same. A comparison of the geometric factors for these two series reveals the conditions required for the cylindrical and planar shielding to be the same.

Only the lengths of the two shields differ significantly, with the length of the plate much shorter than the length of the cylinder. However, this difference should not affect the shielding, since contributions from the ends of the shields should be negligible compared to the contributions from the sides.

The comparison suggests that cylindrical shielding at a given field point can be approximated using an equivalent rectangular shield if the following assumptions are made:

1. Width of the equivalent rectangle and diameter of the cylinder are the same.
2. Length of the equivalent rectangle and length of the cylinder are the same, and are large compared with the diameter.
3. z_s is the same for both types of shields.
4. The longitudinal centerline of the equivalent rectangular plate must coincide with the cylindrical axis of revolution; in addition, the plane of this plate must be perpendicular to the line that is normal to the cylindrical axis of revolution and that passes through the source.

This orientation of the equivalent rectangular plate is shown in figure 25.

Series C1– Comparisons of predicted and measured shielding by the cylinder with the source in the near position (z_s/d = 1.02), are shown in figure 26 for monochromatic sound and broadband noise. An equivalent rectangle described in the previous section was used to calculate the predicted shielding.

The locations of the peaks and valleys were predicted quite well for the monochromatic traverses at all frequencies. At higher frequencies (where the product of the wave number and cylinder diameter, kd, is greater than 34) the agreement between predicted and measured peak magnitudes was good. However, the magnitude agreement was only fair for the monochromatic traverses at lower frequencies, where there were discrepancies in the center of the shadow zone in the order of 2 to 3 dB. These discrepancies can be attributed to wall reflections or to source waveform distortion.

This attribution was substantiated by the much better agreement at the lower frequencies ($kd \leq 34$)

for the broadband traverses,[6] where the predicted and measured peak magnitudes were within 1 dB of each other. At the higher frequencies, the broadband comparisons show excellent agreement deep in the shadow zone, although the predictions show 2 dB less shielding near the visual edge.

Series C2– Comparisons of predicted and measured shielding by the cylinder with the source in the far position (z_s/d = 2.07) are shown in figure 27. The computational approach for the predicted shielding was the same as that used in Series C1.

The locations of the peaks and valleys were predicted quite well for monochromatic and broadband traverses. The agreement between predicted and measured magnitudes of shielding for the monochromatic traverses at lower frequencies ($kd \leqslant 34$) was better than those in Series C1. This was not unexpected since a given error in source location should have less effect with the source in the far position. At the highest frequencies ($kd \geqslant 137$) the shielding deep in the shadow zone was consistently overpredicted by about 2 dB for the monochromatic and broadband traverses; however, this is not a serious deficiency as the measured shielding in this region is relatively large (10 to 15 dB).

Series CH1 and CH3– For these two series the cylinder was positioned so that its axis was parallel to the traverse line (fig. 13(f)). The source was placed in the far position. In series CH1 the source, cylinder axis, and traverse line were all contained in the same horizontal plane. In Series CH3, the traverse line of the microphone was displaced below the horizontal plane containing the source and the cylinder axis. As a result, the entire length of the traverse for Series CH3 was located slightly above the lower visual edge.

Comparisons of the predicted and measured shielding are shown in figures 28 and 29, where the predicted shielding was again based on an equivalent rectangular plate. With a few exceptions, there was excellent agreement between predicted and measured shielding for both series. The exceptions occurred at a kd of 9 for both series, and at a kd of 27 for Series CH1. At the lowest frequency the peaks of the predicted shielding were the same magnitude as the measured shielding. However, the predicted shielding showed an oscillating variation with ϑ which was not evident in the measured shielding. At kd = 27 the measured shielding for series CH3 was considerably smaller than the predicted shielding. A possible source for this discrepancy could be the large variation of shielding incurred by an inadvertent small vertical displacement of the source (i.e., source location error). These large variations are evident in the C2 traverses[7] shown in figure 27 in the region of a traverse angle of 11°.

Wing-Body Combinations

A wing-body combination was simulated by attaching a 50 cm × 160 cm rectangular plate to the cylinder such that the long axis of the plate was perpendicular to the axis of the cylinder. The orientation of this combination with reference to the point source and the microphone traverse line is shown in figure 13. The shielding of a point source by a wing-body combination is complicated by acoustic emission from sources distributed along the surface of a given airframe component due to the direct radiation from the point source, and to the reflected radiation from the other airframe component. Because of these complications, it would be extremely difficult, if not impossible, to accurately predict the shielding by wing-body combinations. It would be much simpler to compare the measured shielding for the cylinder with and without the rectangular plate (i.e., wing) to determine if some gross approximations could be made. These approximations would then be used to formulate some simple predictive models based on the techniques that were previously described. This is the approach that will be used in the next two sections.

Series CH2– The cylinder-source configuration for this series is identical to that for Series CH1. The only addition is the rectangular plate (fig. 13). The measured shielding for these two series is compared in figure 30. Note that the left and right visual edges for the wing are marked on the θ axis with the designations WLVE and WRVE.

Figure 30 shows that the presence of the wing resulted in an increase of up to 8 dB in shielding within the shadow zone of the wing. The incremental

[6] It was pointed out in previous sections that there were no source waveform distortion effects on broadband noise, and that broadband noise was much less affected by source location errors.

[7] A small vertical displacement in Series CH3 at $\theta = 0°$ is equivalent to a small horizontal displacement in Series C2 at $\theta = 11°$.

shielding showed no consistent trend with frequency due to the complexity of the configuration. It may be possible, however, to make a simple approximation that would give acceptable results over most of the range of frequencies. For example, it could be assumed that wing shielding is completely effective within the shadow zone of the wing for this particular configuration. This assumption is equivalent to replacing the wing-body combination by a "three-sided" cylindrical shield, where the fourth side containing the wing-body juncture would not contribute to the acoustic emission. Figure 31 compares the measured shielding with that from an equivalent rectangle with contributions from the bottom and side edges. It can be seen that the three-sided approximation is excellent at the lowest frequency ($kd = 9$) and at the higher frequencies ($kd \geqslant 103$). At the intermediate frequencies, the approximation is only fair, but still superior to using the approximation for the cylinder alone (i.e., four-sided equivalent rectangle).

Outside of the shadow zone of the wing ($|\theta| > 14.5°$) the added shielding due to the wing diminished beyond the wing visual edge with the shielding reaching the levels for the cylinder alone. It can be seen from the comparisons in figure 30 that an adequate representation of this transition is a straight line beginning at the wing visual edges for the three-sided shielding and ending at the cylinder-alone shielding 15° beyond the wing visual edges.

The shieldings based on the approximation described in this section are compared with the measured shielding in figure 32. Although the diffraction patterns could not be predicted, the level of shielding was adequately predicted.

Series C3– The cylinder-source configuration for this series is identical to that for Series C2. The only addition is the rectangular plate (fig. 13). The measured shieldings for these two series are compared in figure 33.

The shielding in the shadow zone and in the right light zone will be discussed first. At the two lowest frequencies ($kd \leqslant 17$) there appear to be no consistent trends, probably the result of large diffractive effects due to large wavelengths overshadowing reflective effects. At higher frequencies, the presence of the wing results in definite increases in shielding in the shadow zone, with the greatest increase at the left visual edge. These variations indicate that the wing-body combination can be replaced by a "three-sided" cylindrical shield, where the fourth side containing the wing-body juncture would not contribute to the acoustic emission.

Figure 33 shows that as θ becomes increasingly negative in the left light zone, the shielding gradually decreases. This is contrary to the behavior expected of a "three-sided" cylindrical shield – a continuous increase in shielding (aside from the diffraction oscillations) as the field point is moved farther away from the right edge of the cylinder. The gradual decrease in shielding shown in figure 33 can be attributed to the increasing contribution of the diffracted waves from three sides of the rectangular plate[8] (i.e., wing) as θ becomes increasingly negative.

Figure 34 compares the measured shielding with two approximations. The first approximation is based on a "three-sided" cylinder where the equivalent rectangle has contributions from the right, top, and bottom edges. The comparison shows that this approximation is good for all θ's to the right of the LVE of the cylinder. The second approximation is based on a "three-sided" rectangle perpendicular to the cylindrical axis and the microphone traverse line. This approximation should be compared with the measured shielding at all θ's to the left of the LVE of the cylinder. Although there are minimal data at negative θ's beyond the LVE, the indications are that the three-sided rectangle is a good approximation at negative θ's 15° beyond the LVE. On the basis of the comparisons of figure 34, we can determine a transition curve from one approximation to the other extending from $\theta = 0°$, on the right-hand side to a negative angle of 15° beyond the LVE, with the shielding at the LVE taken as the arithmetic average of the shielding of the three-sided cylinder and the three-sided rectangle. The approximated shielding for the entire range of θ's is compared with the measured shielding in figure 35. With the exception of the lowest frequency ($kd = 9$), the level of shielding was adequately represented.

SUMMARY OF RESULTS

The present investigation was conducted to evaluate some simple methods for predicting the noise shielding in terms of monochromatic sound and broadband noise of aircraft components. The approach was to make anechoic chamber measurements of the shielding of a point source by geometric

[8]It is assumed that the fourth side of the plate containing the wing-body juncture would not contribute to the acoustic emission.

shapes, and to then compare the measured values with those calculated by the simple approximations. The shielding approximations for all geometric shapes, including wing-body combinations, are based on the superposition of solutions for the shielding by a semi-infinite plane barrier.

In general, the agreement between measured and predicted shielding by rectangular plates was excellent for monochromatic sound and broadband noise in the shadow and light zones. There were two exceptions: (1) for monochromatic traverses, there were large disparities in the vicinity of the diffraction valleys, disparities that can be attributed to experimental errors; and (2) the shielding deep in the shadow zone for certain configurations was underpredicted by as much as 5 dB at the highest frequencies for broadband as well as for monochromatic traverses. The latter deficiency was not considered too important, however, because the measured shielding for these particular traverses was usually more than 20 dB. Aside from these two exceptions, the average deviation between measured and predicted shielding was less than 2 dB.

Edge shape has little effect on shielding in the center of the shadow zone. However, there appeared to be noticeable changes in the diffraction patterns and a shift in level of the order of 2 dB near the visual edges.

Comparisons between measured diffraction patterns from the shielding by the cylinder with those by rectangular plates showed significant similarities. It was concluded from these comparisons that the predicted shielding based on the use of this equivalent rectangle was excellent. Aside from a discrepancy in the vicinity of the diffraction valleys for monochromatic sound at lower frequencies, the average deviation was less than 2 dB.

The shielding of wing-body combinations was predicted by modifications of the approximations used for rectangular or cylindrical shielding. The agreement between predicted and measured shielding was only fair at low frequencies, but were considered good at higher frequencies. The approximations failed to predict the diffraction patterns in certain regions; however, the average level of wing-body shielding could be predicted within 3 dB of the measured values at the higher frequencies.

Ames Research Center
National Aeronautics and Space Administration
Moffett Field, California 94035, June 4, 1979

APPENDIX

COMPUTER PROGRAMS FOR PREDICTING SHIELDING OF A POINT SOURCE BY RECTANGULAR PLATES

General Considerations

Two program listings are included. The first predicts the shielding of a monochromatic point source and the second the shielding of a pink-noise point source. Both programs are for the specific case of a rectangular shield, with the traverse line parallel to one of the edges of the rectangle and in the same horizontal plane as the source. However, the listings can easily be modified to describe shielding by a trapezium with a traverse of any desired orientation and shape (i.e., circular arc).

The programs are identical in setup, with the input and output control cards of the same form. Both programs consist of a main program and three subroutines. Because the three subroutines are identical for the two programs, they are listed only once.

The main program controls all input and output, calculates the geometric parameters, and sums all sides for the final solution. Subroutine EVAL evaluates V_S and V_U for each side. Complex function FRSNL calculates the complex Fresnel integral (eq. (7)). Subroutine THTPLT generates a plot tape to be used on the UCC plotter.

Control Cards

The program was set up to run on the CDC/7600 using the UCC plotter software package (see Ames User Bulletin No. 164). The following control cards are needed to compile and run from a card deck:

```
(JOBNAME), T(NN).
ACCOUNT, (USERID), (JO).
FILE, TAPE 1, RT = U, BT = K, RB = 1,
  MRL = 20000.
STAGE, TAPE 1, POST, HY, VSN = (TAPE
  NUMBER).
ATTACH, UCC, UCCPLOT, ID = AMES UB.
LIBRARY, UCC.
FTN.
LGO.
7/8/9
```

FORTRAN DECK

```
7/8/9
```

DATA DECK

```
6/7/8/9
```

For the monochromatic program, each point generated on a graph requires approximately 0.0012 sec of computer time. For pink noise, each point requires about 0.08 sec of machine time. Therefore, the time needed for a given run can be calculated by multiplying the number of frequencies to be calculated by the number of points per frequency and the number of configurations to be run.

Input

The following input cards are needed for each run:

CARD 1 FORMAT (15)

PARAMETER: NCASE

This is an integer specifying the number of cases to be run. A case is defined as a full range of frequencies for a given configuration.

CARD 2-N FORMAT (7E10.3)

There are NCASE of these

PARAMETERS: A,B,C,D,ASIDE,BSIDE, DELTAZ

A = Horizontal displacement of the source (x_s of fig. 14)

B = Vertical displacement of the source (y_s of fig. 14)

C = Distance from the plate to the source (z_s of fig. 14)

D = Distance from the plate to the microphone at $\theta = 0°$

ASIDE = Half the width of the plate

BSIDE = Half the length of the plate

DELTAZ = Increments along the microphone traverse line.

All linear dimensions are in meters.

The frequencies are given in a data list statement and can be easily modified by changing the card that reads:

```
DATA FI/.....
```

to the required frequencies. This is a sample data deck to run 3 cases:

CARD 1	3						
CARD 2	0.0	0.0	0.25	5.0	0.25	1.0	0.5
CARD 3	0.0	0.0	0.25	2.5	0.5	1.5	0.01
CARD 4	0.0	0.25	0.25	5.0	0.25	1.0	0.05

Output

The major output of the program is the plot tape generated by Subroutine THTPLT. Shielding (SPL) is plotted versus traverse angle (θ). Examples of the plots are given in figures 15 through 34. The input parameters and the number of data points generated for each frequency are printed as a check (Program Lists 1–5).

REFERENCES

1. Grotz, Charles A.: Development of the YC-14 Propulsion System. AIAA Paper 75-1314, Sept. 20–Oct. 1, 1975.
2. Vincent James H.: Quiet Short-Haul Research Aircraft. Phase I: Flight Simulation Investigation. NASA CR-151964, 1977.
3. Primakoff, Henry; Klein, Martin J.; Keller, Joseph B.; and Carstensen, E. L.: Diffraction of Sound Around a Circular Disk. J. Acoust. Soc. Am., vol. 19, no. 1, Jan. 1947, pp. 132–142.
4. Leitner, Alfred: Diffraction of Sound by a Circular Disk. J. Acoust. Soc. Am., vol. 21, no. 4, July 1949, pp. 331–334.
5. Gabrielsen, Ralph E.; and Davis, Joseph E.: Accuracy of the Kirchoff Formula in Determining Acoustic Shielding Due to a Flat Plate. NASA TM-73,261, 1977.
6. Bowman, J. J.; Senior, T. B. A.; and Uslenghi, P. L. E.: Electromagnetic and Acoustic Scattering by Simple Shapes. American Elsevier Publ. Co. Inc., New York, 1969.
7. Conticelli, V. M.; Di Blasi, A.; and O'Keefe, J. V.: Noise Shielding Effects for Engine-Over-Wing Installations. AIAA Paper 75-474, Mar. 24–26, 1975.
8. Dunn, D. G.; Butzel, L. M.; Di Blasi, A.; Filler, L.; and Jacobs, L. D.: Aircraft Configuration Noise Reduction. FAA RD-76-76, vol. 1, June 1976.
9. Olson, Harry F.: Elements of Acoustical Engineering. Second ed., D. Van Nostrand Co. Inc., New York, 1947.
10. Beranek, Leo L.: Acoustics Measurements. John Wiler and Sons, Inc., New York, 1949.

PROGRAM LISTING 1.– SHIELDING OF MONOCHROMATIC SOUND BY RECTANGULAR PLATE

```
      PROGRAM NOISEY(INPUT,OUTPUT,TAPE5=INPUT,TAPE6=OUTPUT,TAPE1)
      COMMON/PLT/PT,TOTR,A,B,C,D,ASD,BSD,F,RVE,XLVE,N,XORG
      COMMON R,R1,RPRIM,FK,PI,PSI,R1R,R1RP
      DIMENSION PT(1000),TOTR(1000)
      DIMENSION FI(14)
      COMPLEX RN1,RN2,RN3,RN4
      COMPLEX C2,VI1,VI2,VI3,VI4
      DIMENSION RRI(8)
      DATA FI/1000.,1950.,2000.,2050.,3900.,4000.,4100.,7800.,
     18000.,8200.,15600.,16000.,16400.,20000./
      RCAP(X,Y,P,Z)=SQRT(X*X+Y*Y-2.0*X*Y*COS(P)+Z*Z)
      NC=0
      EPS=0.0001
      CO=347.412
      DZ=0.5
      PI=3.14159265359
      RAD=57.29577951
      XORG=0.0
      WRITE(6,103)
  103 FORMAT(1HO,37X,36HNOISE REDUCTION - HALF PLANE BARRIER/)
      READ(5,105) NCASE
  105 FORMAT(I5)
    1 CONTINUE
      NC=NC+1
      READ(5,101)A,B,C,D,ASIDE,BSIDE,DELTAZ
      ASD=ASIDE*2.0
      BSD=BSIDE*2.0
      AAC=(ASIDE-A)/C
      ABC=(ASIDE+A)/C
      CD=C+D
      RVE=ATAN(AAC)*RAD
      XLVE=ATAN(ABC)*RAD
      XLVE=-XLVE
      ZRVE=AAC*CD
      ZLVE=-ABC*CD
      ZTEMP=ZRVE
      X1=ZLVE+0.05
      X2=(C+D)*TAN(60.0/RAD)
  110 FORMAT(1HO,6F8.3)
      DO 500 I=1,14
      F=FI(I)
      XLAM=CO/F
      N=0
      FK=2.0*PI*F/CO
      Z=X1
      WRITE(6,104)A,B,C,D,ASIDE,BSIDE,F,CO
  104 FORMAT(1HO,4HA = ,F6.3,2X,4HB = ,F6.3,2X,4HC = ,F6.3,2X,3HD = ,F6.3
     1,2X,8HASIDE = ,F6.3,2X,8HBSIDE = ,F6.3,2X,4HF = ,E12.5,2X,5HCO = ,
     2E12.5/)
   30 CONTINUE
      N=N+1
C
C     DO CASE 1
C
      CODE=1
      BB=BSIDE-B
      BBZ=BB-DELTAZ
      PHIO=ATAN(C/BB)
      THET=ATAN(D/ABS(BBZ))
```

```
      PHI=2.0*PI-THET
      IF(BBZ.LT.0.0) PHI=PI+THET
      ROL=C/SIN(PHIO)
      RL=D/SIN(THET)
      PHIL=PHI-PHIO
      PSI=PI-PHIL
      R=RCAP(RL,ROL,PHIL,Z)
      PHIL=PHI+PHIO
      RPRIM=RCAP(RL,ROL,PHIL,Z)
      R1=RCAP(RL,ROL,PI,Z)
      RTST1=2.0*RL*ROL*(1.0+COS(PHI-PHIO))/R1**4
      RTST2=2.0*RL*ROL*(1.0+COS(PHI+PHIO))/R1**4
      R1R=R1-R
      IF(RTST1.LE.EPS) R1R=RL*ROL*(1.0+COS(PHI-PHIO))/R1
      R1RP=R1-RPRIM
      IF(RTST2.LE.EPS) R1RP=RL*ROL*(1.0+COS(PHI+PHIO))/R1
      CALL EVAL(RN1)
      RTEM=CABS(RN1)
      RNA=20.0*ALOG10(RTEM)
C
C     DO CASE 2
C
      CODE=2
      BB=BSIDE+B
      BBZ=BB+DELTAZ
      PHIO=ATAN(C/BB)
      THET=ATAN(D/ABS(BBZ))
      ROL=C/SIN(PHIO)
      RL=D/SIN(THET)
      PHI=2.0*PI-THET
      IF(BBZ.LT.0.0) PHI=PI+THET
      PHIL=PHI-PHIO
      PSI=PI-PHIL
      R=RCAP(RL,ROL,PHIL,Z)
      PHIL=PHI+PHIO
      RPRIM=RCAP(RL,ROL,PHIL,Z)
      R1=RCAP(RL,ROL,PI,Z)
      RTST1=2.0*RL*ROL*(1.0+COS(PHI-PHIO))/R1**4
      RTST2=2.0*RL*ROL*(1.0+COS(PHI+PHIO))/R1**4
      R1R=R1-R
      IF(RTST1.LE.EPS) R1R=RL*ROL*(1.0+COS(PHI-PHIO))/R1
      R1RP=R1-RPRIM
      IF(RTST2.LE.EPS) R1RP=RL*ROL*(1.0+COS(PHI+PHIO))/R1
      CALL EVAL(RN2)
      RTEM=CABS(RN2)
      RNB=20.0*ALOG10(RTEM)
C
C     DO CASE 3
C
      CODE=3
      AA=ASIDE-A
      IF(AA.LT.1.E-12) GO TO 40
      PHIO=ATAN(C/AA)
      GO TO 41
   40 PHIO=PI/2.0
   41 CONTINUE
      ALPHA=ATAN((Z-AA)/D)
      PHI=3.0*PI/2.0-ALPHA
      RL=D/COS(ALPHA)
      ROL=C/SIN(PHIO)
```

PROGRAM LISTING 1.– CONTINUED

```
      PHIL=PHI-PHIO
      PSI=PI-PHIL
      PSI3=PSI
      R=RCAP(RL,ROL,PHIL,DELTAZ)
      PHIL=PHI+PHIO
      RPRIM=RCAP(RL,ROL,PHIL,DELTAZ)
      R1=RCAP(RL,ROL,PI,DELTAZ)
      RTST1=2.0*RL*ROL*(1.0+COS(PHI-PHIO))/R1**4
      RTST2=2.0*RL*ROL*(1.0+COS(PHI+PHIO))/R1**4
      R1R=R1-R
      IF(RTST1.LE.EPS)  R1R=RL*ROL*(1.0+COS(PHI-PHIO))/R1
      R1RP=R1-RPRIM
      IF(RTST2.LE.EPS)  R1RP=RL*ROL*(1.0+COS(PHI+PHIO))/R1
      CALL EVAL(RN3)
      RTEM=CABS(RN3)
      RNC=20.0*ALOG10(RTEM)
C
C     DO CASE 4
C
      CODE=4
      AA=ASIDE+A
      IF(AA.LT.1.E-12) GO TO 50
      PHIO=ATAN(C/AA)
      GO TO 51
   50 PHIO=PI/2.0
   51 CONTINUE
      ALPHA=ATAN((Z+AA)/D)
      PHI=3.0*PI/2.0+ALPHA
      RL=D/COS(ALPHA)
      ROL=C/SIN(PHIO)
      PHIL=PSI-PHIO
      PSI=PI-PHIL
      R=RCAP(RL,ROL,PHIL,DELTAZ)
      PHIL=PHI+PHIO
      RPRIM=RCAP(RL,ROL,PHIL,DELTAZ)
      R1=RCAP(RL,ROL,PI,DELTAZ)
      RTST1=2.0*RL*ROL*(1.0+COS(PHI-PHIO))/R1**4
      RTST2=2.0*RL*ROL*(1.0+COS(PHI+PHIO))/R1**4
      R1R=R1-R
      IF(RTST1.LE.EPS) R1R=RL*ROL*(1.0+COS(PHI-PHIO))/R1
      R1RP=R1-RPRIM
      IF(RTST2.LE.EPS) R1RP=RL*ROL*(1.0+COS(PHI+PHIO))/R1
      CALL EVAL(RN4)
      RTEM=CABS(RN4)
      RND=20.0*ALOG10(RTEM)
C
C     CALCULATE TOTAL NOISE REDUCTION
      RN4=0.0
      TOTRN=CABS(RN1+RN2+RN3+RN4)
      TOTRN=20.0*ALOG10(TOTRN)
      TOTR(N)=TOTRN
      PT(N)=ATAN(Z/(C+D))*RAD
  100 FORMAT(8E15.5)
  101 FORMAT(7E10.3)
      PTN=PT(N)+DZ
```

PROGRAM LISTING 1.–CONCLUDED

```
175                 Z=(C+D)*TAN(PTN/RAD)
                    IF(Z.LE.X2) GO TO 30
                    CALL THTPLT
                500 CONTINUE
                    IF(NC.LT.NCASE) GO TO 1
180                 CALL ENPLT(12.0,0.0)
                    STOP
                    END
```

PROGRAM LISTING 2.– SUBROUTINE FOR CALCULATION OF V_s AND u FOR SEMI-INFINITE BARRIER

```
 1                  SUBROUTINE EVAL(RN)
                    COMMON R,R1,RPRIM,FK,PI,PSI,R1R,R1RP
                    COMPLEX C4,C6,TERM1,TERM2,TERM3,FRSNL
                    COMPLEX CC2,RN
 5                  NAMELIST/NAM2/TERM1,TERM2,TERM3,RN,C1,C2,C5,W1,W2
                C
                C   EVALUATES THE EXPRESSION FOR RN
                C
                    C1=R*SQRT(2.0)
10                  C2=1.0
                    CC2=CMPLX(1.0,0.0)
                    C3=PI*R1
                    C4=CMPLX(0.0,C3)
                    C5=FK*(RPRIM-R)
15                  C6=CMPLX(0.0,C5)
                    TERM1=C1/(C2*CSQRT(C4))
                    W1=SQRT(FK*R1R)
                    TERM2=FRSNL(W1)/SQRT(R1+R)
                    W2=SQRT(FK*R1RP)
20                  TERM3=CEXP(C6)*FRSNL(W2)/SQRT(R1+RPRIM)
                    IF(PSI.LT.0.0) GO TO 10
                    RN=CC2-TERM1*(TERM2-TERM3)
                    GO TO 11
                 10 RN=TERM1*(TERM2+TERM3)
25               11 RETURN
                    END
```

PROGRAM LISTING 3.– SUBROUTINE FOR CALCULATION OF FRESNEL INTEGRAL

```
      COMPLEX FUNCTION FRSNL(W1)
      DATA EPS/1.E-6/
      NAMELIST /NAM3/FR,FI,C,S
      FAC=SQRT(3.14159265359/2.)
      W=W1/FAC
      IF(ABS(W).GT.1.E-12) GO TO 10
      C=0.0
      S=0.0
      GO TO 500
   10 X=W*W/.636619772368
      X2=-X*X
      IF(X.GE.13.1) GO TO 200
C
C     SERIES COMPUTATION OF C AND S
C
      FRS=X/3.
      N=5
      TERM=X*X2/6.
      FRSI=FRS+TERM/7.
  100 IF(ABS(FRS-FRSI).LE.EPS*ABS(FRS)) GO TO 101
      FRS=FRSI
      TERM=TERM*X2/(N*N-N)
      FRSI=FRS+TERM/(2*N+1)
      N=N+2
      GO TO 100
  101 S=FRSI*W
      FRC=1.
      N=4
      TERM=X2/2
      FRCI=1.+TERM/5.
  110 IF(ABS(FRC-FRCI).LE.EPS*ABS(FRC)) GO TO 111
      FRC=FRCI
      TERM=TERM*X2/(N*N-N)
      FRCI=FRC+TERM/(2*N+1)
      N=N+2
      GO TO 110
  111 C=FRCI*W
      GO TO 500
C
C     ASYMPTOTIC SERIES FOR C AND S CALCULATION
C
  200 X2=4.*X2
      TERM=3./X2
      S1=1.+TERM
      N=8
      DO 210 I=1,6
      N=N+4
      TERM=TERM*(N-7)*(N-5)/X2
      S1=S1+TERM
      IF(ABS(TERM).LE.EPS/2.) GO TO 211
  210 CONTINUE
  211 TERM=0.5/X
      S2=TERM
      N=4
      DO 220 I=1,6
      N=N+4
      TERM=TERM*(N-5)*(N-3)/X2
      S2=S2+TERM
      IF(ABS(TERM).LE.EPS/2.) GO TO 221
```

PROGRAM LISTING 3.– CONCLUDED

```
      220 CONTINUE
      221 HALF=-.5
          IF(W.LT.0.) GO TO 222
          HALF=0.5
      222 TERM=COS(X)
          TEMP=SIN(X)
          X2=3.14159265359*W
          C=HALF+(TEMP*S1-TERM*S2)/X2
          S=HALF-(TERM*S1+TEMP*S2)/X2
C
C     COMPUTE FRSNL FROM C AND S
C
      500 FR=FAC*(.5-C)
          FI=FAC*(0.5-S)
          FRSNL=CMPLX(FR,FI)
          RETURN
          END
```

PROGRAM LISTING 4.– SUBROUTINE FOR GENERATION OF PLOT TAPE

```
      SUBROUTINE THTPLT
      COMMON/PLT/PT,TOTR,A,B,C,D,ASIDE,BSIDE,F,RVE,XLVE,N,XORG
      DIMENSION PT(1000),TOTR(1000),P(1000),TOT(1000),XAX(10),YAX(7)
      DATA XAX/-30.,-20.,-10.,0.,10.,20.,30.,40.,50.,60./
      DATA YAX/0.,-5.,-10.,-15.,-20.,-25.,-30./
      N=N
  100 FORMAT(I10)
      XORG=12.
      CALL GRID(1.5,2.0,0.66,0.6042,0.,0.,10,7)
      WRITE(6,100) N
C
C     LABEL X AXIS
C
      XP=1.25
      YP=1.5575
      XD=0.0
      DO 600 I=1,10
      XI=0.
      IF(I.EQ.4) XI=0.25
      IF(I.EQ.5) XI=-0.125
      XP=XP+XD+XI
      CALL NUMPLT(XP,YP.0.,.125,XAX(I),-1)
      XD=0.66
  600 CONTINUE
  102 FORMAT(2F8.3)
C
C     LABEL Y AXIS
C
      YP=5.625
      DO 601 I=1,7
      XP=0.875
      IF(I.EQ.1) XP=XP+0.25
      IF(I.EQ.2) XP=XP+0.125
      CALL NUMPLT(XP,YP,0.,0.125,YAX(I),-1)
      YP=YP-0.6042
  601 CONTINUE
C
C     PUT IN CHARACTER LABELS
C
      CALL CHAR(3.5,1.10,0.,0.2,7HDEGREES,7)
      CALL CHAR(0.5,3.25,1.57,0.2,8HDECIBELS,8)
C
C     PUT HEADER AND DATA INFORMATION AT TOP OF PLOT
C
      CALL CHAR(1.06,9.5,0.,0.2,34HNOISE REDUCTION-HALF PLANE BARRIER,
     134)
      CALL CHAR(1.5,8.5,0.,0.2,7HASIDE = ,7)
      CALL NUMPLT(3.25,8.5,0.,0.2,ASIDE,3)
      CALL CHAR(4.5,8.5,0.,0.2,7HBSIDE = ,7)
      CALL NUMPLT(6.25,8.5,0.,0.2,BSIDE,3)
      CALL CHAR(1.06,7.9,0.,0.2,4HA = ,4)
      CALL NUMPLT(1.66,7.9,0.,0.2,A,3)
      CALL CHAR(2.86,7.9,0.,0.2,4HB = ,4)
      CALL NUMPLT(3.46,7.9,0.,0.2,B,3)
      CALL CHAR(4.76,7.9,0.,0.2,4HC = ,4)
      CALL NUMPLT(5.36,7.9,0.,.2,C,3)
      CALL CHAR(6.46,7.9,0.,.2,4HD = ,4)
      CALL NUMPLT(7.06,7.9,0.,0.2,D,3)
      CALL CHAR(1.5,7.3,0.,0.2,11HRVE(DEG) = ,11)
```

PROGRAM LISTING 4.– CONCLUDED

```
      CALL NUMPLT(3.625,7.3,0.,0.2,RVE,2)
      CALL CHAR(4.700,7.3,0.,0.2,11HLVE(DEG) = ,11)
      CALL NUMPLT(6.7,7.3,0.,0.2,XLVE,2)
      CALL CHAR(2.5,6.5,0.,0.2,12HFREQUENCY = ,12)
      CALL NUMPLT(4.9,6.5,0.,0.2,F,1)
C
C     DO ACTUAL PLOTTING
C
      CALL ORIGIN(1.5,2.0,0)
      NC=0
      DO 11 I=1,N
      IF(TOTR(I).LT.(-30.)) TOTR(I)=-32.0
      IF(TOTR(I).GT.(5.0)) TOTR(I)=5.0
      IF(PT(I).GE.(-30.).AND.PT(I).LE.60.) GO TO 10
      GO TO 11
   10 NC=NC+1
      P(NC)=PT(I)
      TOT(NC)=TOTR(I)
  101 FORMAT(I5,2F8.3)
   11 CONTINUE
      CALL SCALF(0.066,0.1208,1)
      CALL OFFST(-30.,-30.,1)
      IF(NC.LT.2) GO TO 15
C
C     PLOT 1ST POINT
C
      CALL PLOT(P(1),TOT(1), 3)
      DO 12 I=2,NC
      CALL PLOT(P(I),TOT(I),2)
   12 CONTINUE
   15 CONTINUE
C
C     RESET SCALES, OFFSETS, AND ORIGIN
C
      CALL RESET
      CALL ORIGIN(0.0,0.0,0)
      CALL PLOT(XORG,0.,-3)
      RETURN
      END
```

PROGRAM LISTING 5.– SHIELDING OF PINK NOISE BY RECTANGULAR PLATE

```
      PROGRAM NOISEY(INPUT,OUTPUT,TAPE5=INPUT,TAPE6=OUTPUT,TAPE1)
      COMMON/PLT/PT,TOTR,A,B,C,D,ASD,BSD,F,RVE,XLVE,N,XORG
      COMMON R,R1,RPRIM,FK,PI,PSI
      DIMENSION PT(1000),TOTR(1000)
      DIMENSION FI(10)
      COMPLEX RN1,RN2,RN3,RN4
      COMPLEX C2,VI1,VI2,VI3,VI4
      DIMENSION RR1(8)
      DATA FI/1000.,1950.,2000.,2050.,3000.,4000.,8000.,12000.,16000.,
     120000./
      RCAP(X,Y,P,Z)=SQRT(X*X+Y*Y-2.0*X*Y*COS(P)+Z*Z)
      NC=0
      NJ=99
      CO=347.412
      AZ=ALOG10(2.0)
      IY=2
      DZ=0.5
      PI=3.14159265359
      RAD=57.29577951
      XORG=0.0
      WRITE(6,103)
  103 FORMAT(1HO,37X,36HNOISE REDUCTION - HALF PLANE BARRIER/)
      READ(5,105) NCASE
  105 FORMAT(I5)
    1 CONTINUE
      NC=NC+1
      READ(5,101)A,B,C,D,ASIDE,BSIDE,DELTAZ
      ASD=ASIDE*2.0
      BSD=BSIDE*2.0
      AAC=(ASIDE-A)/C
      ABC=(ASIDE+A)/C
      CD=C+D
      RVE=ATAN(AAC)*RAD
      XLVE=ATAN(ABC)*RAD
      XLVE=-XLVE
      ZRVE=AAC*CD
      ZLVE=-ABC*CD
      ZTEMP=ZRVE
          X1=XLVE
      X2=(C+D)*TAN(60.0/RAD)
  110 FORMAT(1HO,6F8.3)
      NTRY=NJ
      XNTRY=NTRY
      NT1=NTRY+1
      DO 500 I=1,10
      F=FI(I)
      FL=0.889*F
      FU=1.120*F
      N=0
      Z=X1
      WRITE(6,104)A,B,C,D,ASIDE,BSIDE,F,CO
  104 FORMAT(1HO,4HA = ,F6.3,2X,4HB = ,F6.3,2X,4HC = ,F6.3,2X,3HD = ,F6.3
     1,2X,8HASIDE = ,F6.3,2X,8HBSIDE = ,F6.3,2X,4HF = ,E12.5,2X,5HCO = ,
     2E12.5/)
   30 CONTINUE
      N=N+1
      TOTG=0.0
      TOTV=0.0
      DO 501 J=1,NT1
```

```
      JM=J-1
      XJM=J-1
      F=FL+(XJM/XNTRY)*(FU-FL)
      FZ=ALOG10(FL)
      F1=ALOG10(F)
      AMPLG=AZ+0.5*(FZ-F1)
      AMP=10.0**AMPLG
      FK=2.0*PI*F/CO
C
C     DO CASE 1
C
      CODE=1
      BB=BSIDE-B
      BBZ=BB-DELTAZ
      PHIO=ATAN(C/BB)
      THET=ATAN(D/ABS(BBZ))
      PHI=2.0*PI-THET
      IF(BBZ.LT.0.0) PHI=PI+THET
      ROL=C/SIN(PHIO)
      RL=D/SIN(THET)
      PHIL=PHI-PHIO
      PSI=PI-PHIL
      R=RCAP(RL,ROL,PHIL,Z)
      PHIL=PHI+PHIO
      RPRIM=RCAP(RL,ROL,PHIL,Z)
      R1=RCAP(RL,ROL,PI,Z)
      CALL EVAL(RN1)
      C1=EK*R
      C2=CMPLX(0.0,C1)
      VI1=CEXP(C2)/C1
      RN1=VI1*RN1
      RTEM=CABS(RN1)
      RNA=20.0*ALOG10(RTEM)
C
C     DO CASE 2
C
      CODE=2
      BB=BSIDE+B
      BBZ=BB+DELTAZ
      PHIO=ATAN(C/BB)
      THET=ATAN(D/ABS(BBZ))
      ROL=C/SIN(PHIO)
      RL=D/SIN(THET)
      PHI=2.0*PI-THET
      IF(BBZ.LT.0.0) PHI=PI+THET
      PHIL=PHI-PHIO
      PSI=PI-PHIL
      R=RCAP(RL,ROL,PHIL,Z)
      PHIL=PHI+PHIO
      RPRIM=RCAP(RL,ROL,PHIL,Z)
      R1=RCAP(RL,ROL,PI,Z)
      CALL EVAL(RN2)
      C1=FK*R
      C2=CMPLX(0.0,C1)
      VI2=CEXP(C2)/C1
      RN2=VI2*RN2
      RTEM=CABS(RN2)
      RNB=20.0*ALOG10(RTEM)
C
C     DO CASE 3
```

PROGRAM LISTING 5.– CONTINUED

```
120         C
                CODE=3
                AA=ASIDE-A
                IF(AA.LT.1.E-12) GO TO 40
                PHIO=ATAN(C/AA)
125             GO TO 41
             40 PHIO=PI/2.0
             41 CONTINUE
                ALPHA=ATAN((Z-AA)/D)
                PHI=3.0*PI/2.0-ALPHA
130             RL=D/COS(ALPHA)
                ROL=C/SIN(PHIO)
                PHIL=PHI-PHIO
                PSI=PI-PHIL
                PSI3=PSI
135             R=RCAP(RL,ROL,PHIL,DELTAZ)
                PHIL=PHI+PHIO
                RPRIM=RCAP(RL,ROL,PHIL,DELTAZ)
                R1=RCAP(RL,ROL,PI,DELTAZ)
                CALL EVAL(RN3)
140             C1=EK*R
                C2=CMPLX(0.0,C1)
                VI3=CEXP(C2)/C1
                RN3=VI3*RN3
                RTEM=CABS(RN3)
145             RNC=20.0*ALOG10(RTEM)
            C
            C     DO CASE 4
            C
                CODE=4
150             AA=ASIDE+A
                IF(AA.LT.1.E-12) GO TO 50
                PHIO=ATAN(C/AA)
                GO TO 51
             50 PHIO=PI/2.0
155          51 CONTINUE
                ALPHA=ATAN(Z+AA)/D)
                PHI=3.0*PI/2.0+ALPHA
                RL=D/COS(ALPHA)
                ROL=C/SIN(PHIO)
160             PHIL=PHI-PHIO
                PSI=PI-PHIL
                R=RCAP(RL,ROL,PHIL,DELTAZ)
                PHIL=PHI+PHIO
                RPRIM=RCAP(RL,ROL,PHIL,DELTAZ)
165             R1=RCAP(RL,ROL,PI,DELTAZ)
                CALL EVAL(RN4)
                C1=FK*R
                C2=CMPLX(0.0,C1)
                VI4=CEXP(C2)/C1
170             RN4=VI4*RN4
                RTEM=CABS(RN4)
                RND=20.0*ALOG10(RTEM)
                IE(NC.EQ.2) RN1=0.0
                TOTG=TOTG+CABS((RN1+RN2+RN3+RN4)*AMP*FK)
175             TOTV=TOTV+CABS(VI1*AMP*FK)
             501 CONTINUE
            C
            C     CALCULATE TOTAL NOISE REDUCTION
                TOTRN=TOTG/TOTV
```

PROGRAM LISTING 5.– CONCLUDED

```
180          TOTRN=20.0*ALOG10(TOTRN)
             TOTR(N)=TOTRN
             PT(N)=ATAN(Z/(C+D))*RAD
         100 FORMAT(8E15.5)
         101 FORMAT(7E10.3)
185          PTN=PT(N)+DZ
             Z=(C+D)*TAN(PTN/RAD)
             IF(Z.LE.X2) GO TO 30
             CALL THTPLT
         500 CONTINUE
190          IF(NC.LT.NCASE) GO TO 1
             CALL ENPLT(12.0,0.0)
             STOP
             END
```

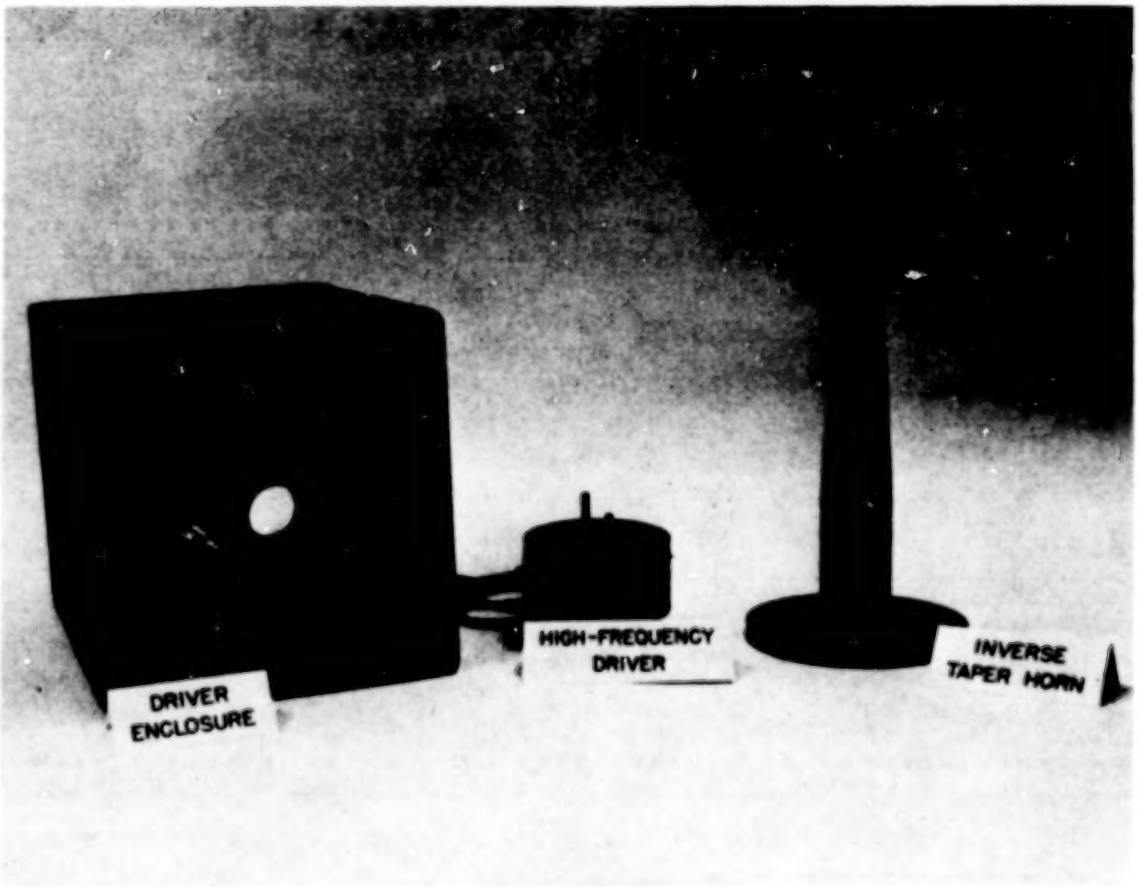

Figure 1.– Components of sound source.

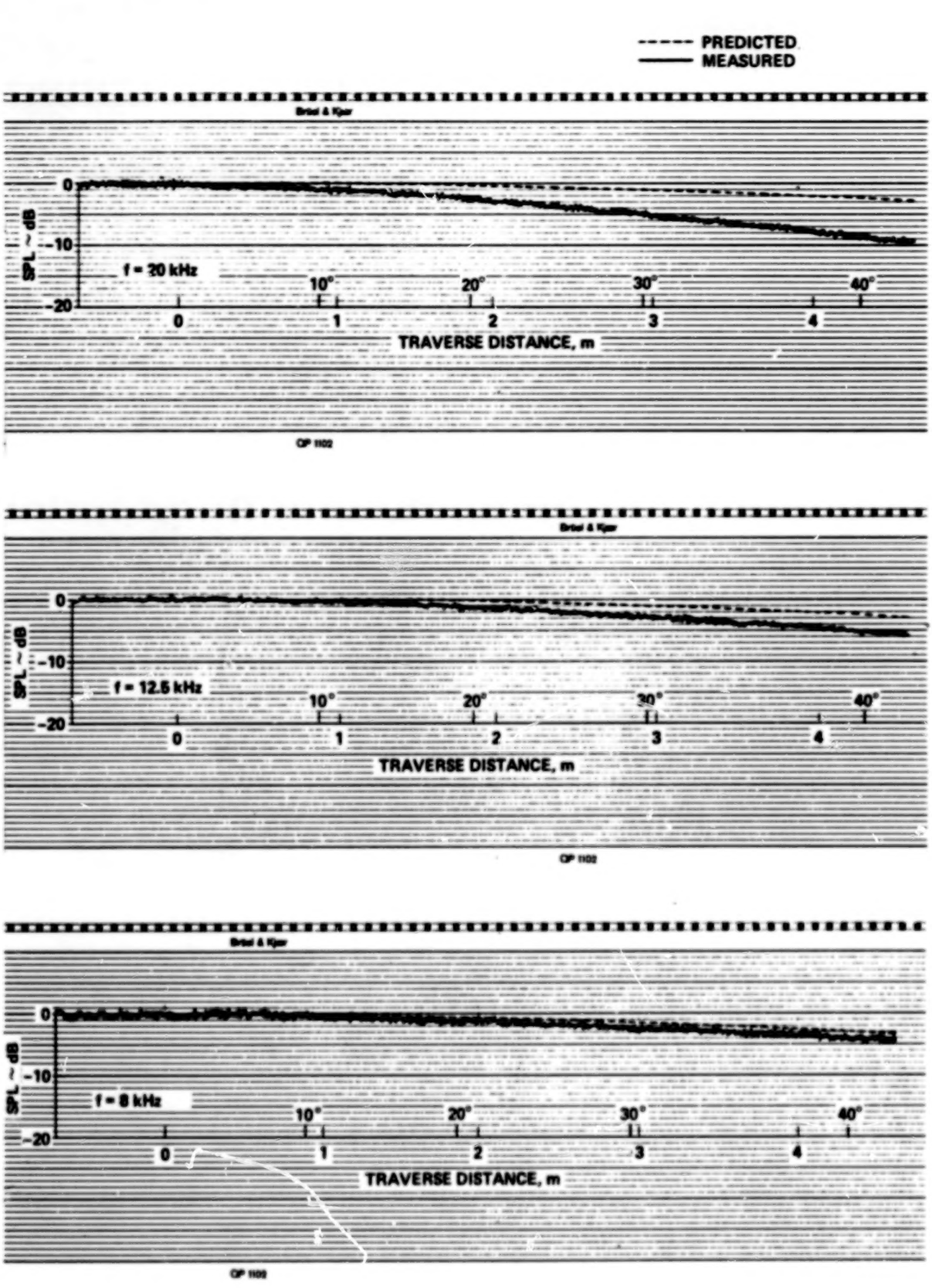

Figure 2.– Directionality of unshielded SPL at high frequencies for pink noise source.

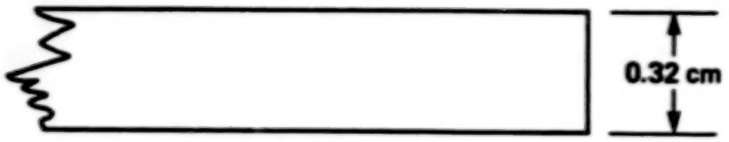

(a) SQUARE EDGE

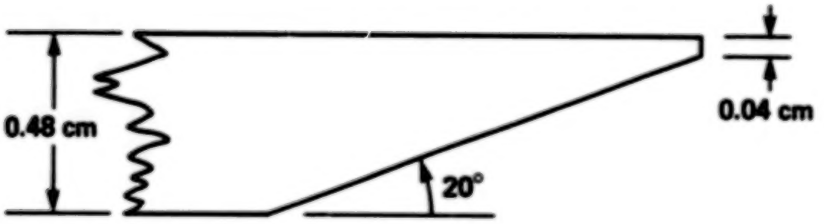

(b) SHARP EDGE

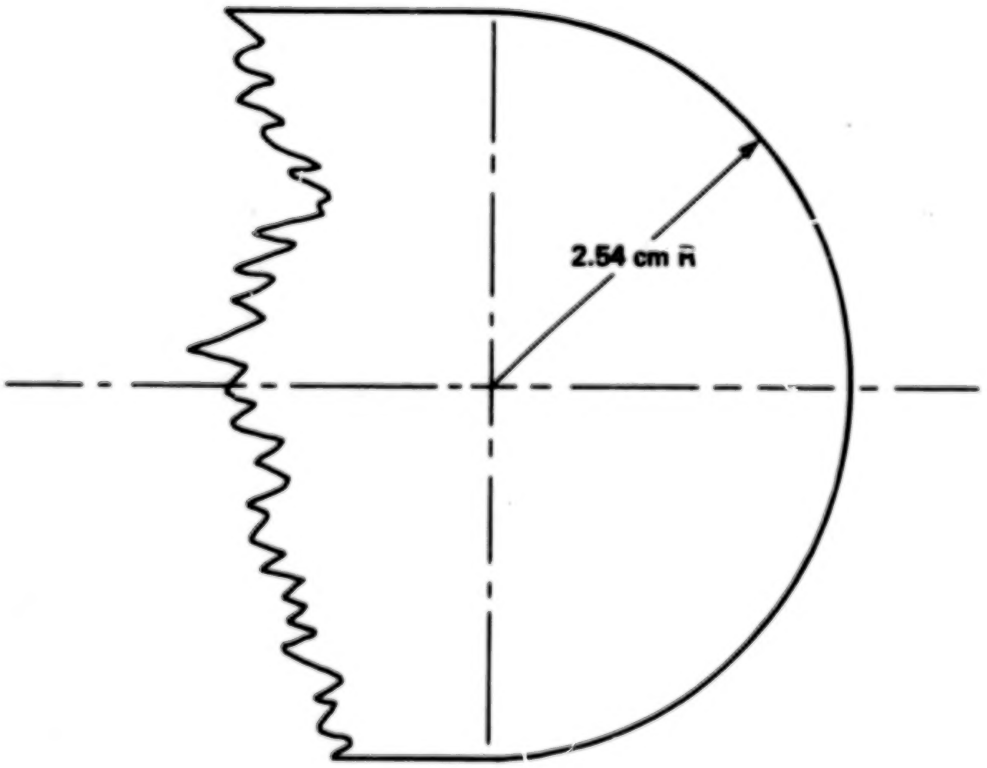

(c) ROUND EDGE

Figure 3.– Edge configurations for rectangular shields.

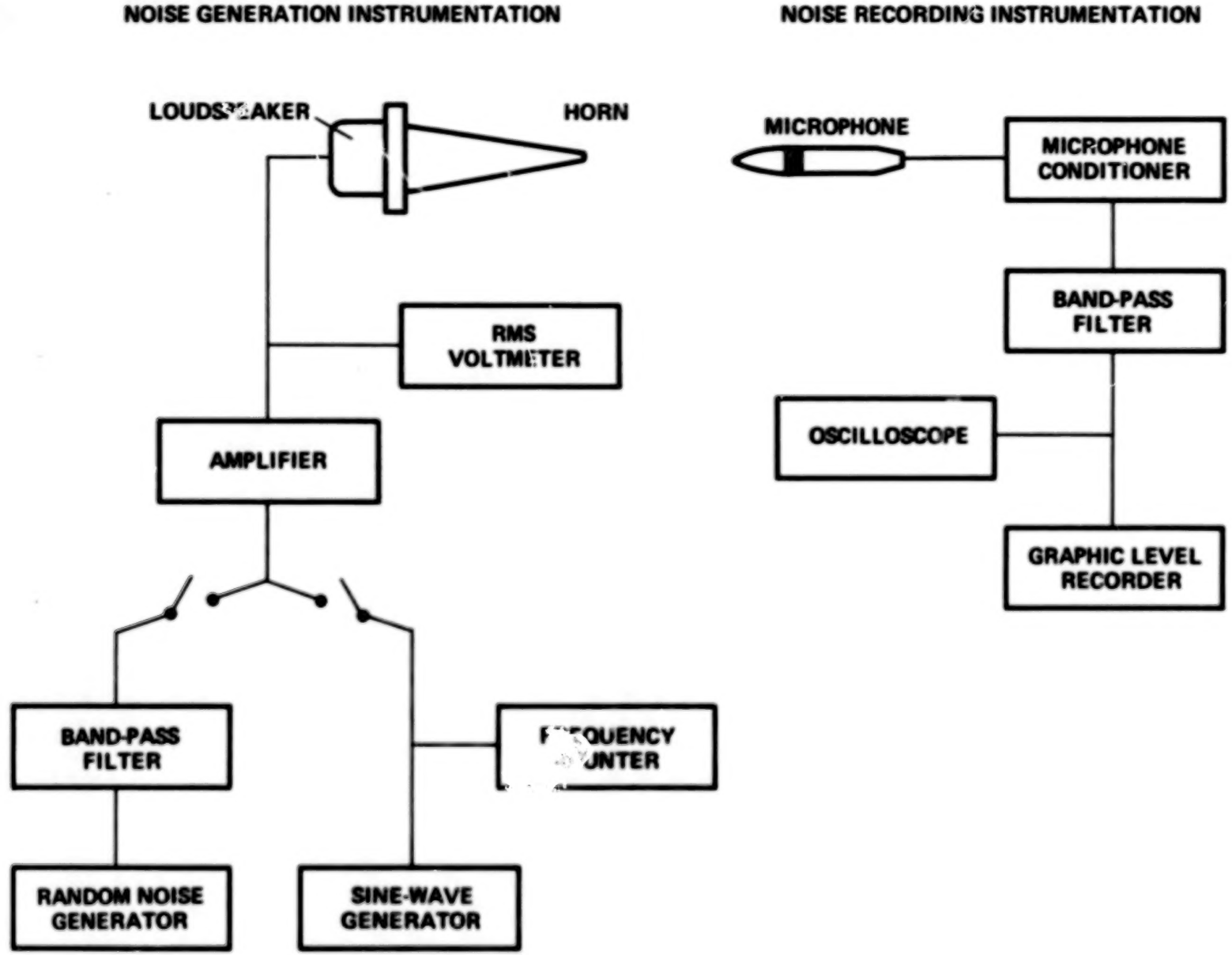

Figure 4.– Instrumentation for shielding experiment.

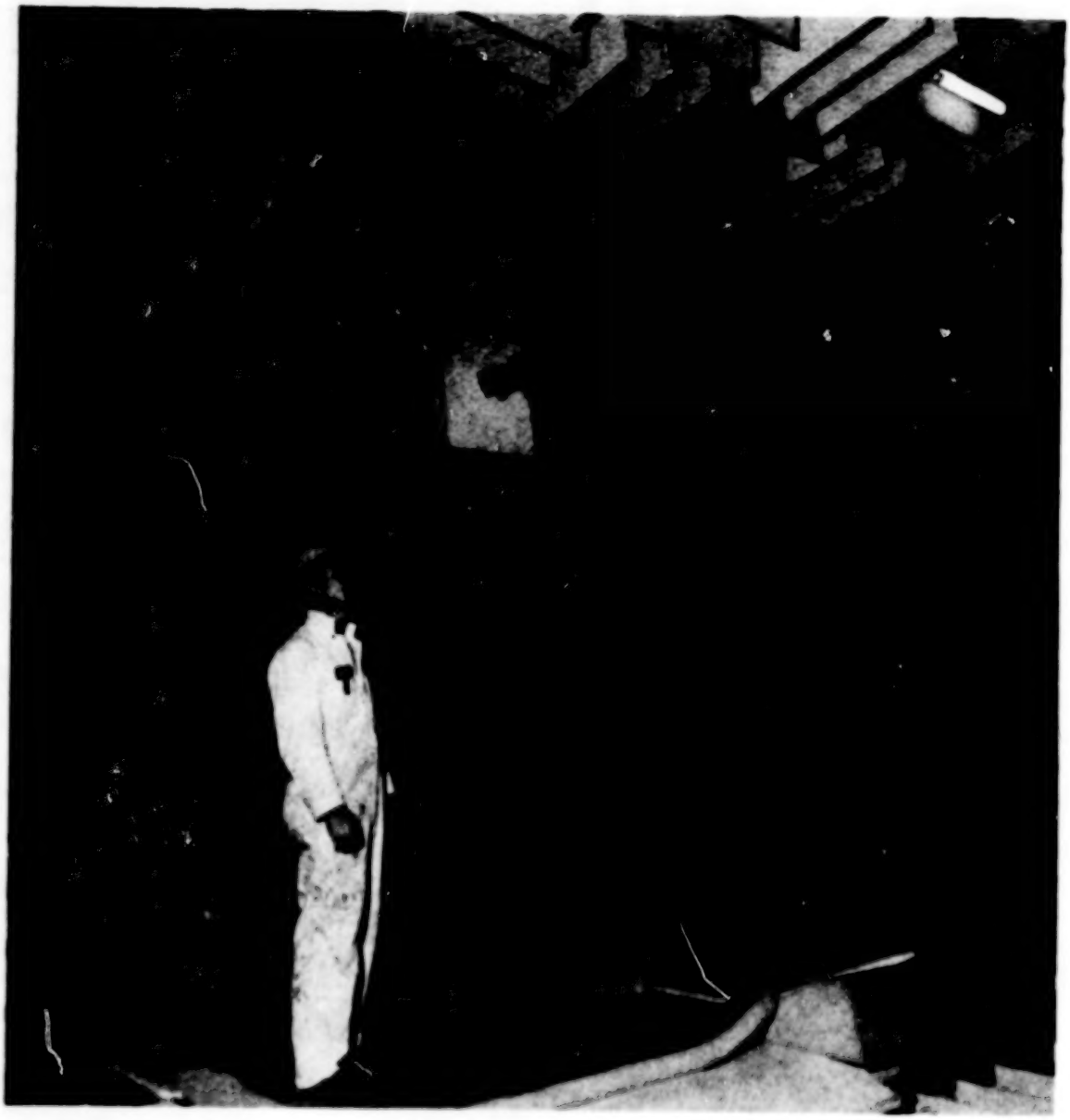

(a) Cylindrical shield.

Figure 5.– Source, shield, and microphone installations in anechoic chamber.

(b) Traversing microphone.

Figure 5.– Concluded.

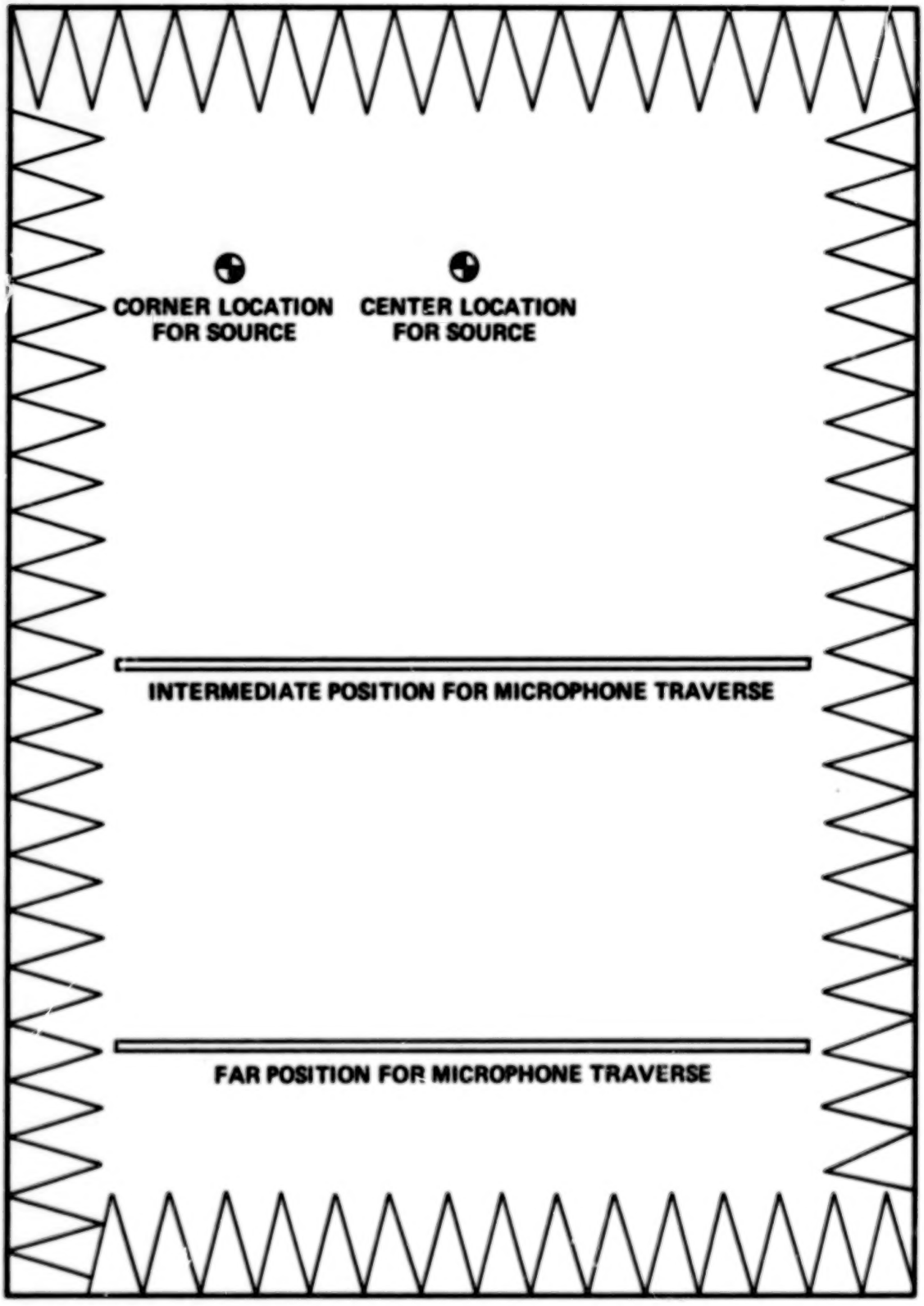

Figure 6.– Source-microphone-traverse combinations.

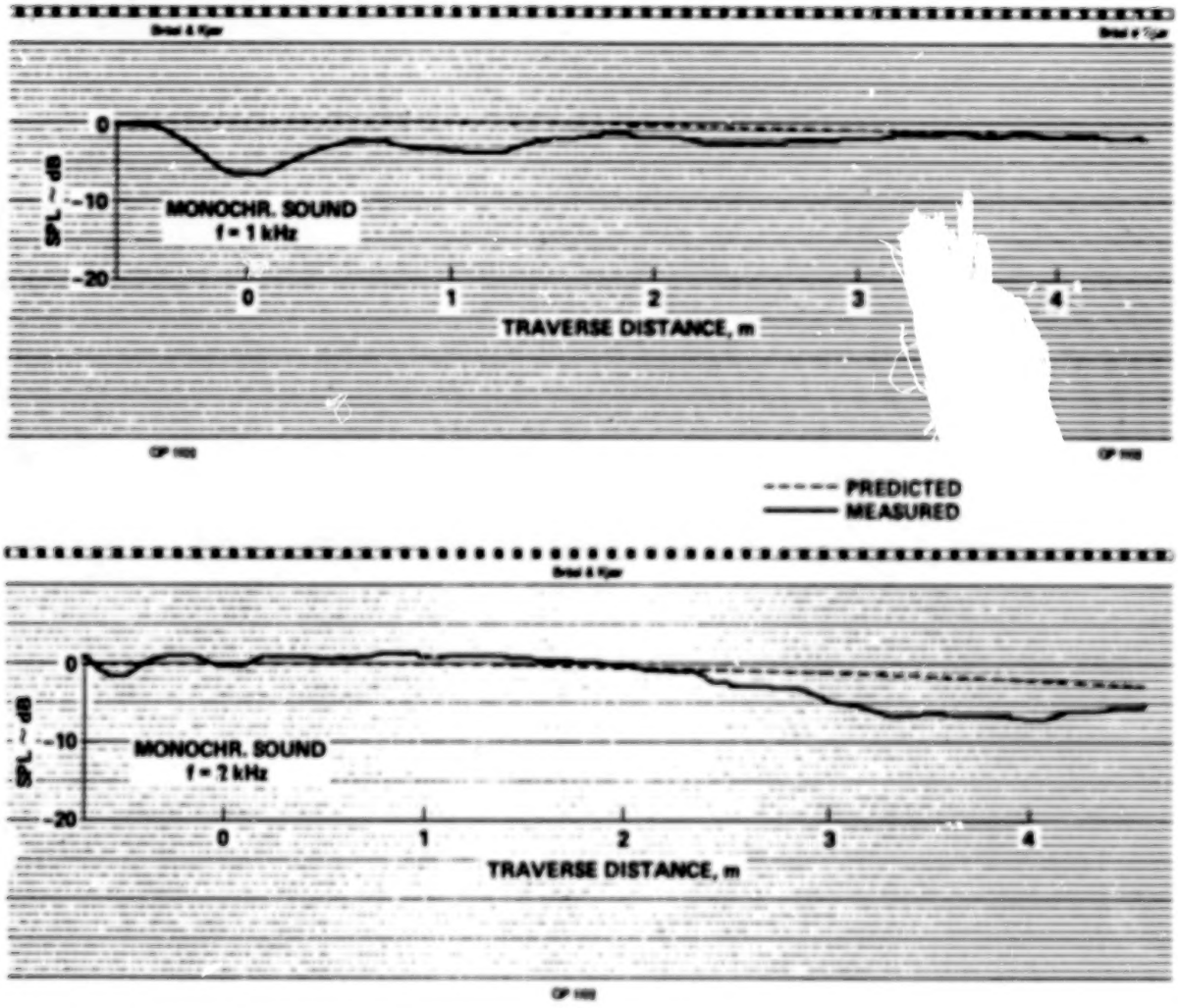

Figure 7.– Variation of unshielded SPL with traverse distance at low frequencies for Configuration A.

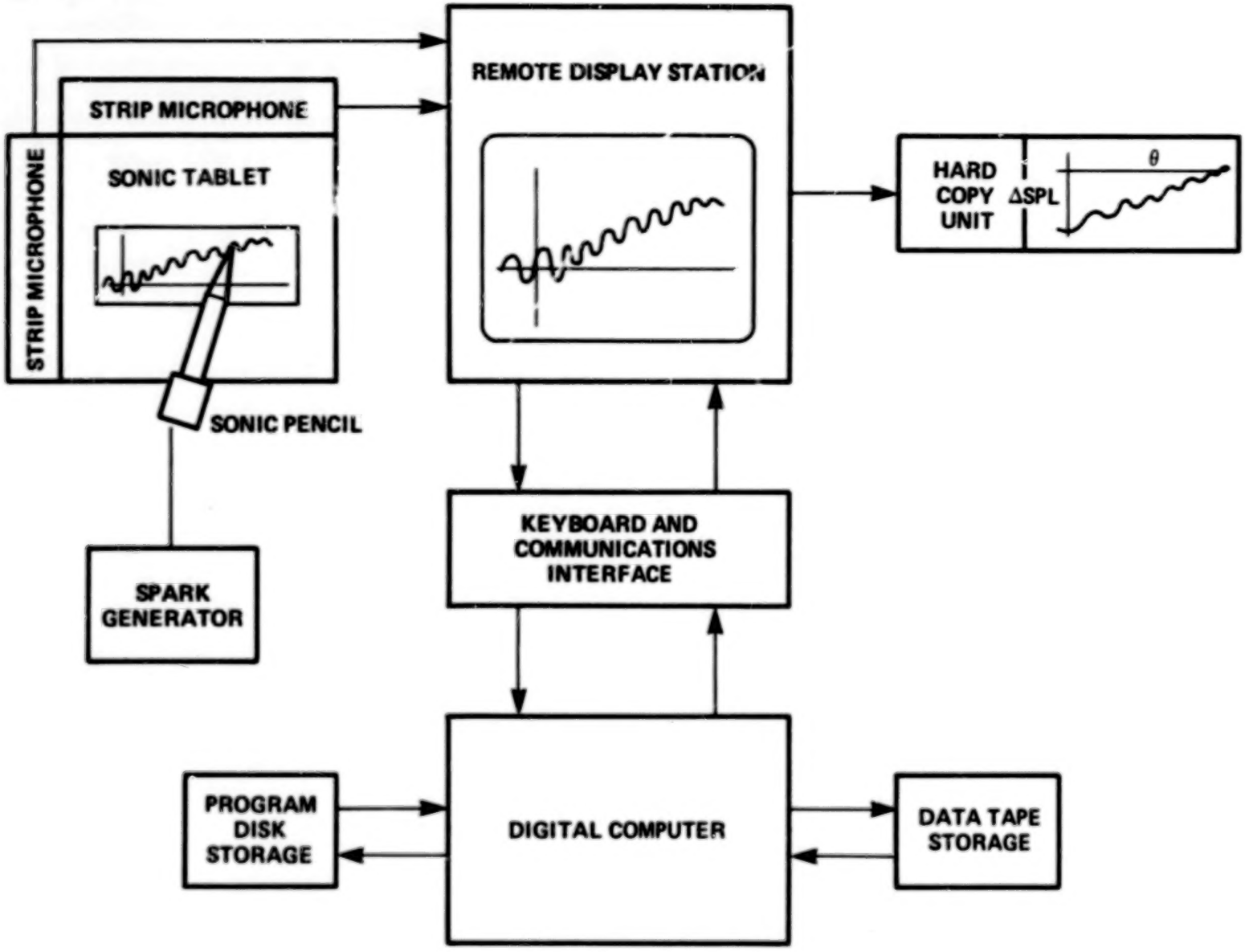

Figure 8.– Schematic diagram for data reduction system.

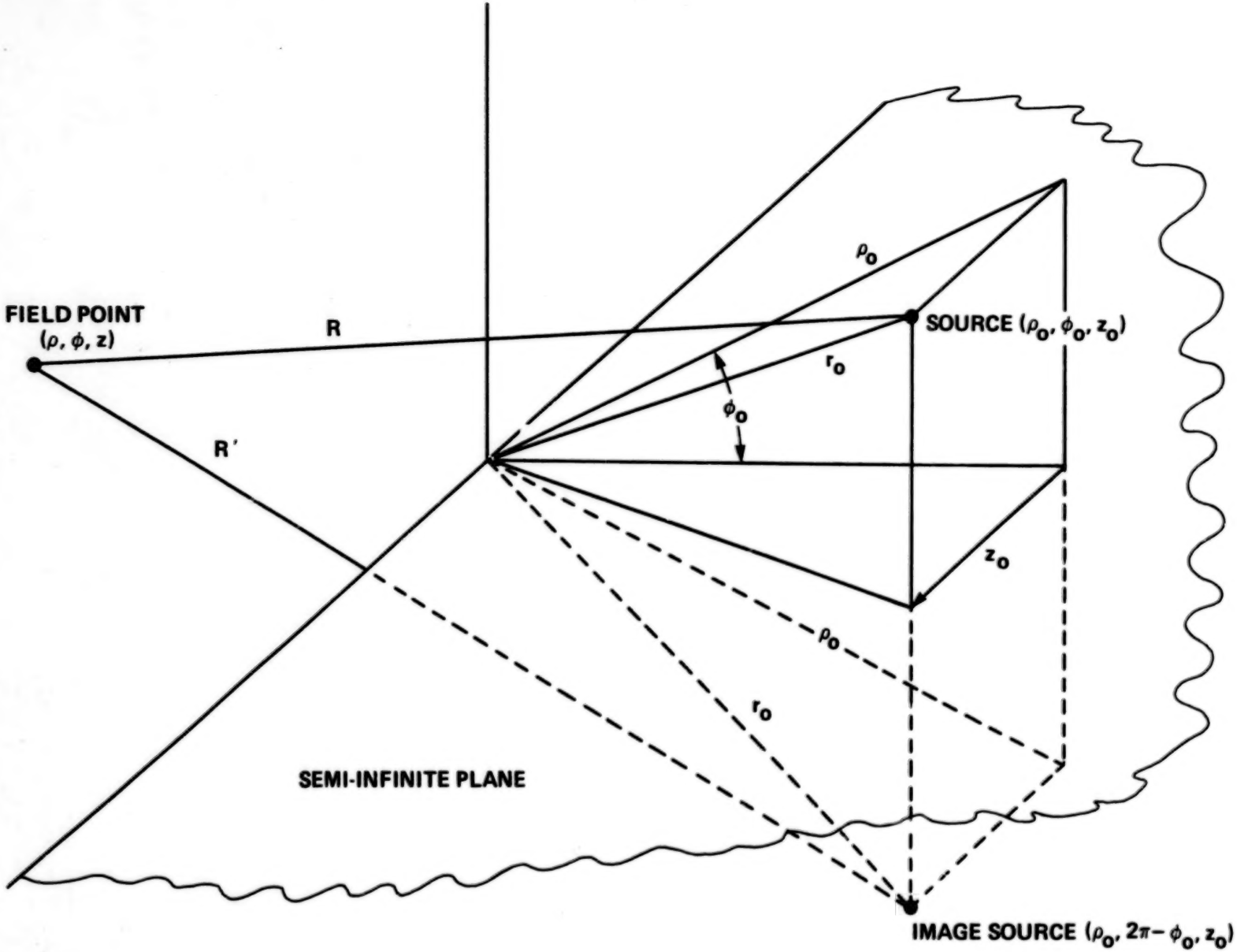

Figure 9.– Geometry for semi-infinite barrier shielding of a point source.

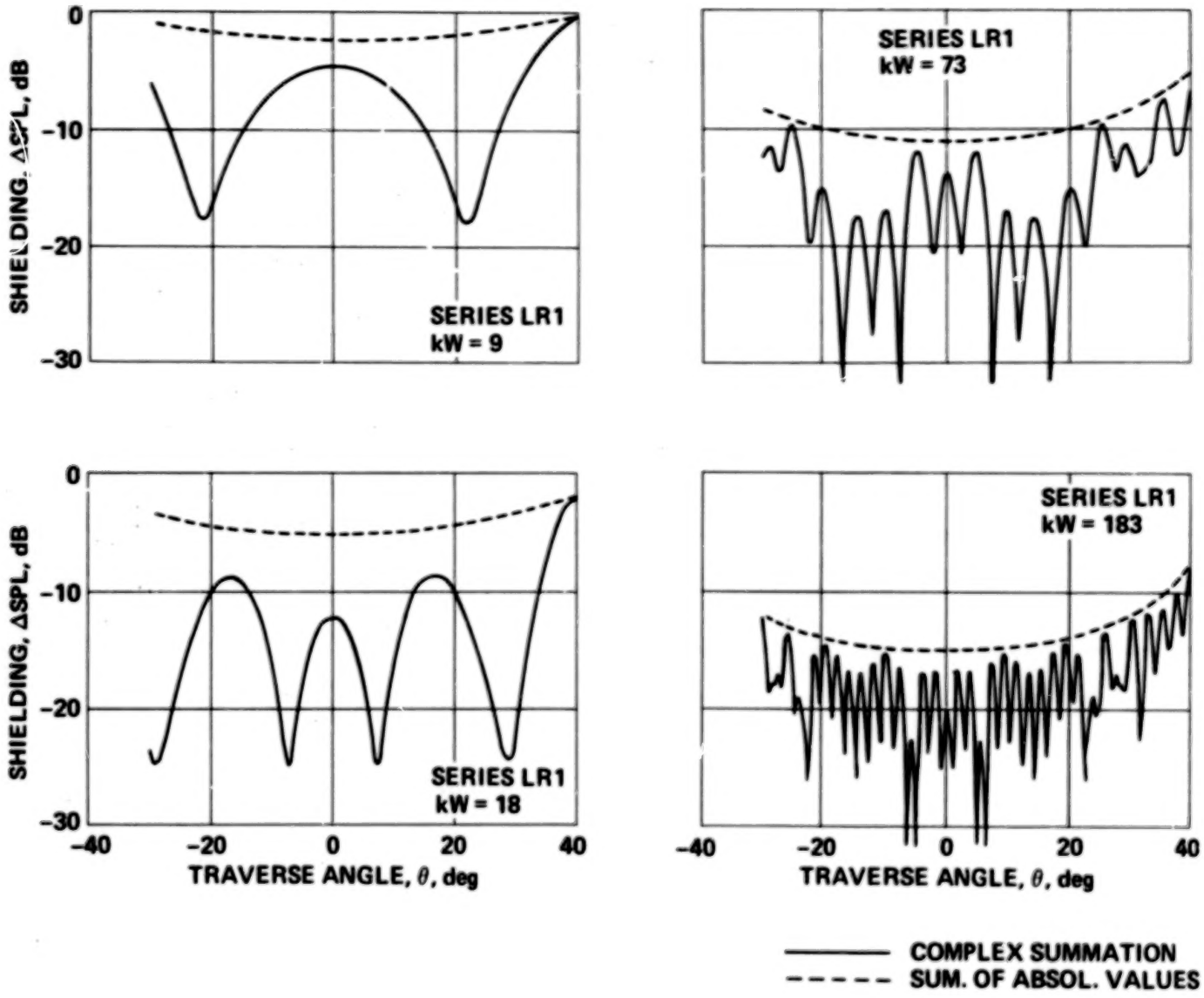

Figure 10.– Effect of superposition mode on predicted shielding of rectangular plate.

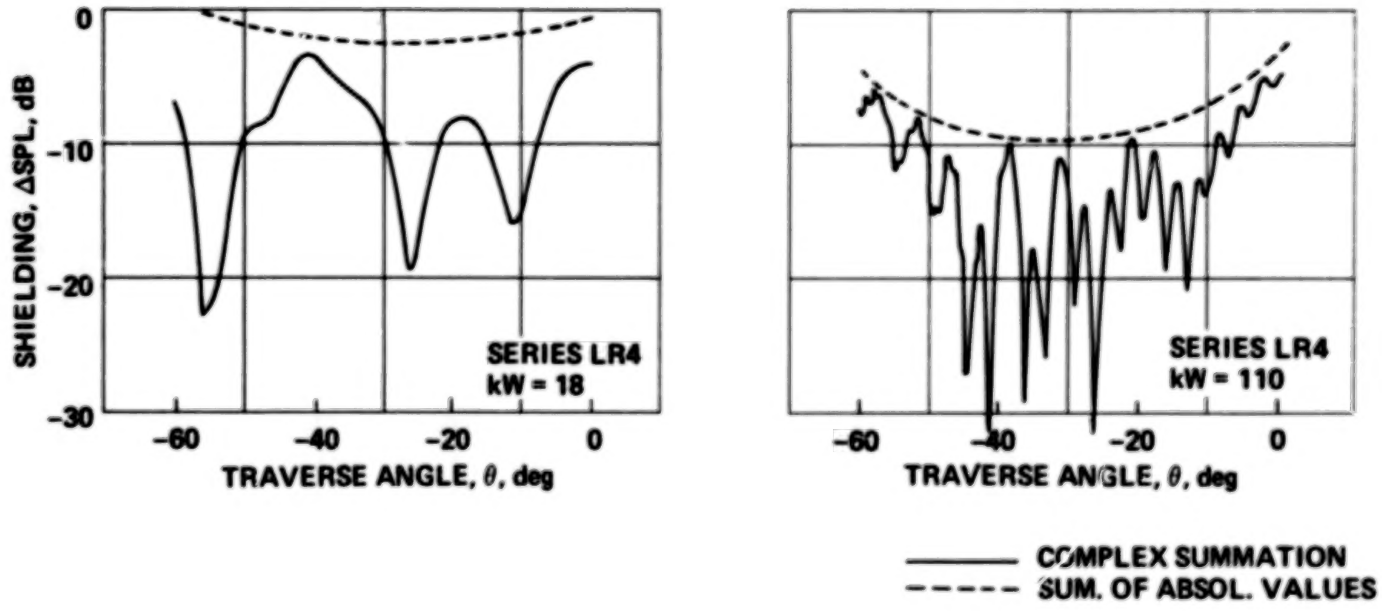

Figure 10.– Concluded.

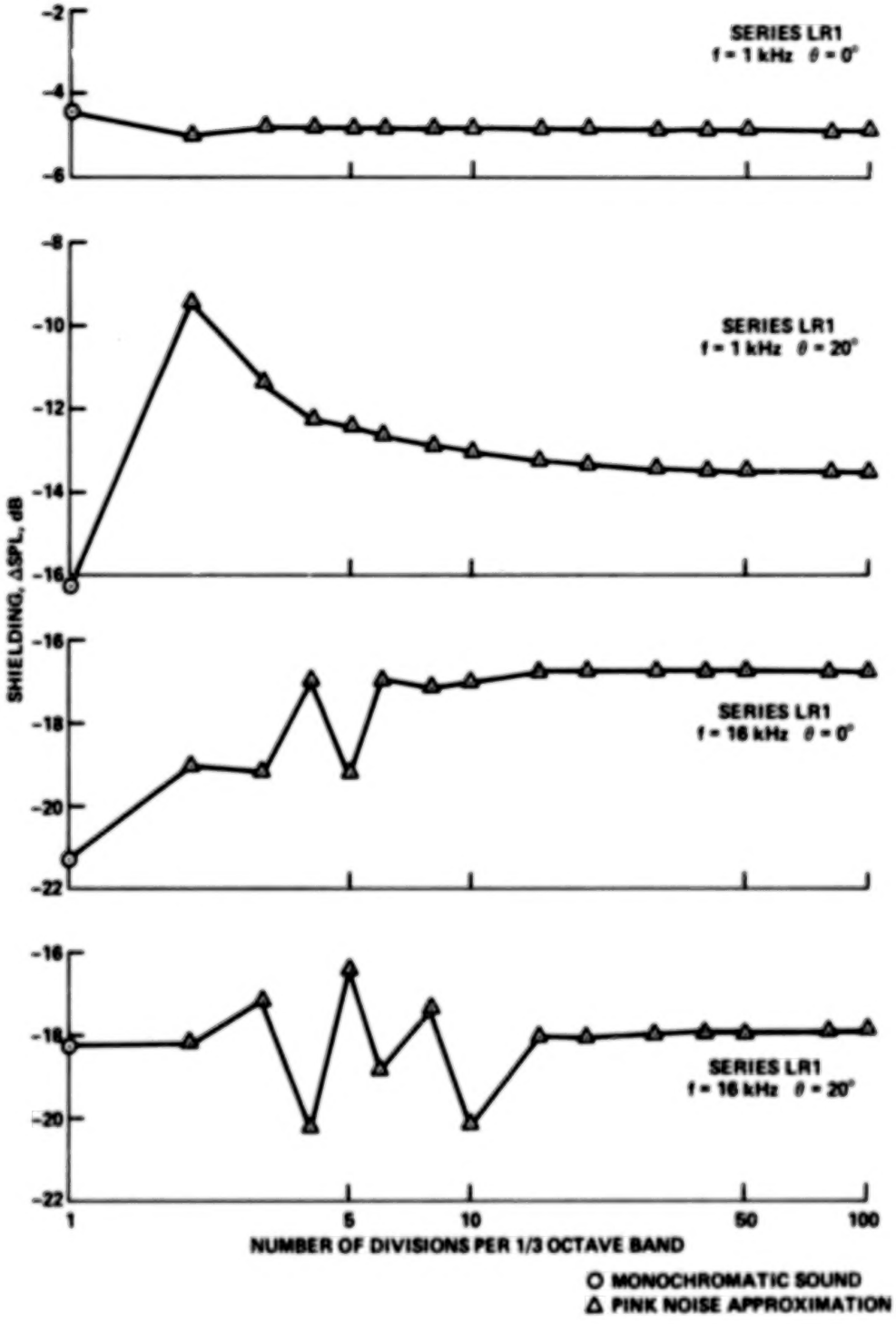

Figure 11.– Effect of frequency band division on predicted broadband shielding of rectangular plate.

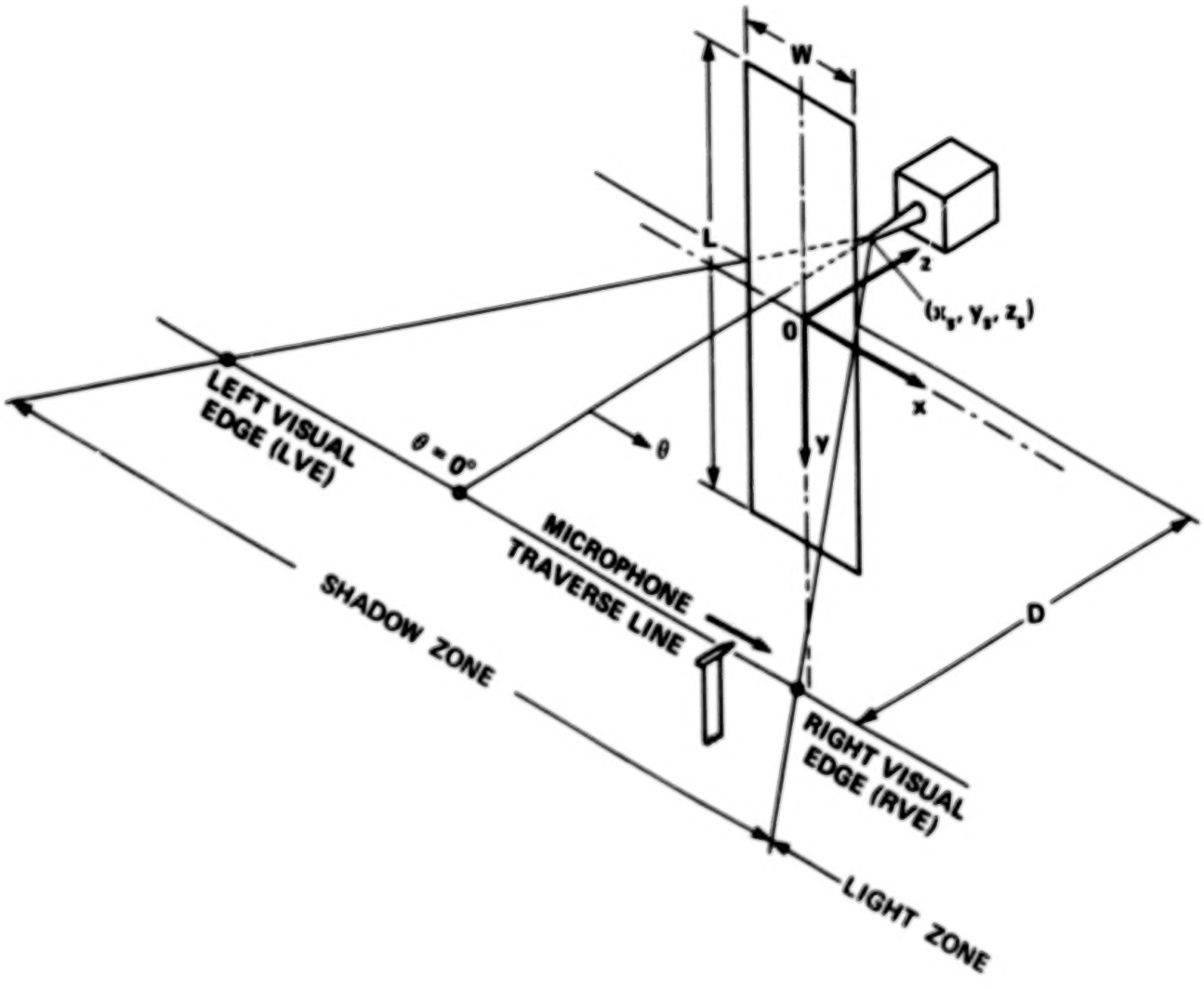

Figure 12.– Coordinate system for rectangular plate shielding.

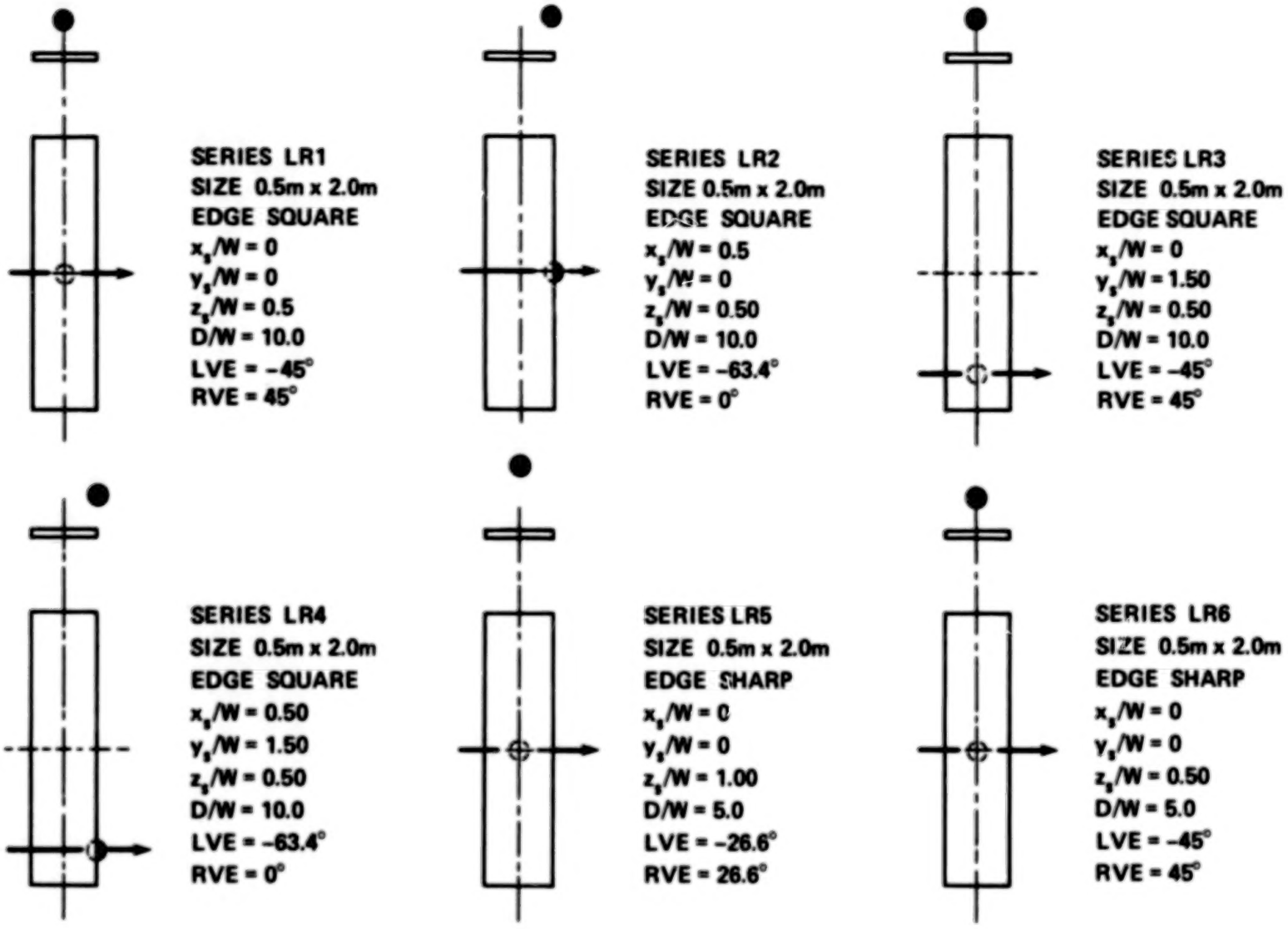

Figure 13.– Source, shield, and microphone – traverse configurations.

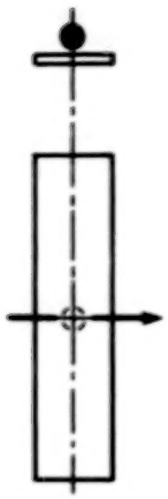

SERIES LR7
SIZE 0.5m x 2.0m
EDGE SHARP
$x_s/W = 0$
$y_s/W = 0$
$z_s/W = 0.25$
D/W = 5.0
LVE = -63.4°
RVE = 63.4°

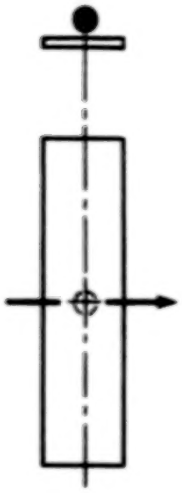

SERIES LR8
SIZE 0.5m x 2.0m
EDGE SHARP
$x_s/W = 0$
$y_s/W = 0$
$z_s/W = 0.25$
D/W = 10.0°
LVE = -63.4°
RVE = 63.4°

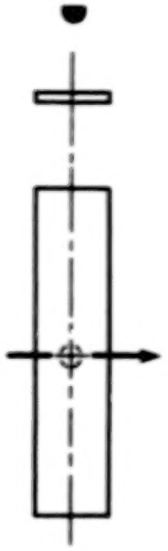

SERIES LR9
SIZE 0.5m x 2.0m
EDGE SHARP
$x_s/W = 0$
$y_s/W = 0$
$z_s/W = 1.00$
D/W = 10.0
LVE = -26.6°
RVE = 26.6°

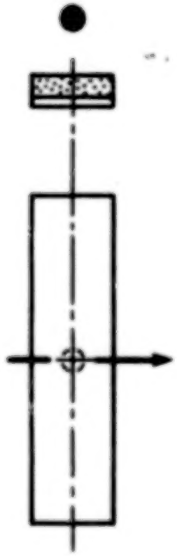

SERIES LR10
SIZE 0.5m x 2.0m
EDGE SQUARE
$x_s/W = 0$
$y_s/W = 0$
$z_s/W = 0.50$
D/W = 10.0
LVE = -45°
RVE = 45°

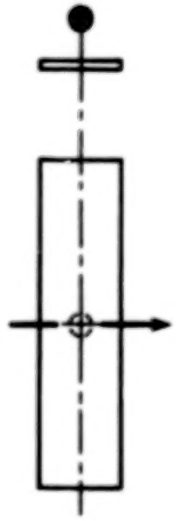

SERIES LR11
SIZE 0.5m x 2.0m
EDGE SHARP
$x_s/W = 0$
$y_s/W = 0$
$z_s/W = 0.50$
D/W = 10.0
LVE = -45°
RVE = 45°

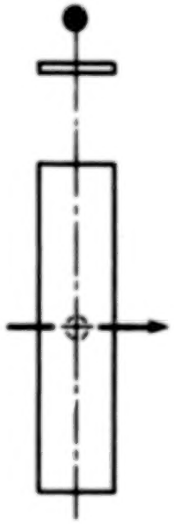

SERIES LR12
SIZE 0.5m x 2.0m
EDGE ROUNDED
$x_s/W = 0$
$y_s/W = 0$
$z_s/W = 0.50$
D/W = 10.0
LVE = -45°
RVE = 45°

Figure 13.– Continued.

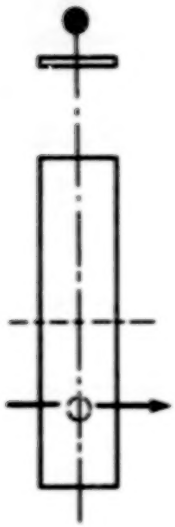

SERIES LR13
SIZE 0.5m x 2.0m
EDGE SQUARE
$x_s/W = 0$
$y_s/W = 1.00$
$z_s/W = 0.50$
D/W = 10.0
LVE = –45°
RVE = 45°

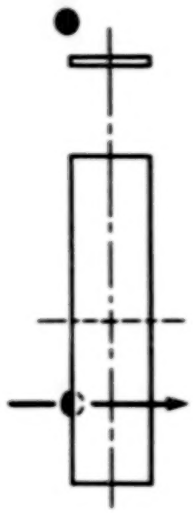

SERIES LR14
SIZE 0.5m x 2.0m
EDGE SQUARE
$x_s/W = -0.50$
$y_s/W = 1.00$
$z_s/W = 0.50$
D/W = 10.0
LVE = 0°
RVE = 63.4°

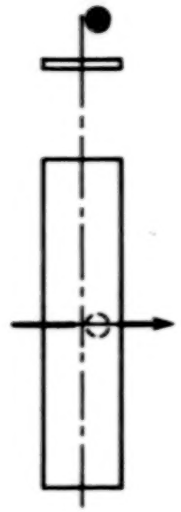

SERIES LR15
SIZE 0.5m x 2.0m
EDGE SHARP
$x_s/W = 0.25$
$y_s/W = 0$
$z_s/W = 0.50$
D/W = 10.0
LVE = –56.3°
RVE = 26.6°

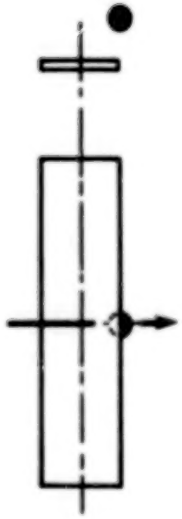

SERIES LR16
SIZE 0.5m x 2.0m
EDGE SHARP
$x_s/W = 0.50$
$y_s/W = 0$
$z_s/W = 0.50$
D/W = 5.0
LVE = –63.4°
RVE = 0°

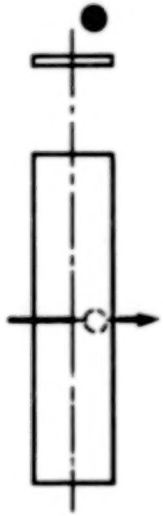

SERIES LR17
SIZE 0.5m x 2.0m
EDGE SHARP
$x_s/W = 0.25$
$y_s/W = 0$
$z_s/W = 0.50$
D/W = 5.0
LVE = –56.3°
RVE = 26.6°

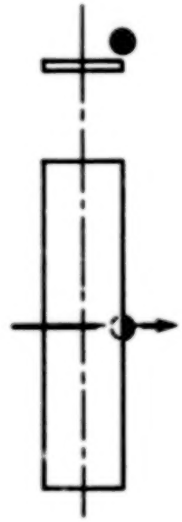

SERIES LR18
SIZE 0.5m x 2.0m
EDGE SHARP
$x_s/W = 0.50$
$y_s/W = 0$
$z_s/W = 0.25$
D/W = 5.0
LVE = –76°
RVE = 0°

Figure 13.– Continued.

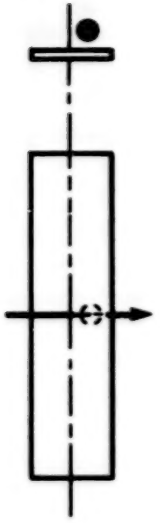

SERIES LR19
SIZE 0.5m x 2.0m
EDGE SHARP
$x_s/W = 0.25$
$y_s/W = 0$
$z_s/W = 0.25$
D/W = 5.0
LVE = –71.6°
RVE = 45°

SERIES SR1
SIZE 0.25m x 1.0m
EDGE SQUARE
$x_s/W = 0$
$y_s/W = 0$
$z_s/W = 1.00$
D/W = 20.0
LVE = –26.6°
RVE = 26.6°

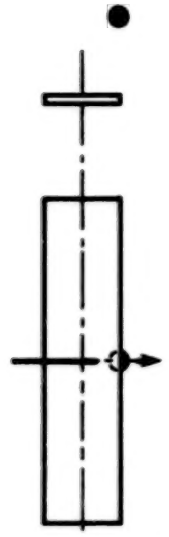

SERIES SR2
SIZE 0.25m x 1.0m
EDGE SQUARE
$x_s/W = 0.50$
$y_s/W = 0$
$z_s/W = 1.00$
D/W = 20.0
LVE = –45°
RVE = 0°

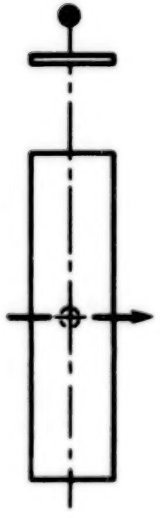

SERIES SR3
SIZE 0.25m x 1.0m
EDGE SQUARE
$x_s/W = 0$
$y_s/W = 0$
$z_s/W = 0.50$
D/W = 20.0
LVE = –45°
RVE = 45°

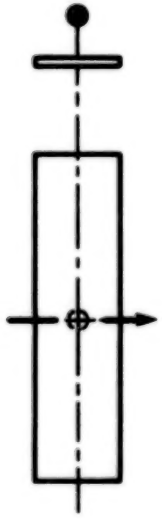

SERIES SR4
SIZE 0.25m x 1.0m
EDGE SQUARE
$x_s/W = 0$
$y_s/W = 0$
$z_s/W = 0.50$
D/W = 10.0
LVE = –45°
RVE = 45°

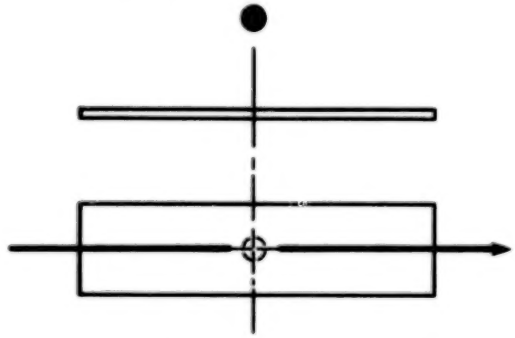

SERIES SRH
SIZE 1.0m x 0.25m
EDGE SQUARE
$x_s/W = 0$
$y_s/W = 0$
$z_s/W = 1.00$
D/W = 20.0
LVE = –63.4°
RVE = 63.4°

Figure 13.– Continued.

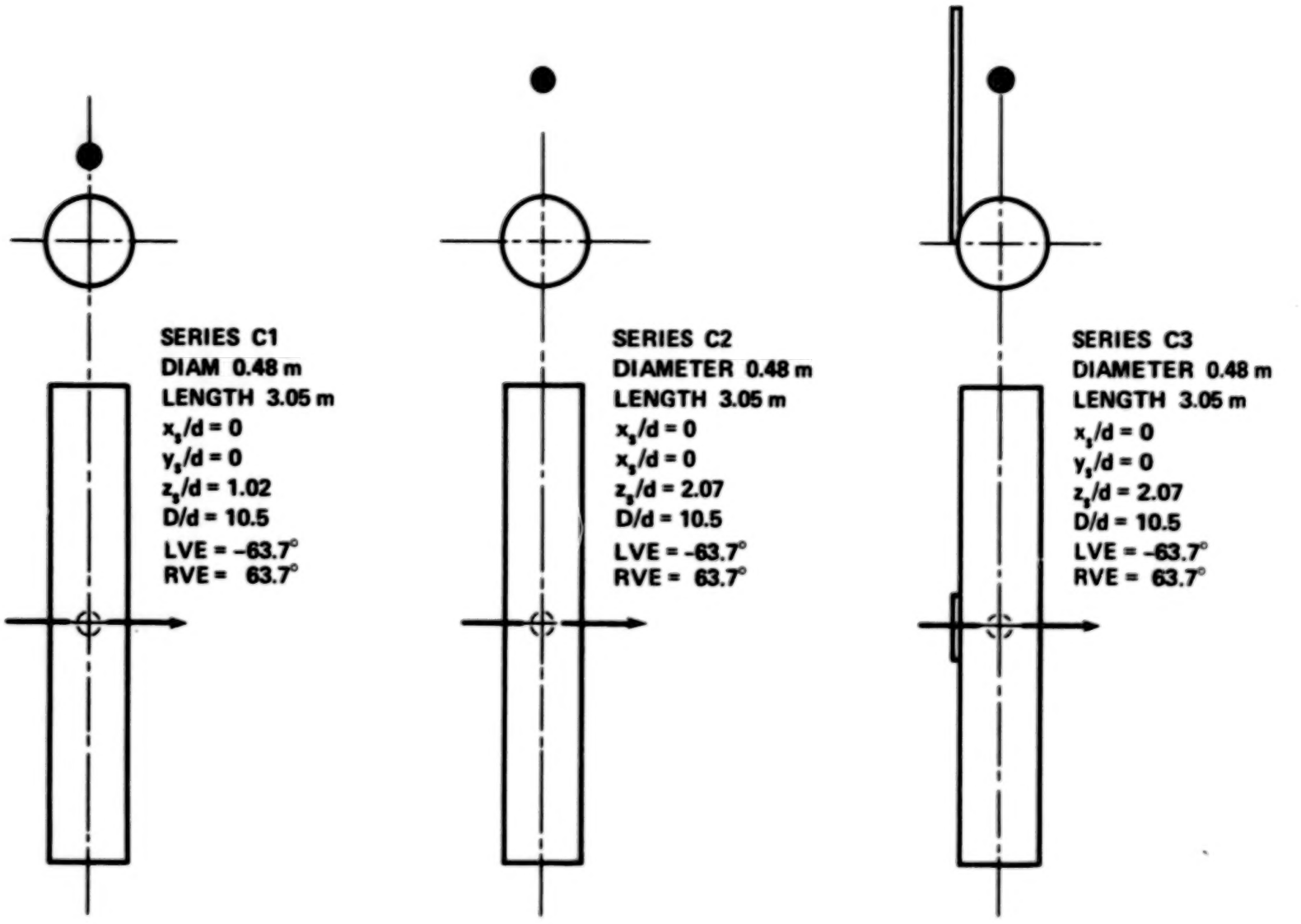

Figure 13.– Continued.

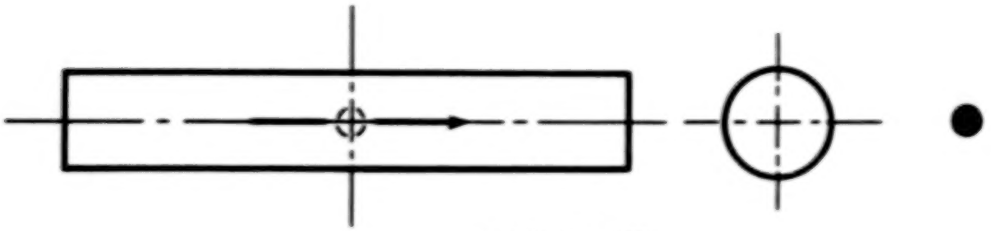

SERIES CH1

DIAMETER 0.48 m	$z_s/d = 2.07$
LENGTH 3.05 m	D/d = 10.5
$x_s/d = 0$	LVE = −14°
$y_s/d = 0$	RVE = 14°

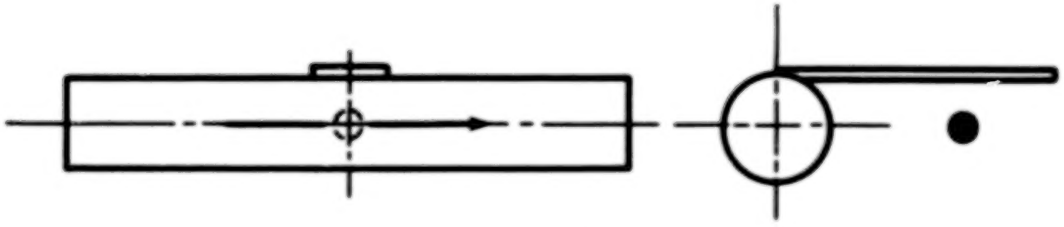

SERIES CH2

DIAMETER 0.48 m	$z_s/d = 2.07$
LENGTH 3.05 m	D/d = 10.5
$x_s/d = 0$	LVE = −14°
$y_s/d = 0$	RVE = 14°

SERIES CH3

DIAMETER 0.48 m	$z_s/d = 2.07$
LENGTH 3.05 m	D/d = 10.5
$x_s/d = 0$	LVE = −14°
$y_s/d = 0$	RVE = 14°

Figure 13.– Concluded.

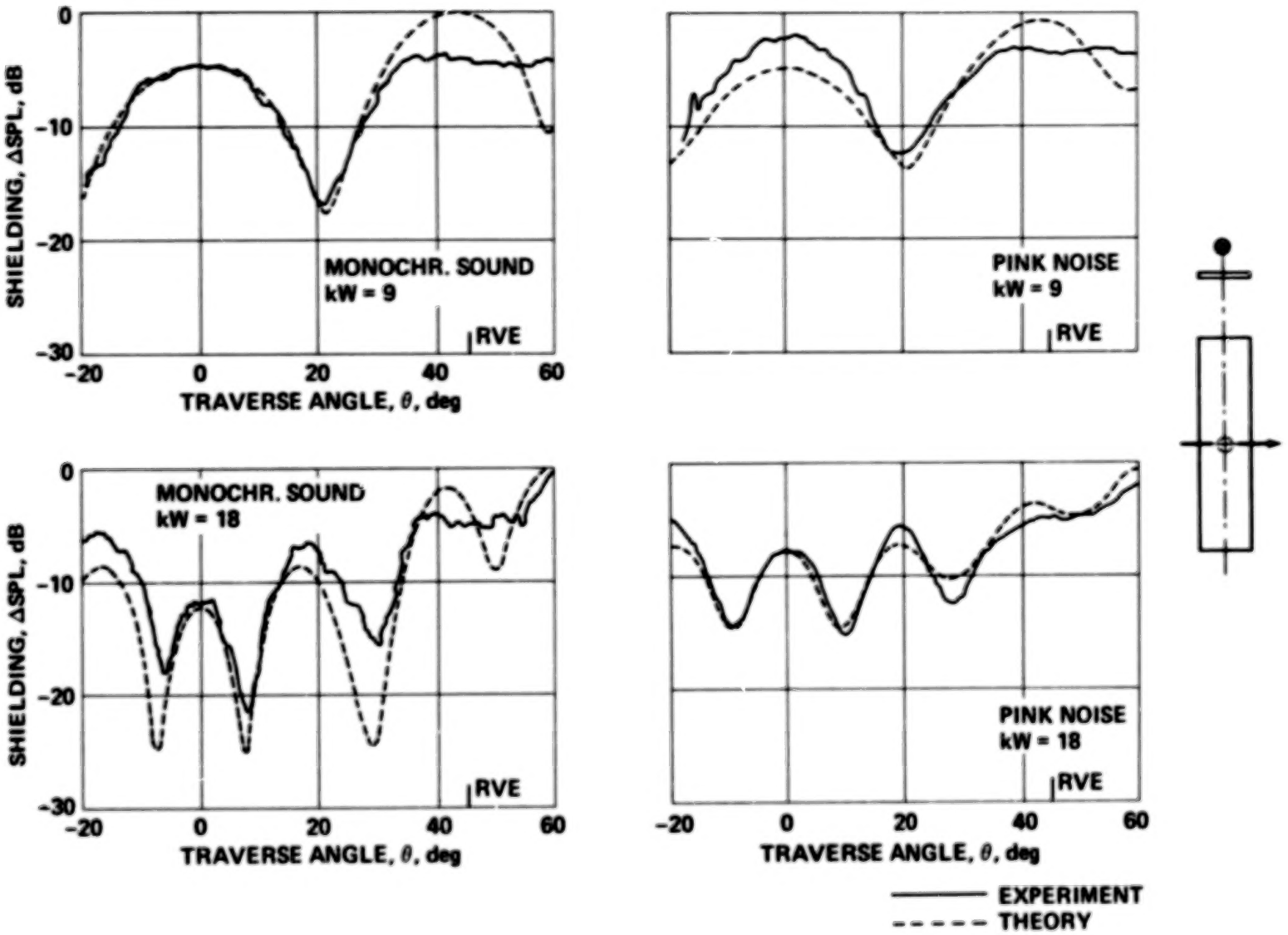

Figure 14.– Comparison of experimental shielding with theoretical shielding for rectangular plate – Series LR1.

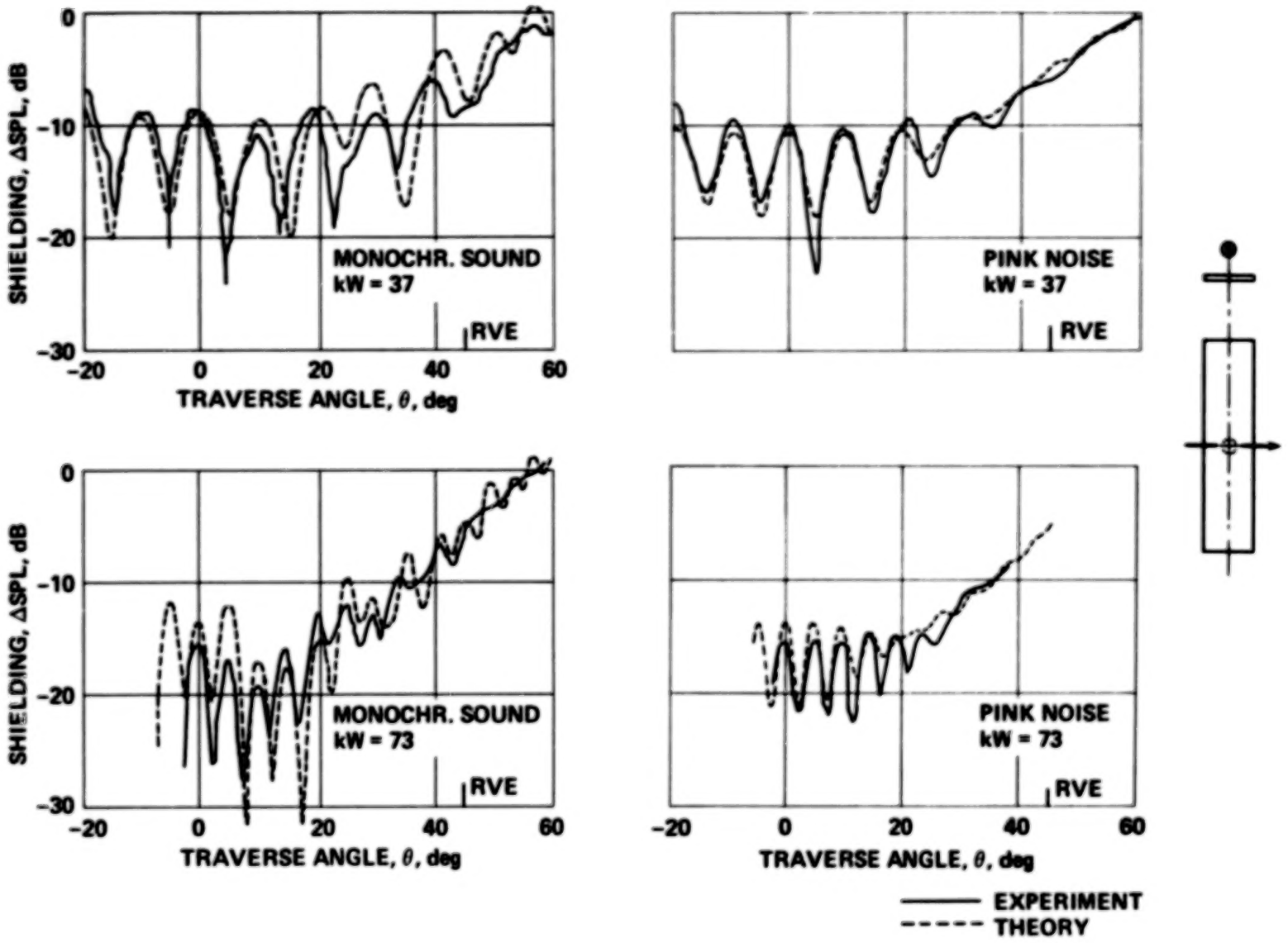

Figure 14.– Continued.

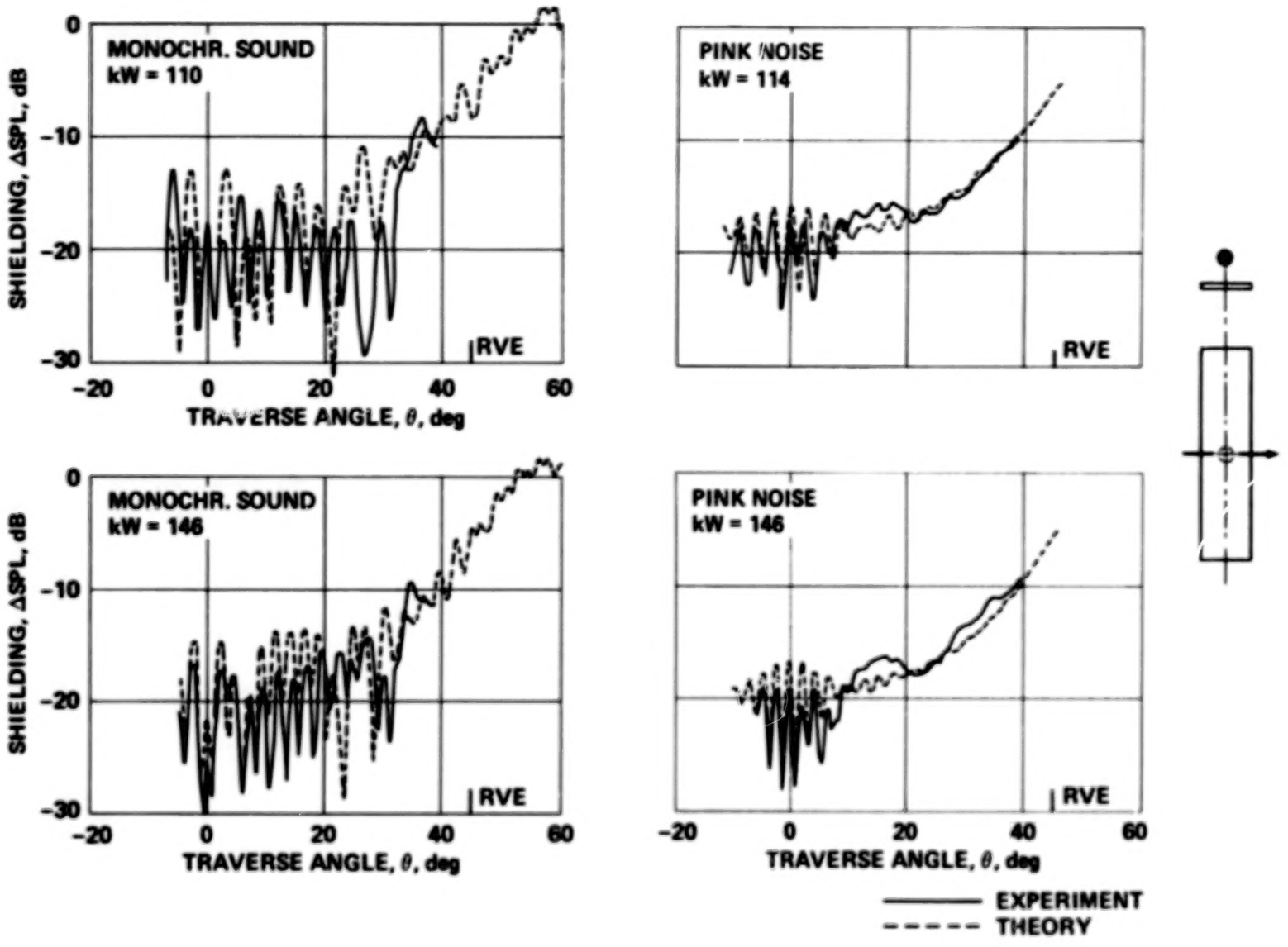

Figure 14.– Continued.

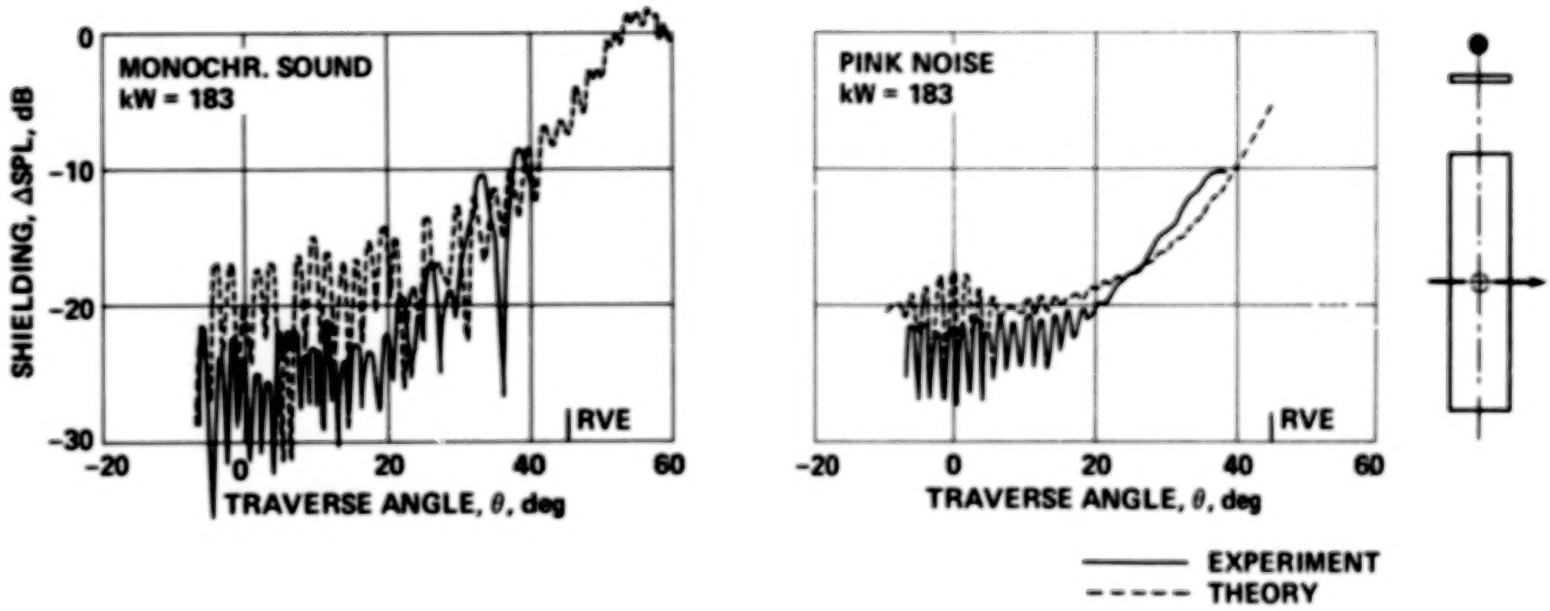

Figure 14.– Concluded.

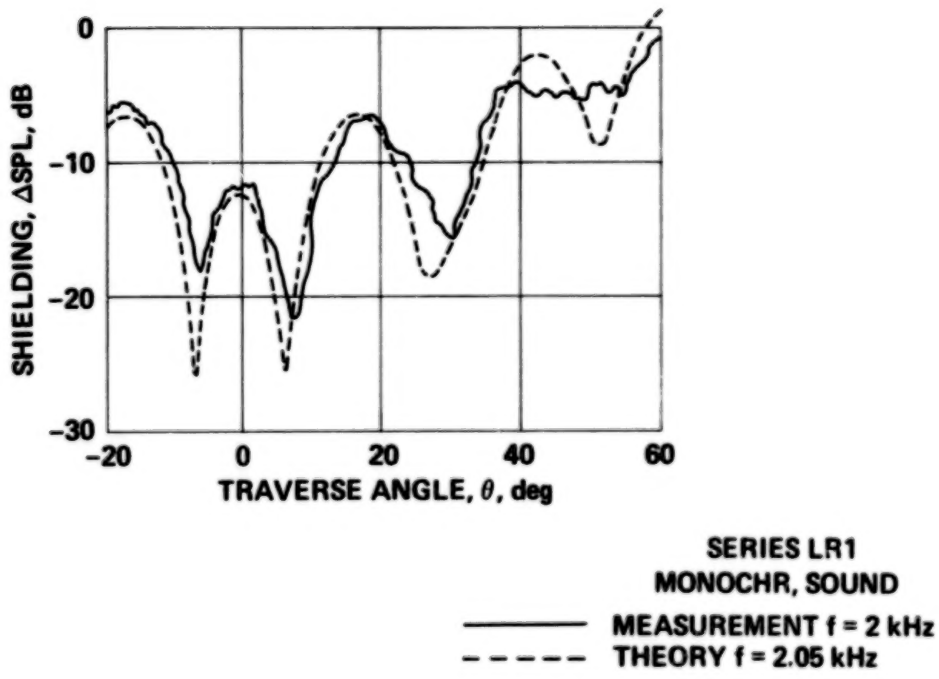

Figure 15.– Effect of small frequency change on rectangular plate shielding.

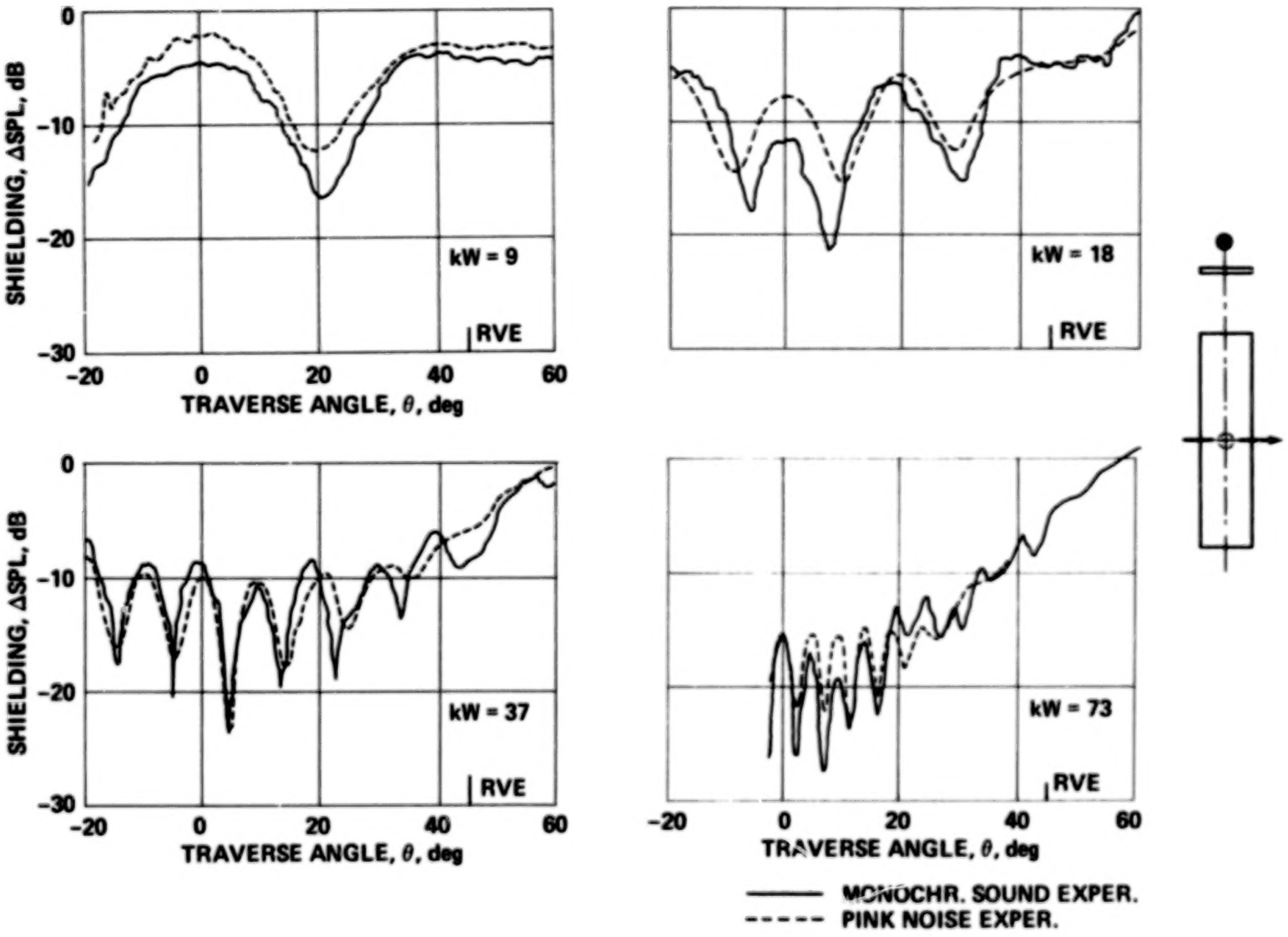

Figure 16.– Comparison of measured shielding of monochromatic sound with that for pink noise – Series LR1.

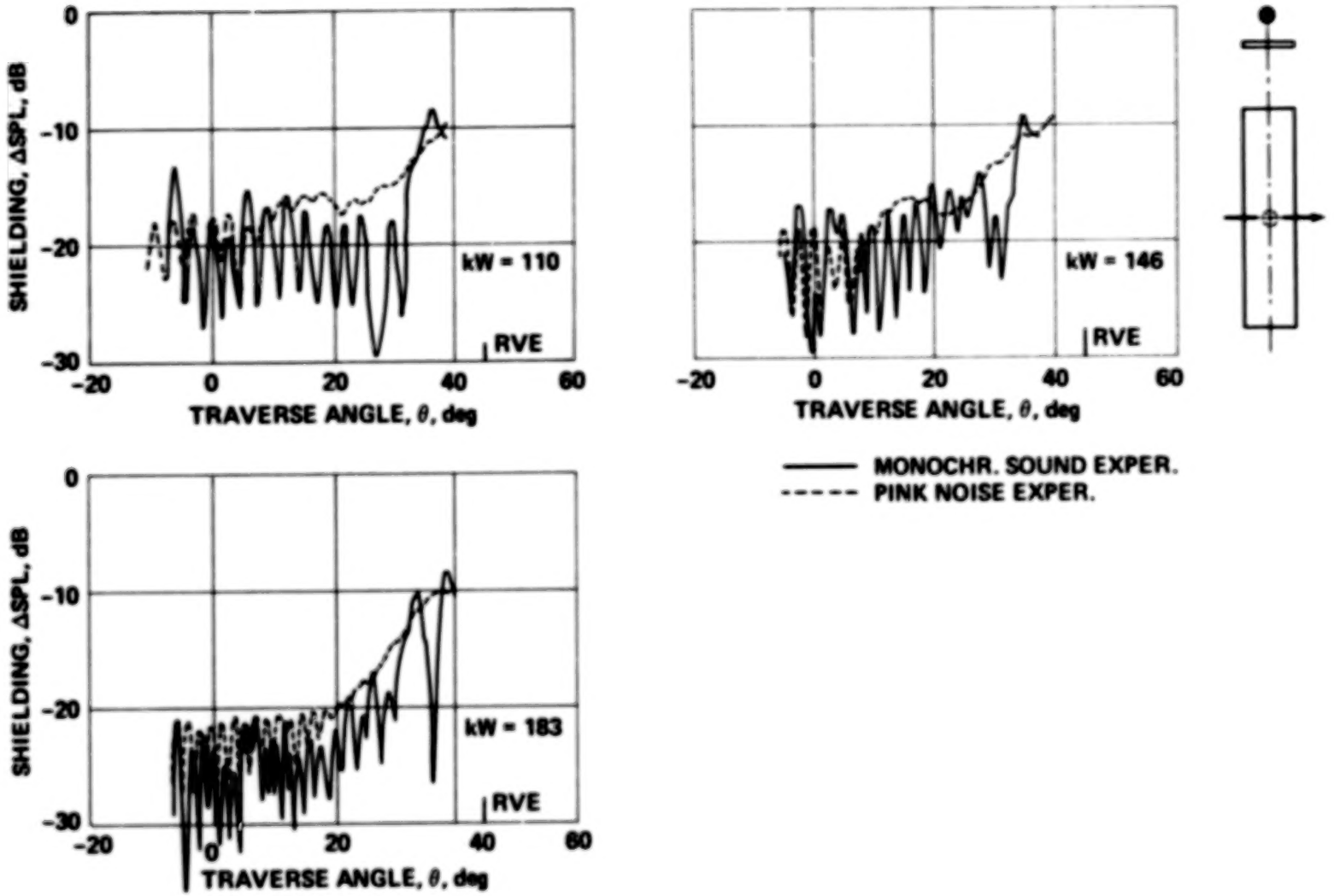

Figure 16.– Concluded.

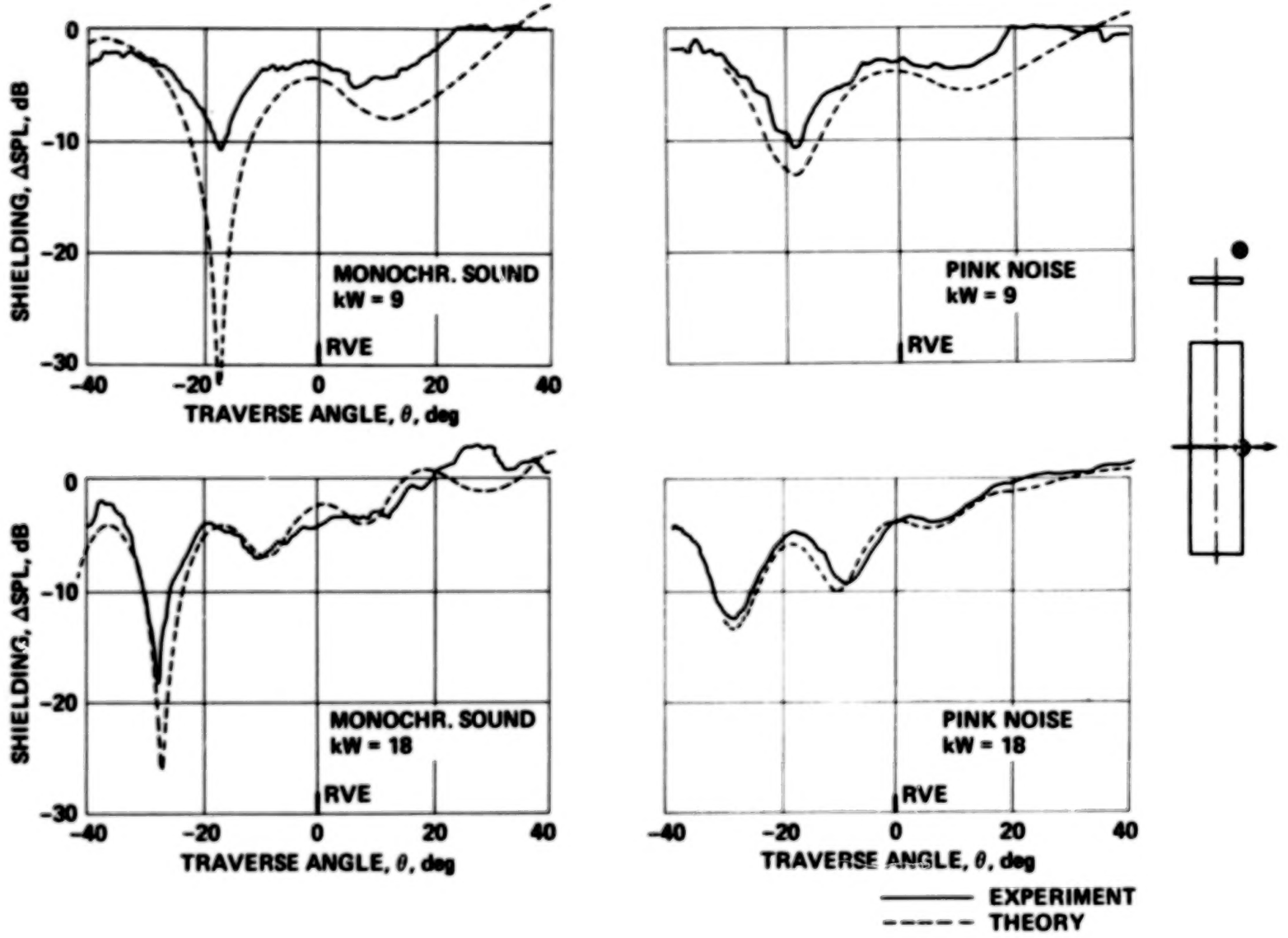

Figure 17.– Comparison of experimental shielding with theoretical shielding for rectangular plate – Series LR2.

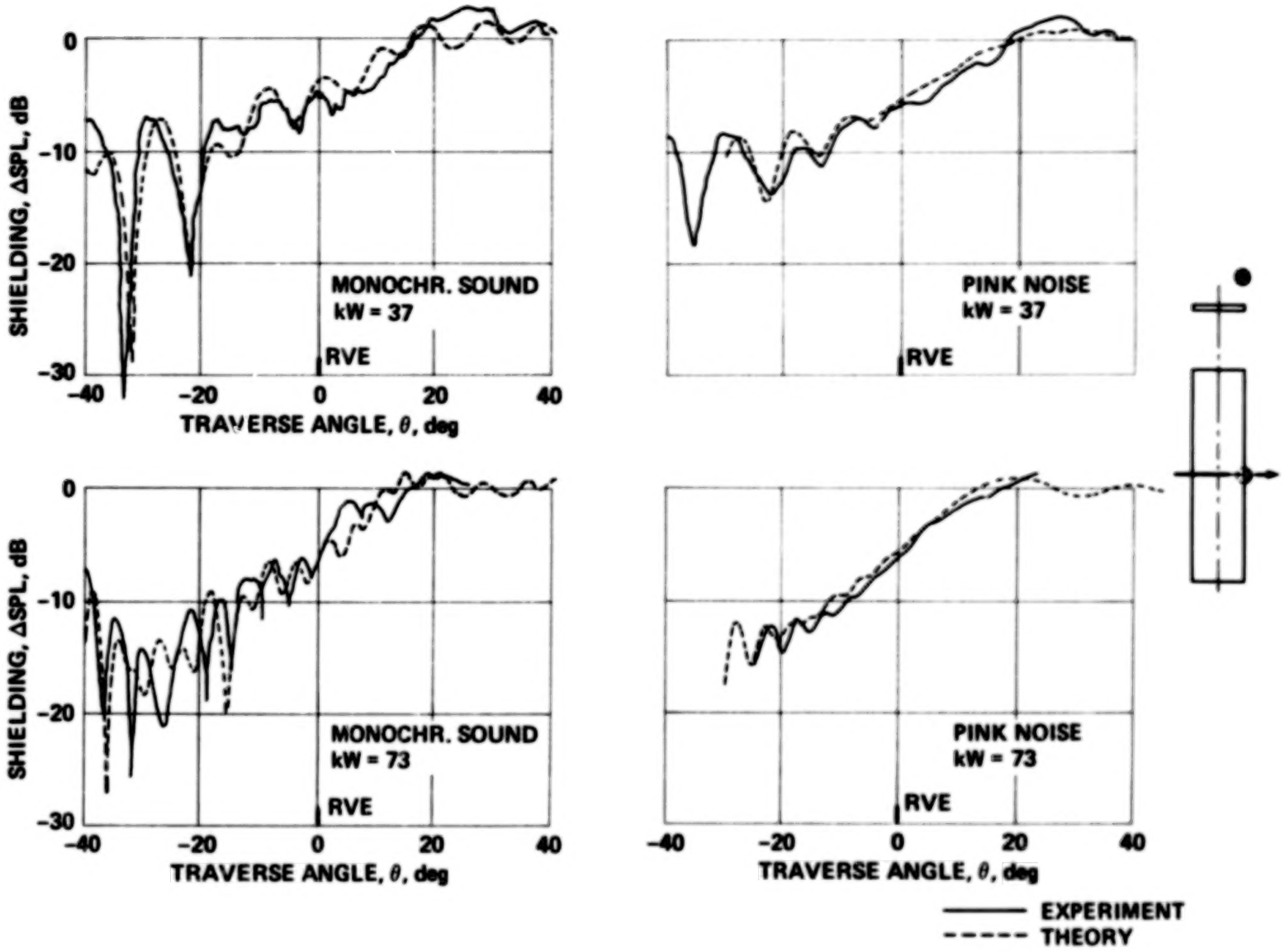

Figure 17.– Continued.

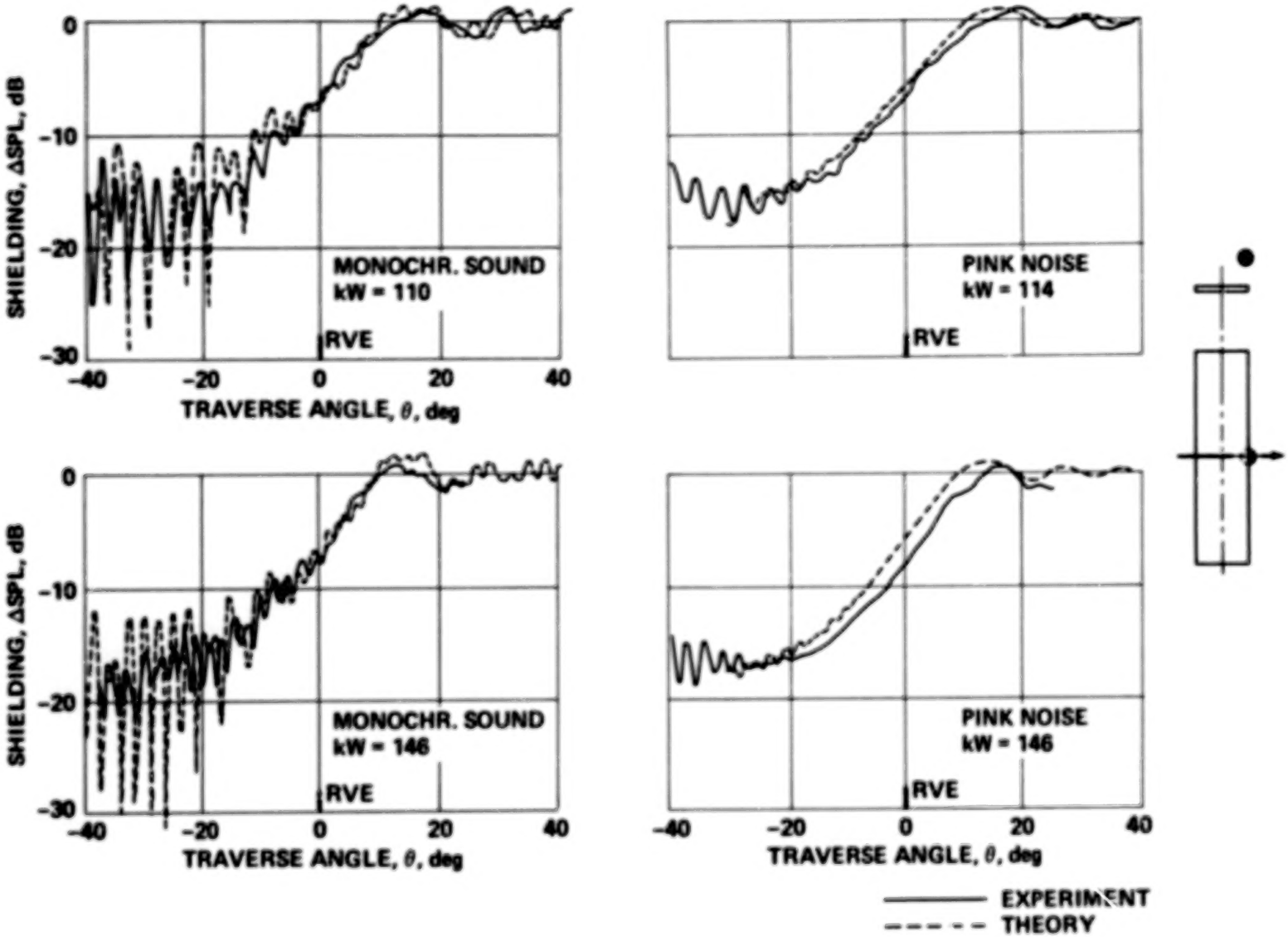

Figure 17.– Continued.

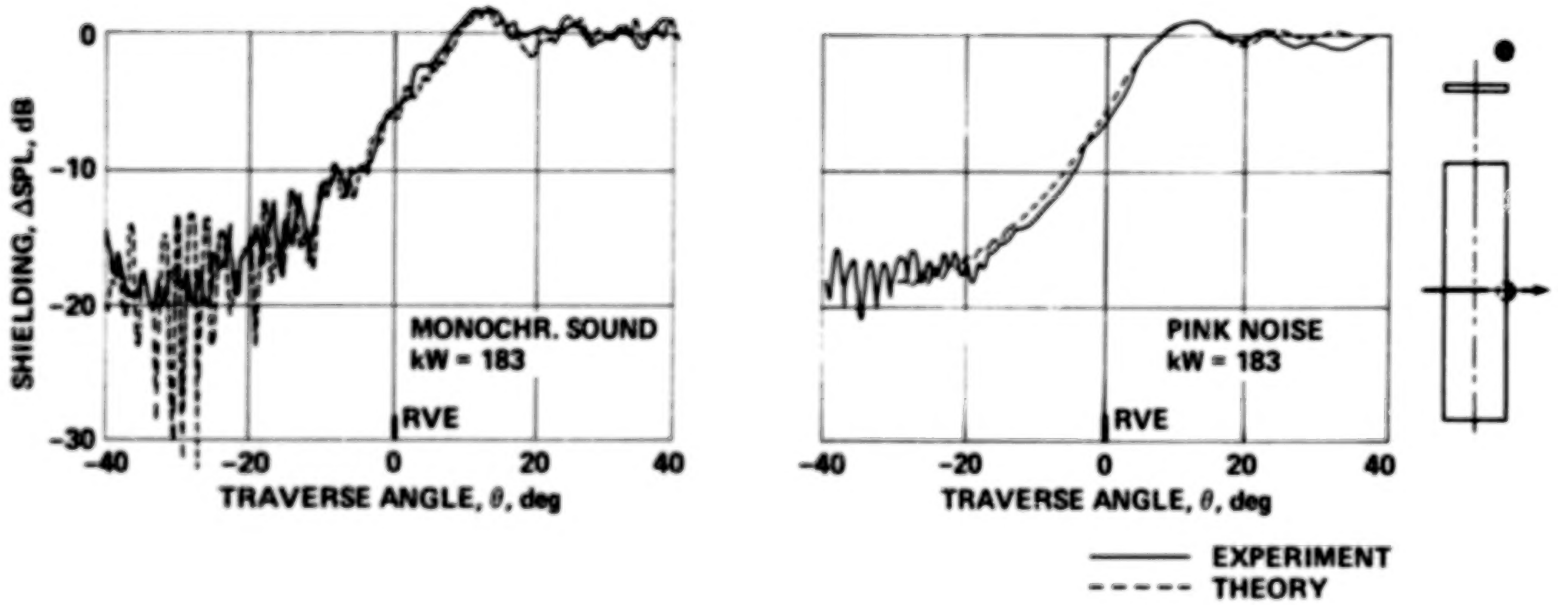

Figure 17.– Concluded.

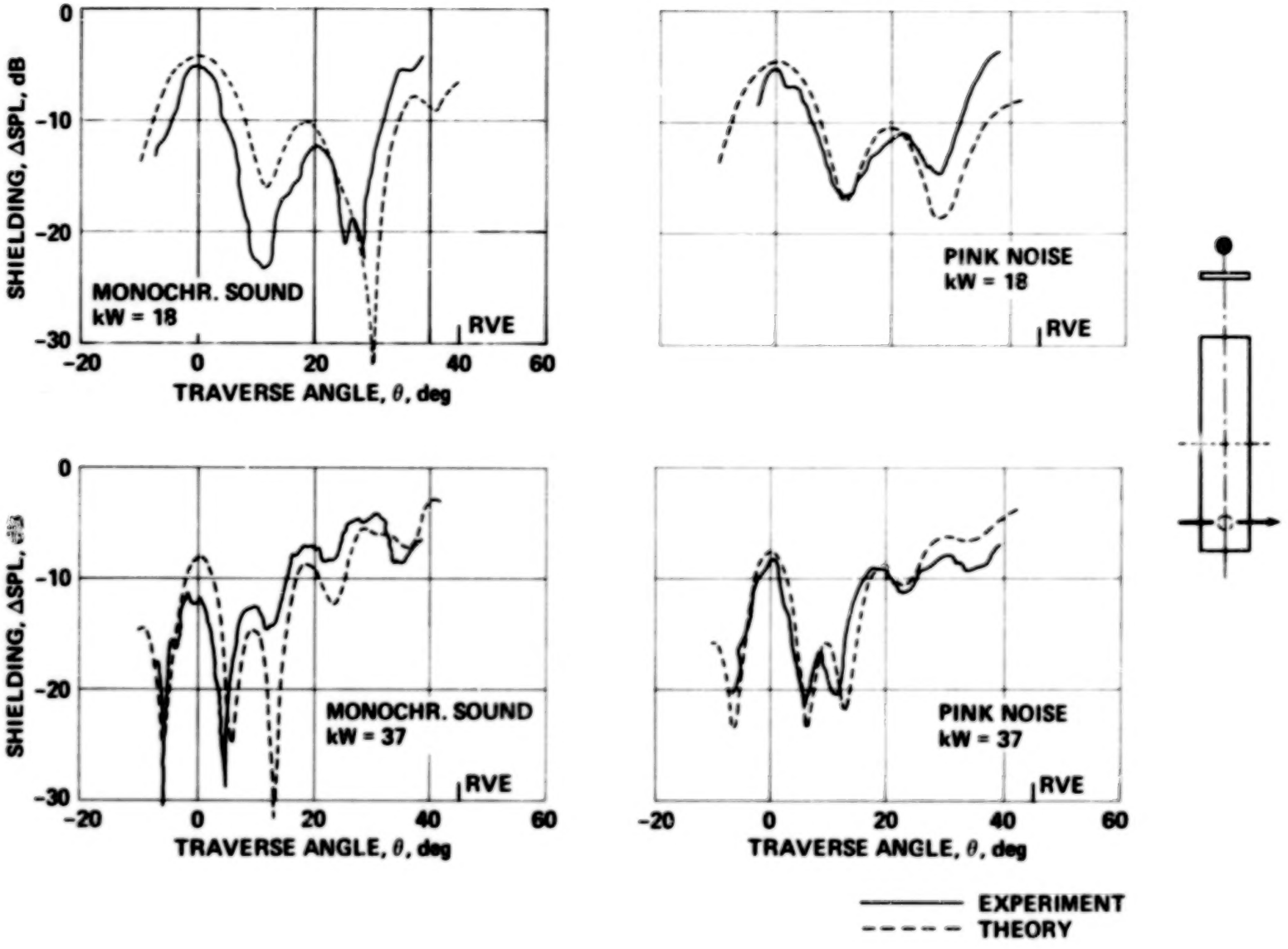

Figure 18.– Comparison of experimental shielding with theoretical shielding for rectangular plate – Series LR3.

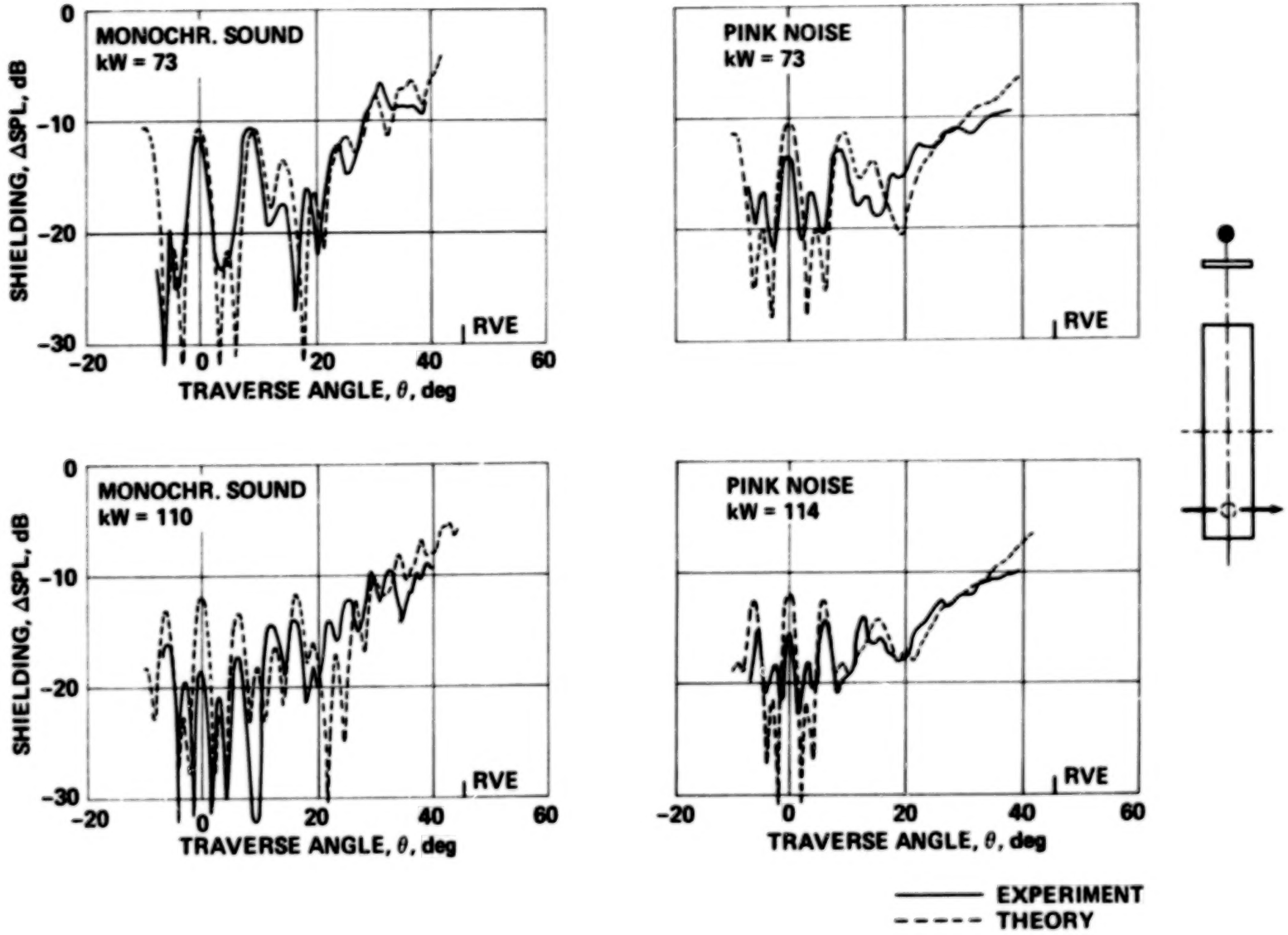

Figure 18.– Continued.

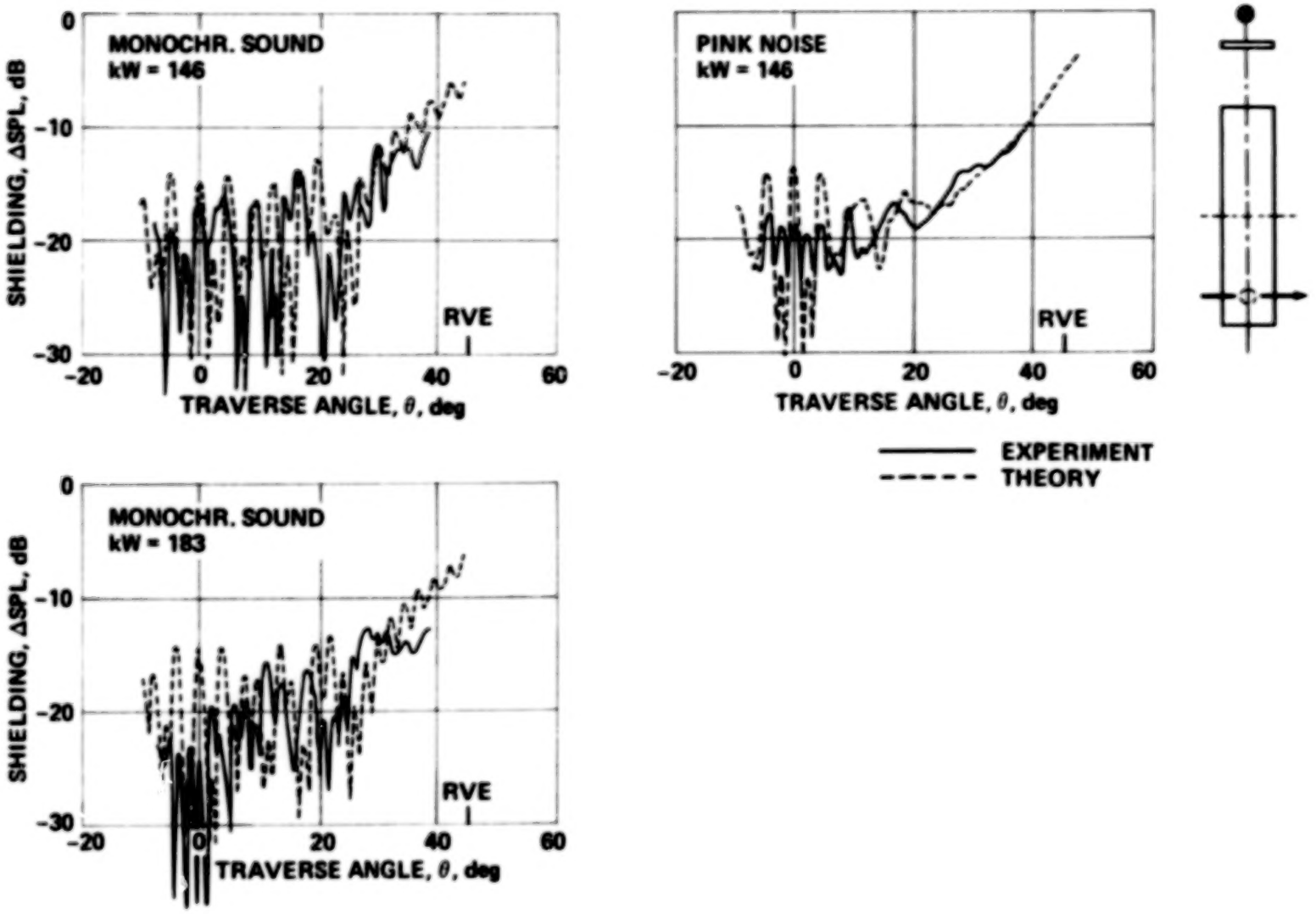

Figure 18.– Concluded.

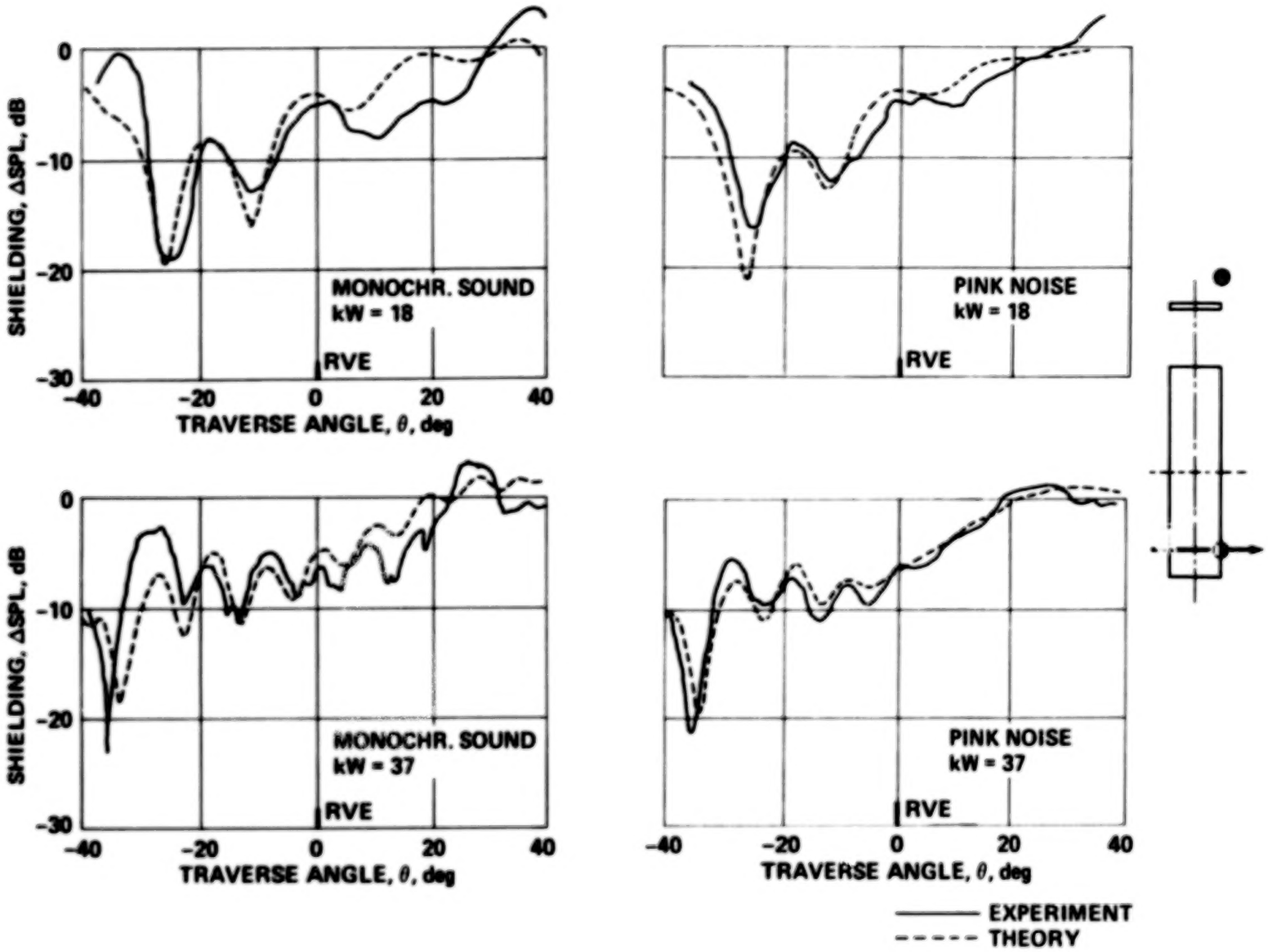

Figure 19.– Comparison of experimental shielding with theoretical shielding for rectangular plate – Series LR4.

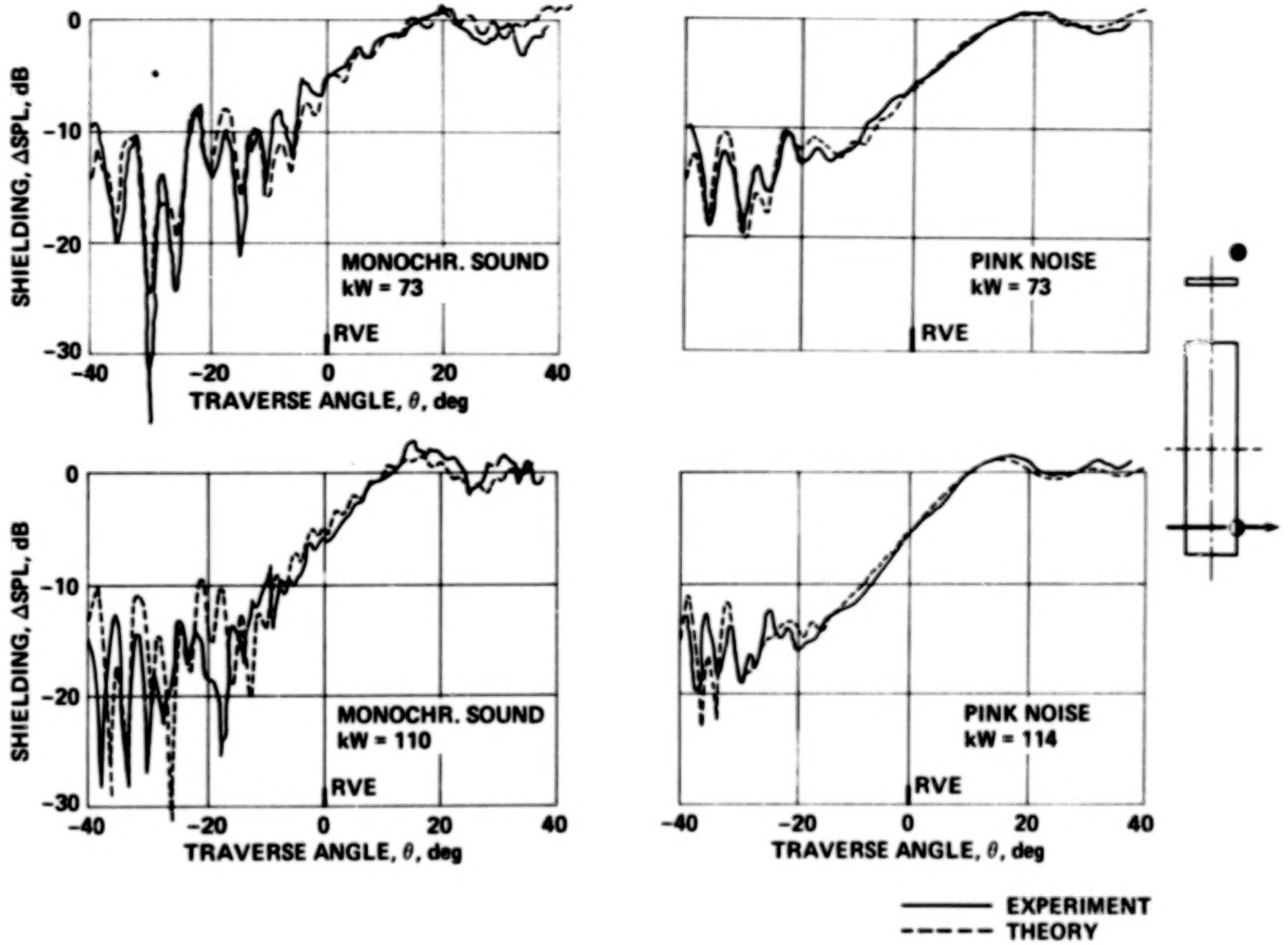

Figure 19.– Continued.

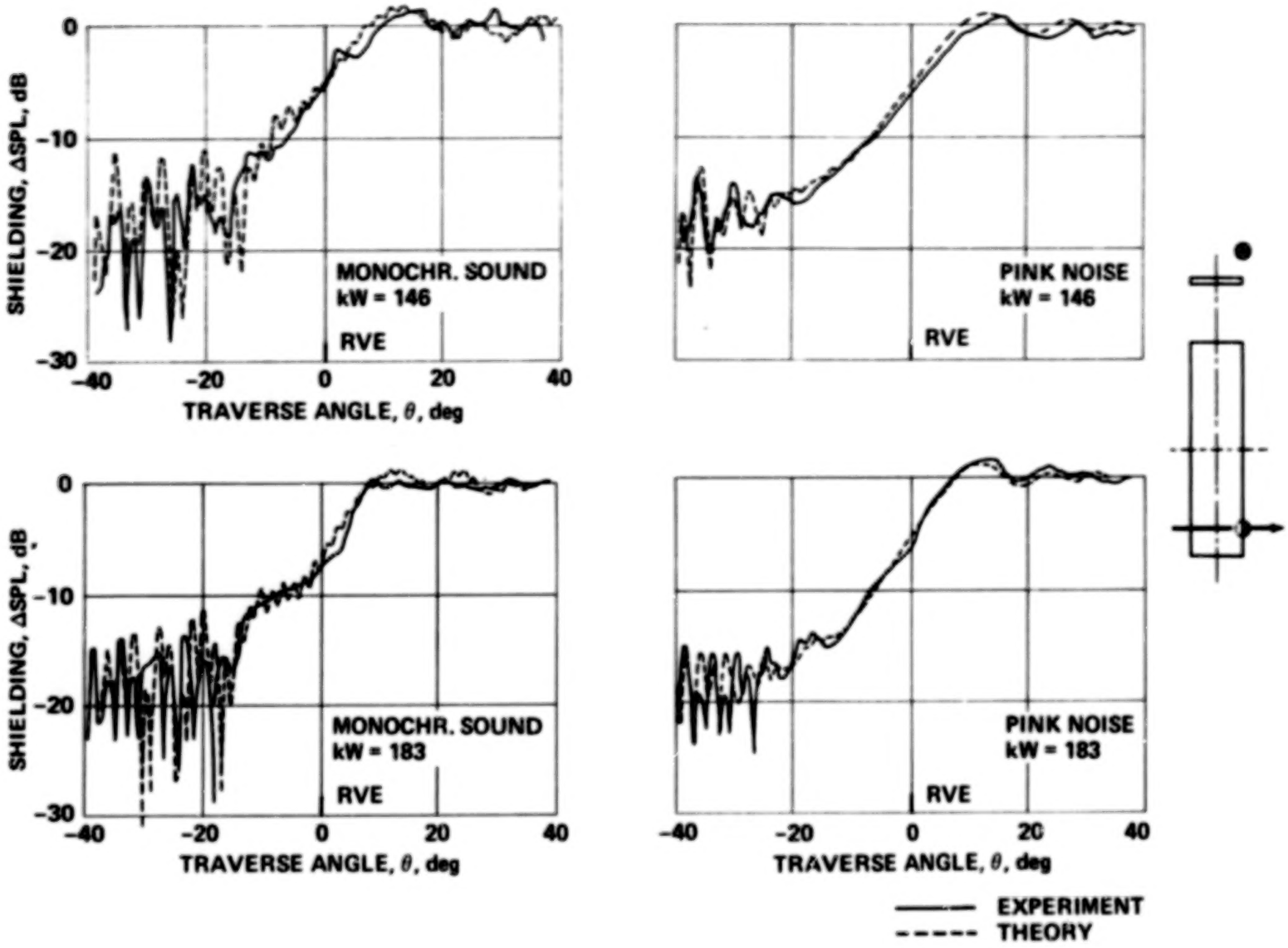

Figure 19.– Concluded.

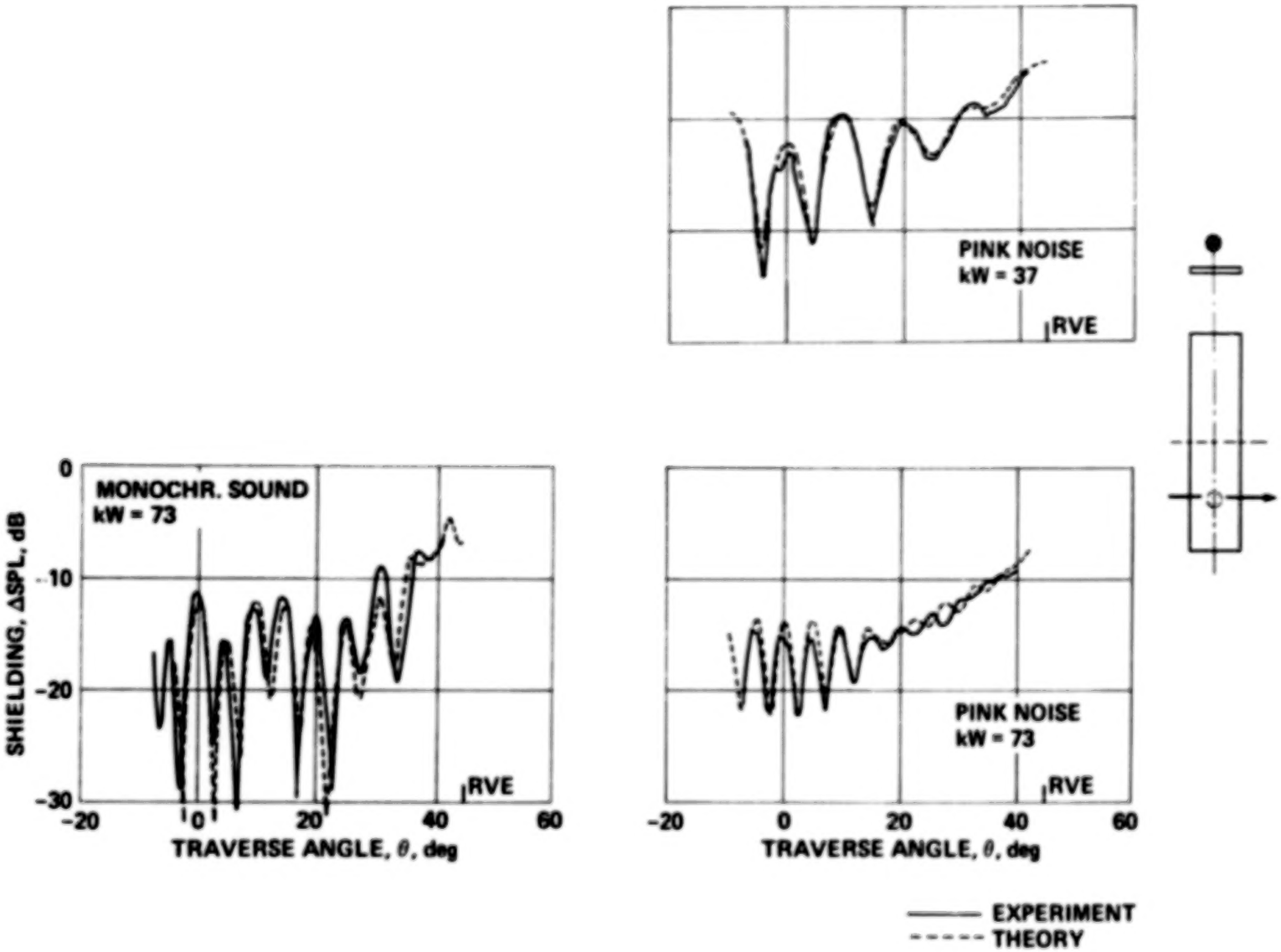

Figure 20.– Comparison of experimental shielding with theoretical shielding for rectangular plate – Series LR13.

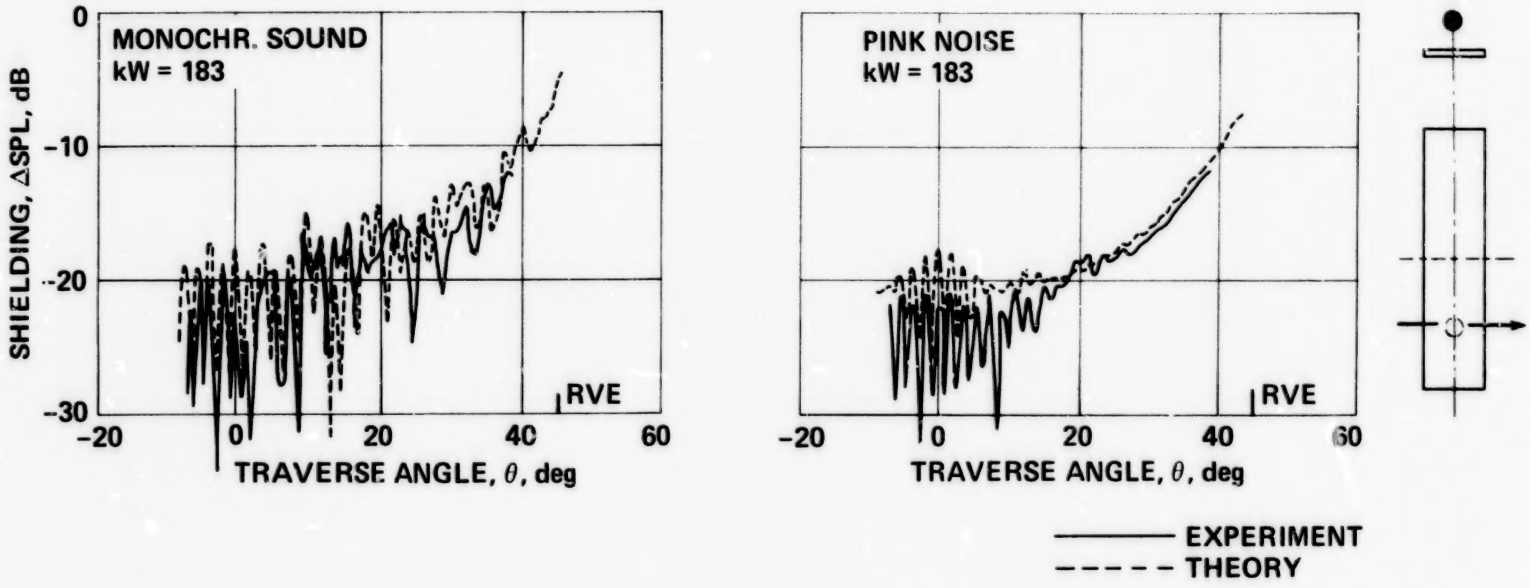

Figure 20.– Concluded.

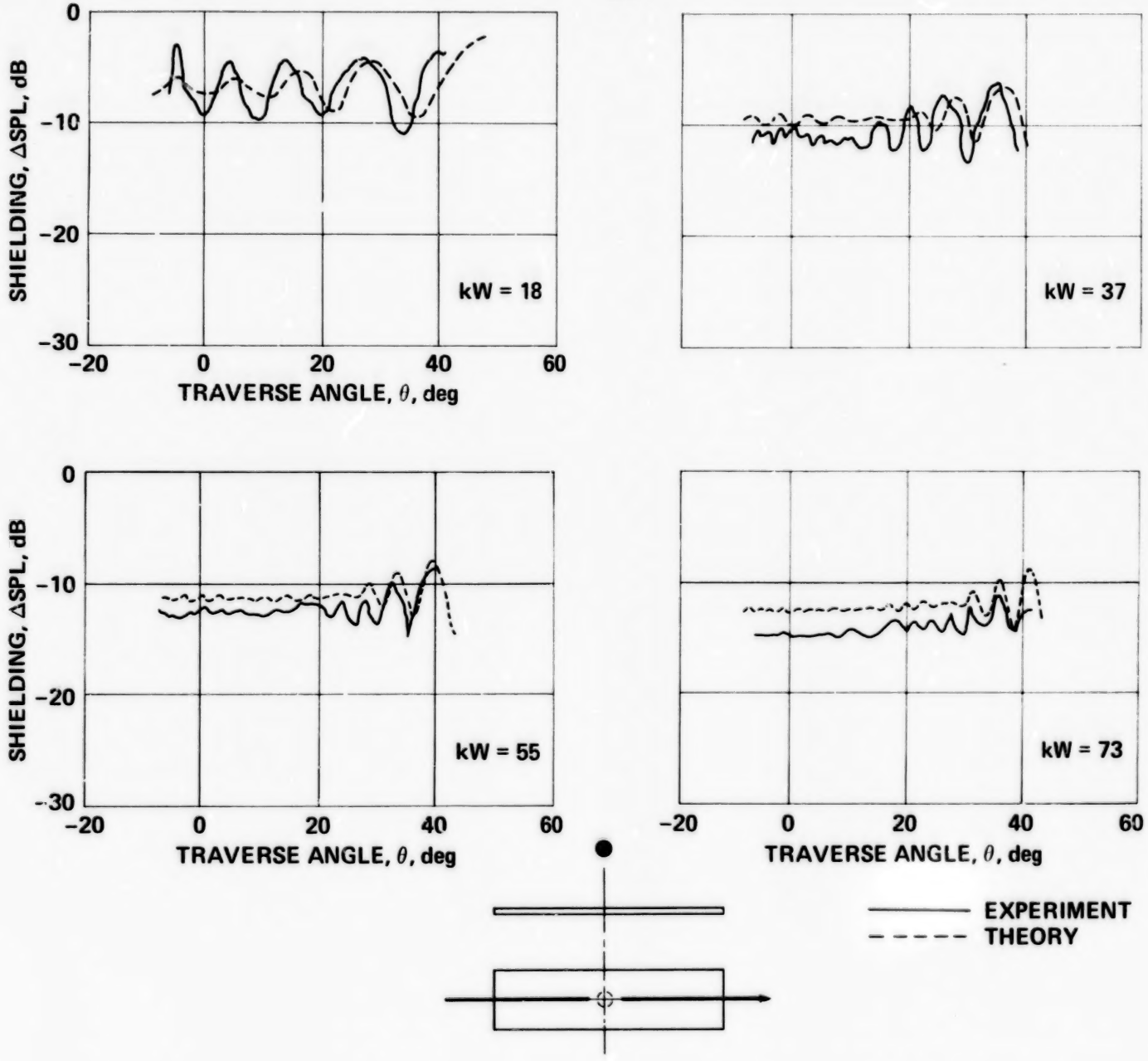

Figure 21.– Comparison of experimental shielding with theoretical shielding for rectangular plate – Series SRH, pink noise.

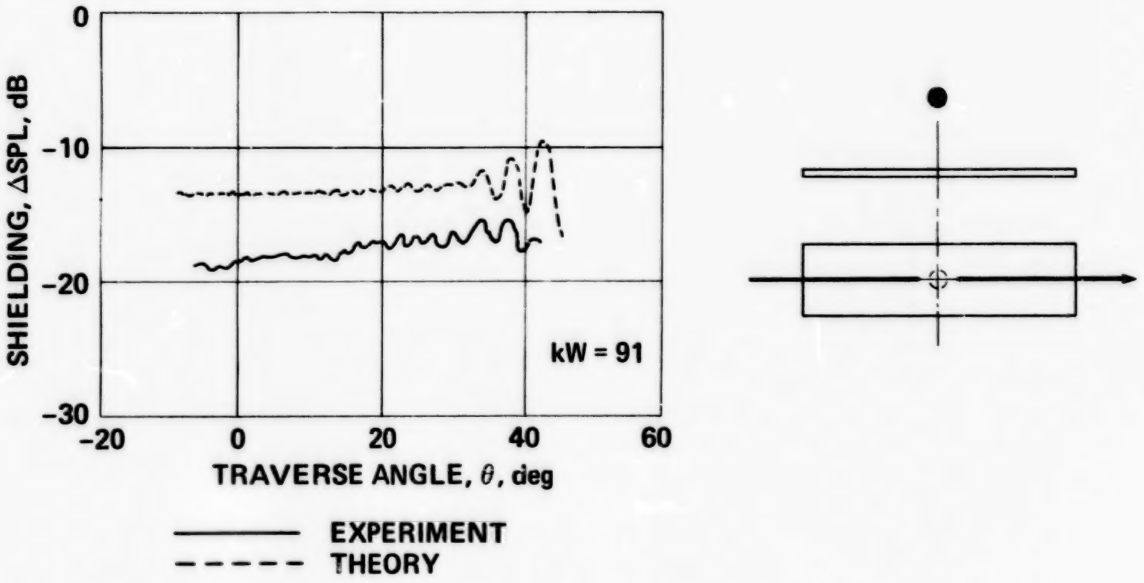

Figure 21.– Concluded.

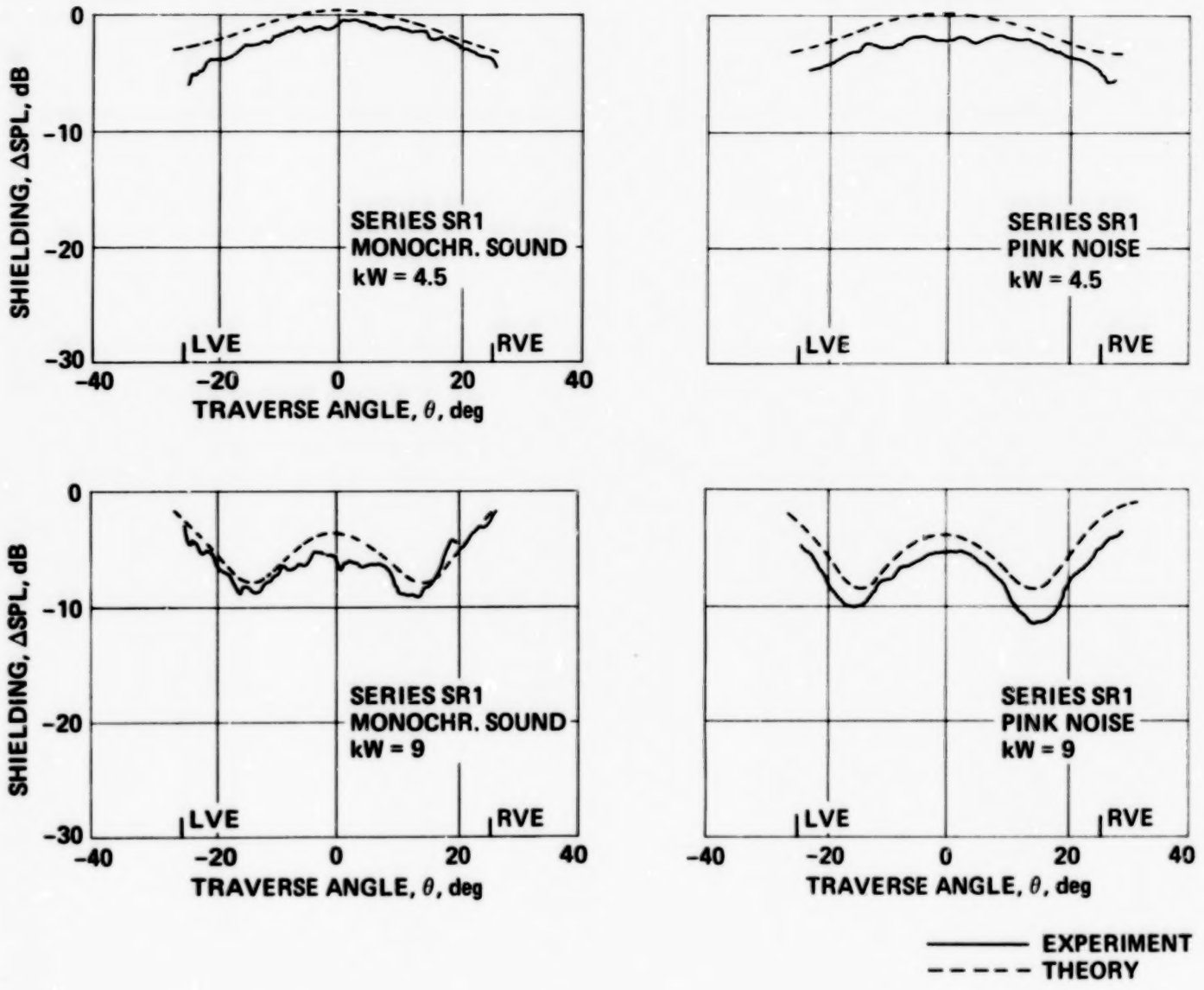

Figure 22.– Comparison of experimental shielding with theoretical shielding for rectangular plate at low frequencies.

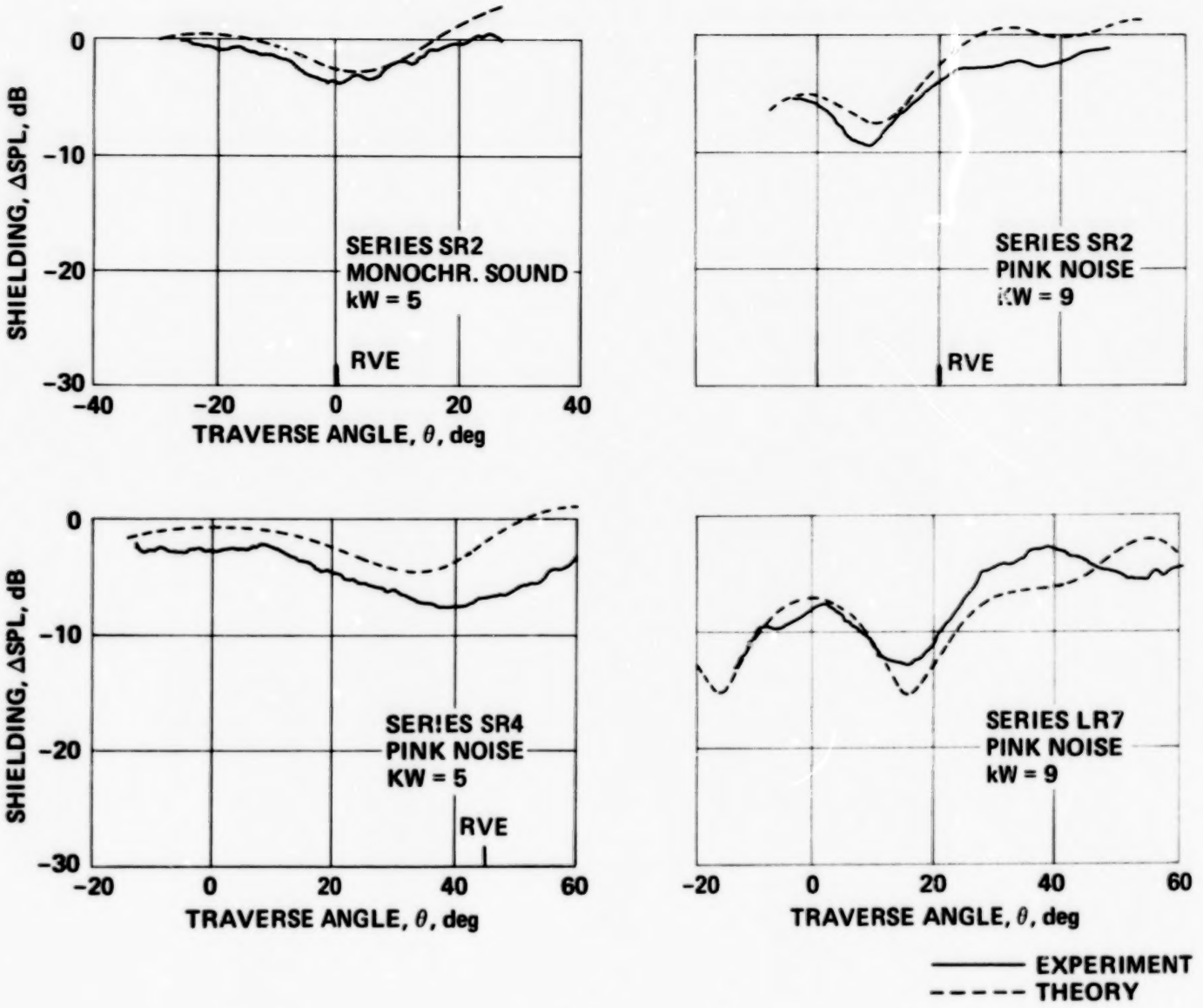

Figure 22.– Continued.

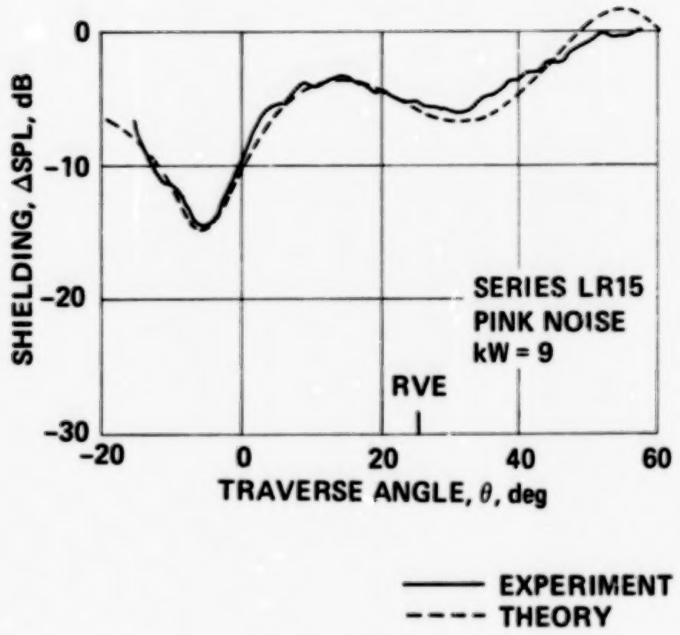

Figure 22.– Concluded.

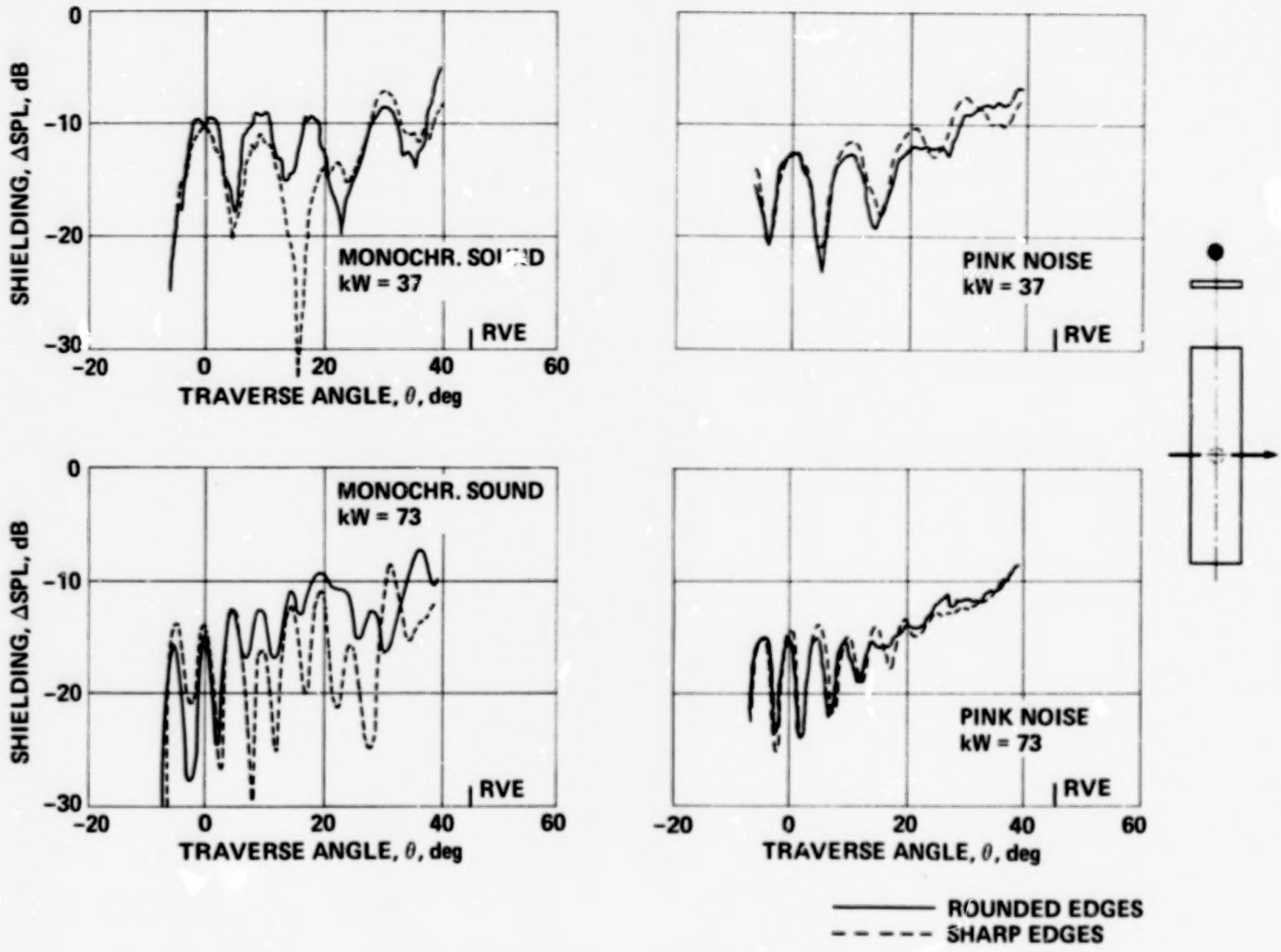

Figure 23.-- Effect of edge shape on rectangular shielding.

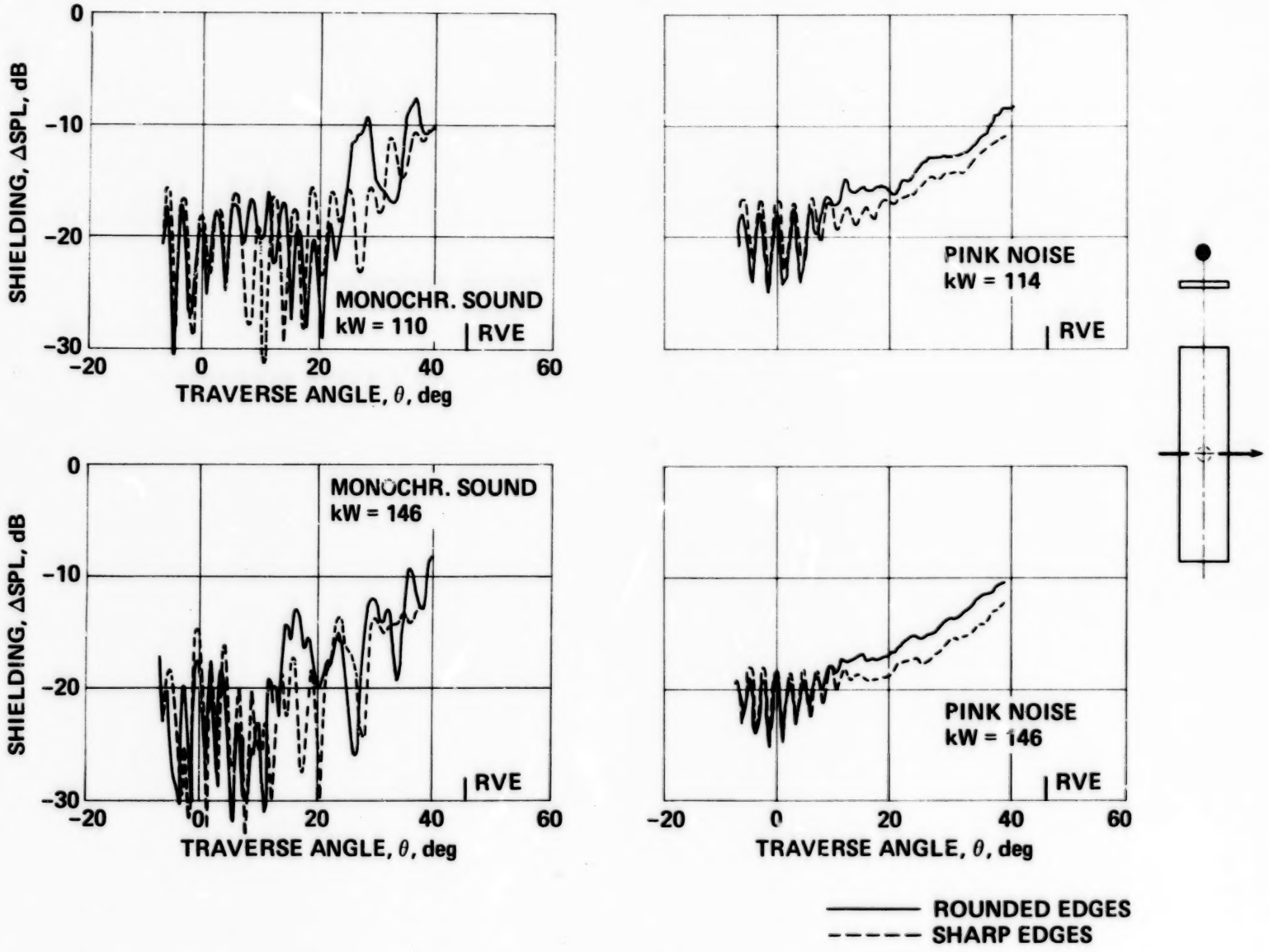

Figure 23.– Continued.

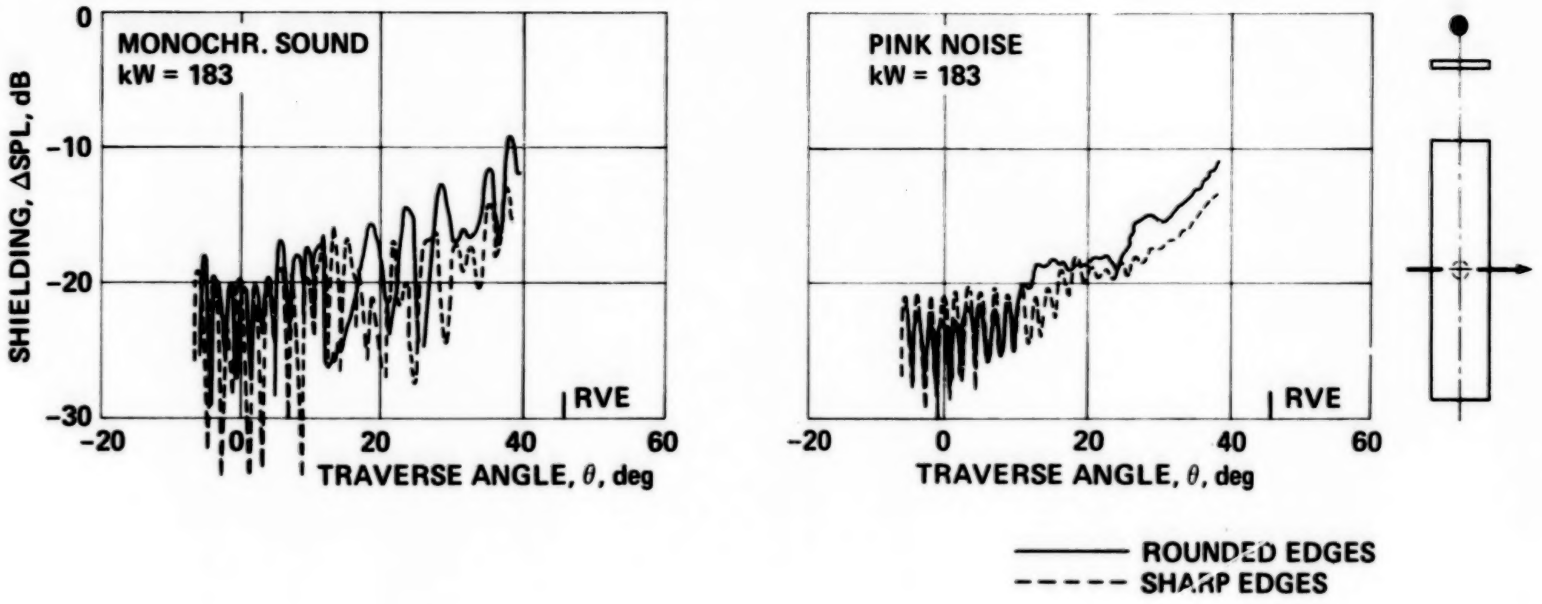

Figure 23.– Concluded.

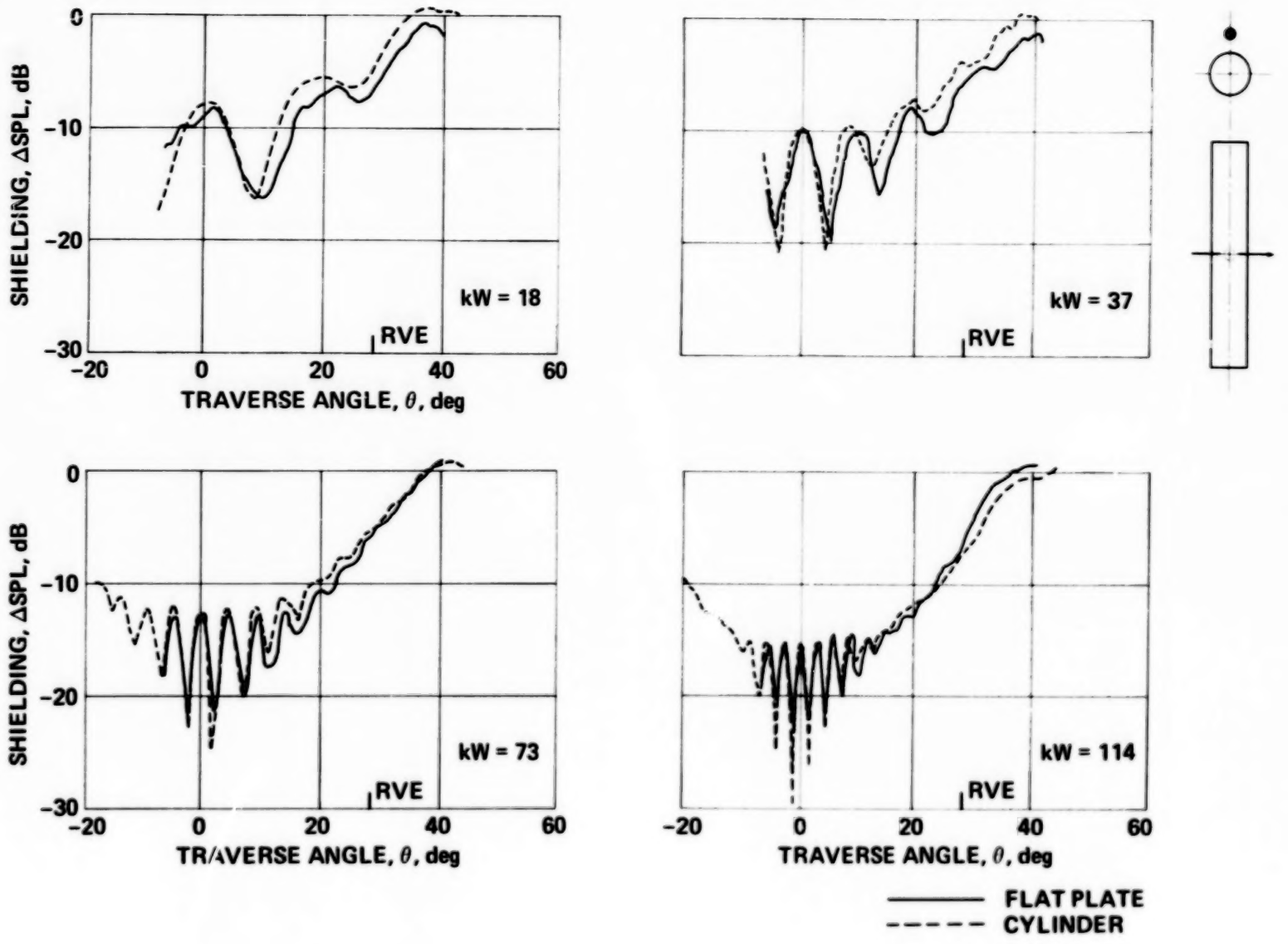

Figure 24.– Comparison of measured shielding for rectangular plate with that for circular cylinder.

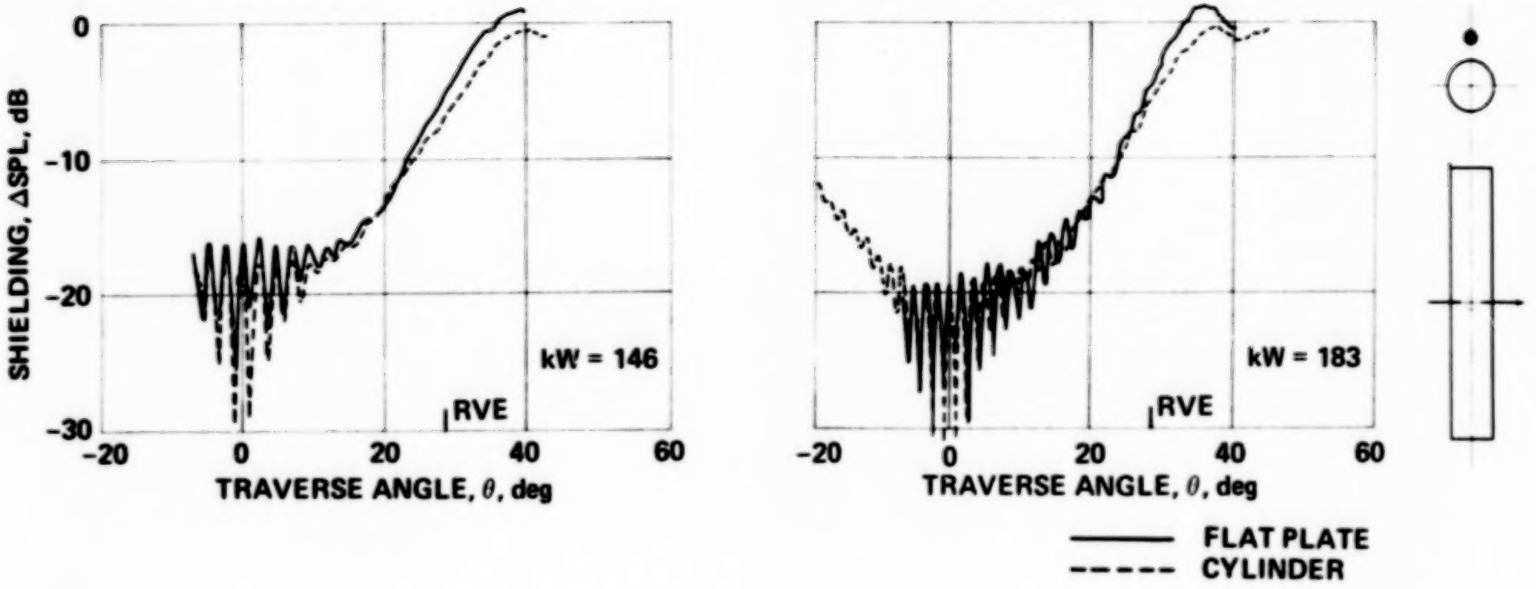

Figure 24.– Concluded.

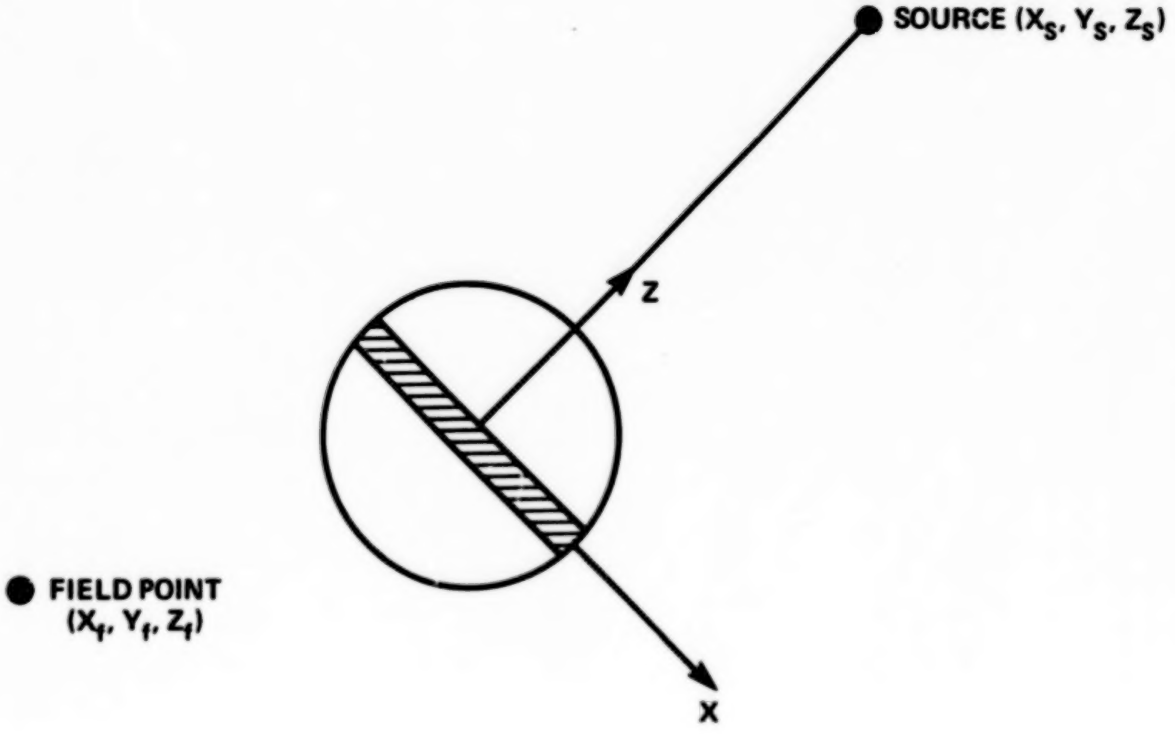

Figure 25.– Crientation of equivalent rectangular plate.

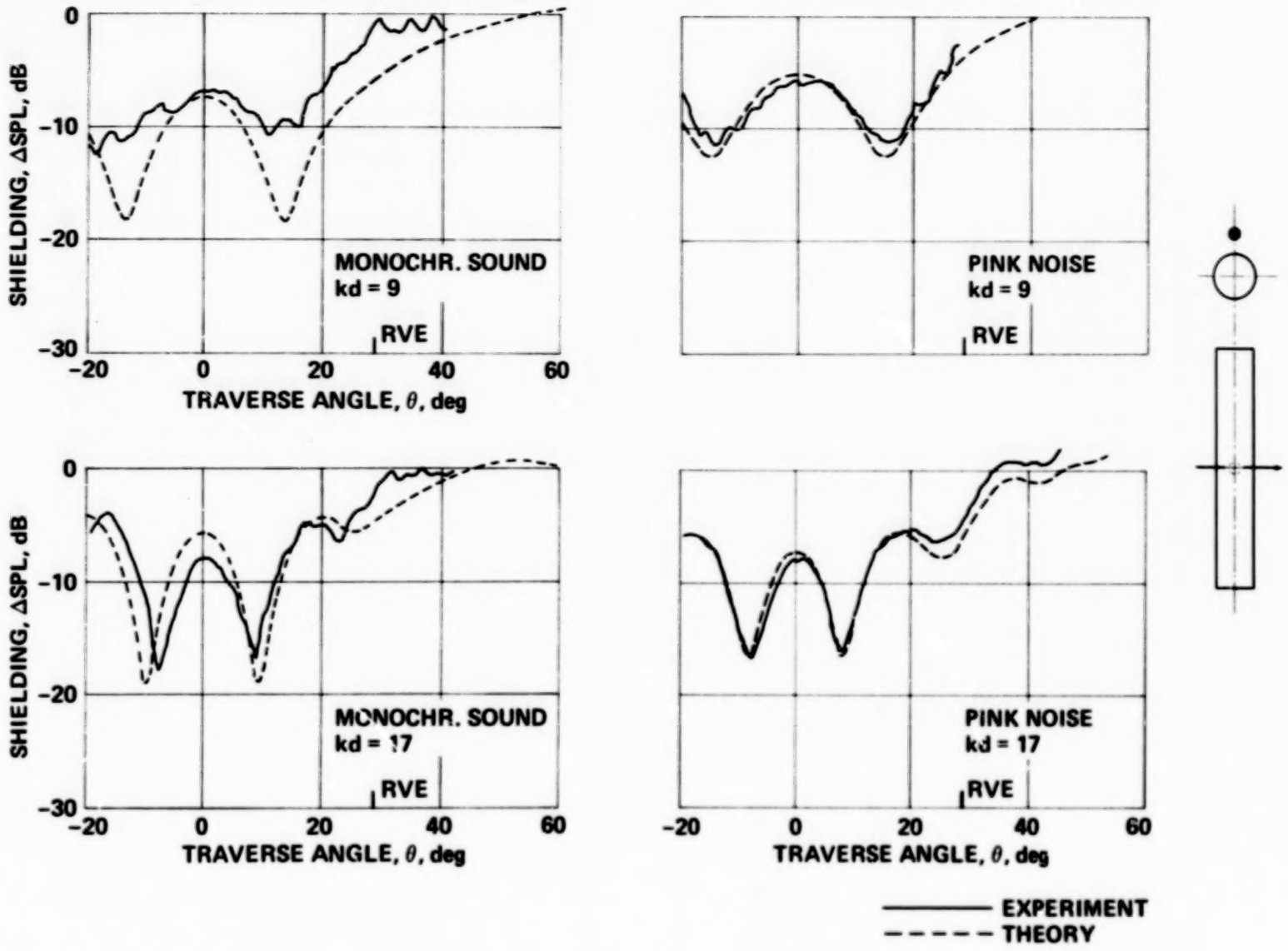

Figure 26.– Comparison of experimental shielding with theoretical shielding for circular cylinder – Series C1.

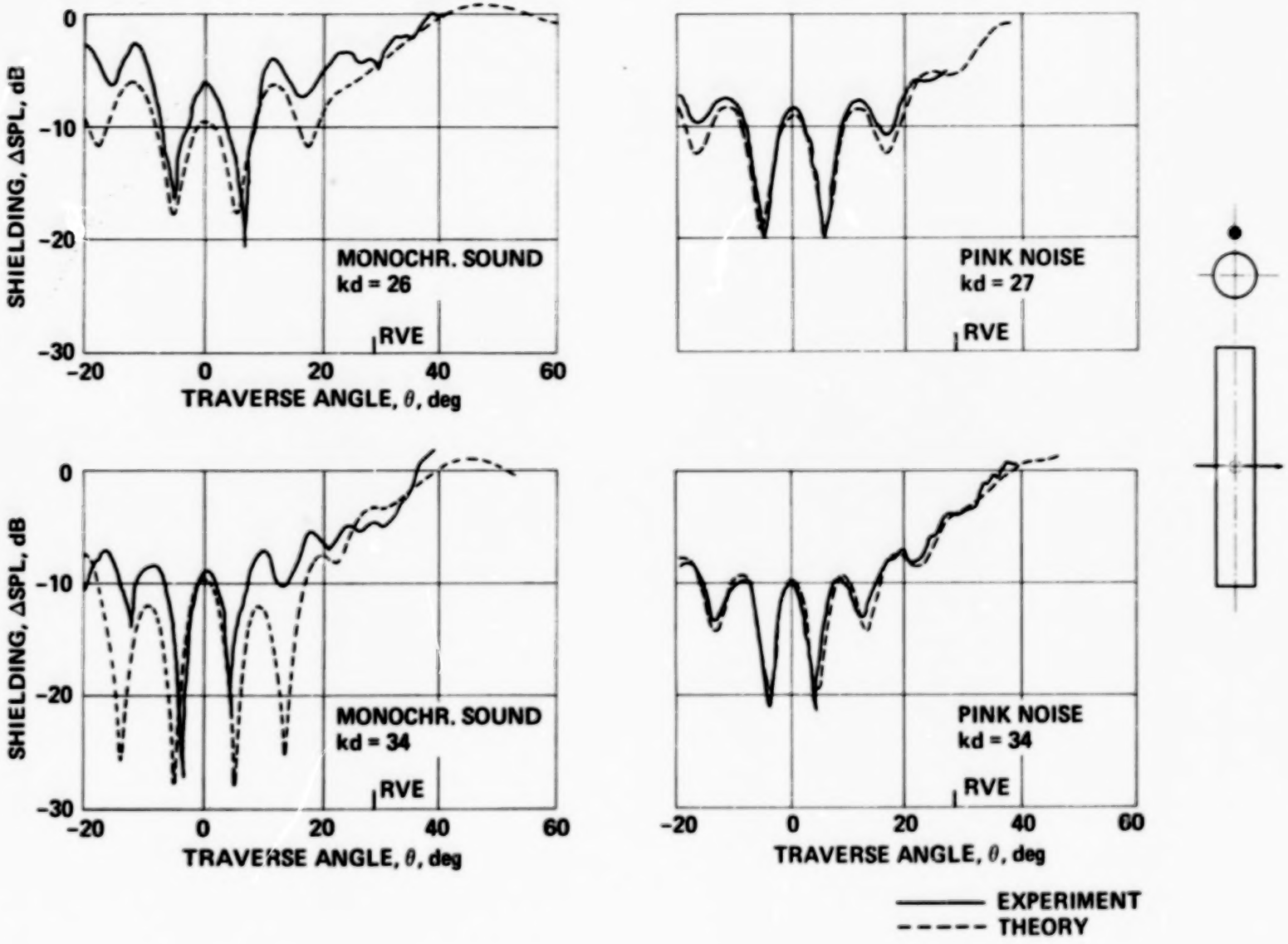

Figure 26.– Continued.

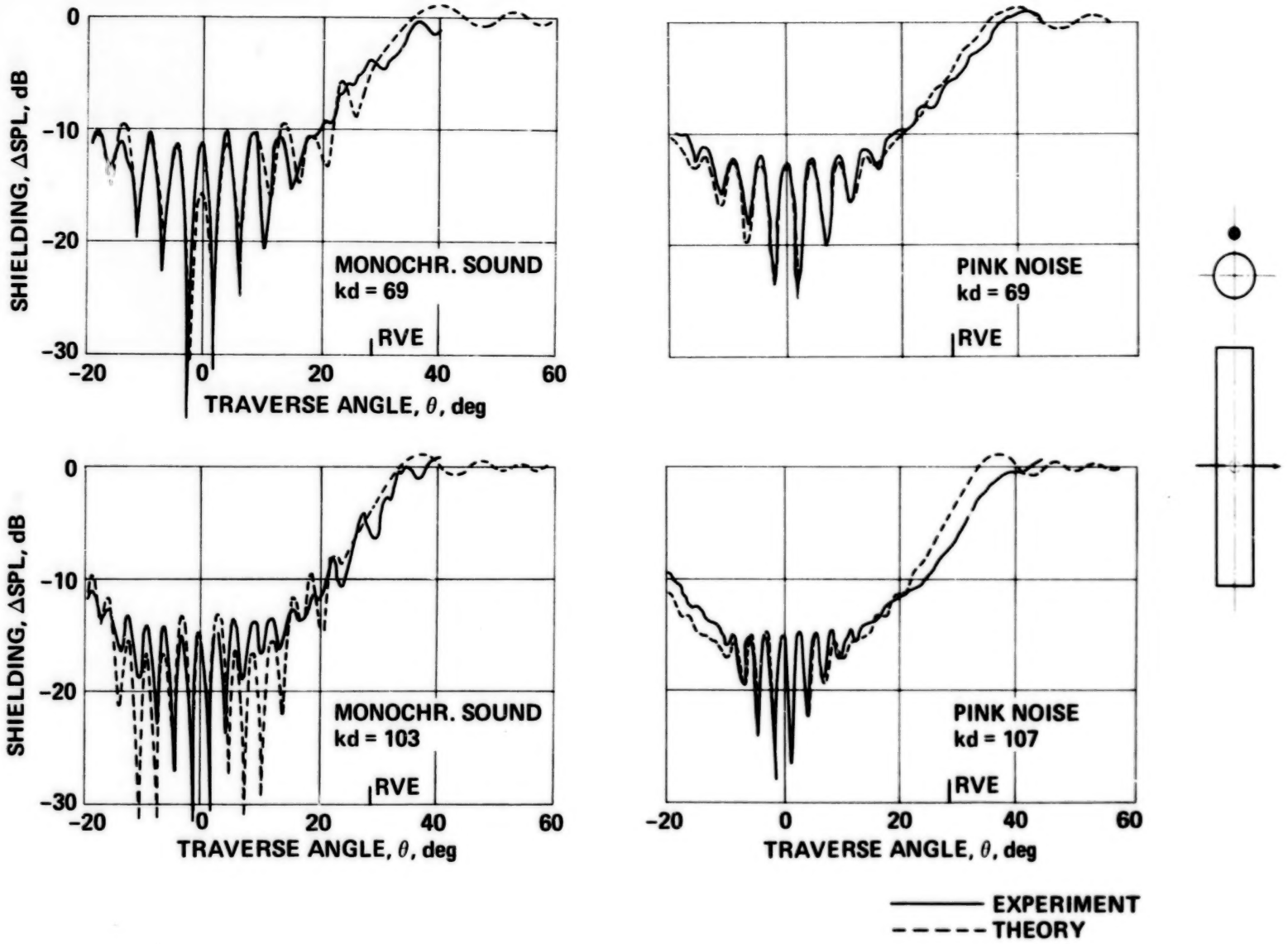

Figure 26.– Continued.

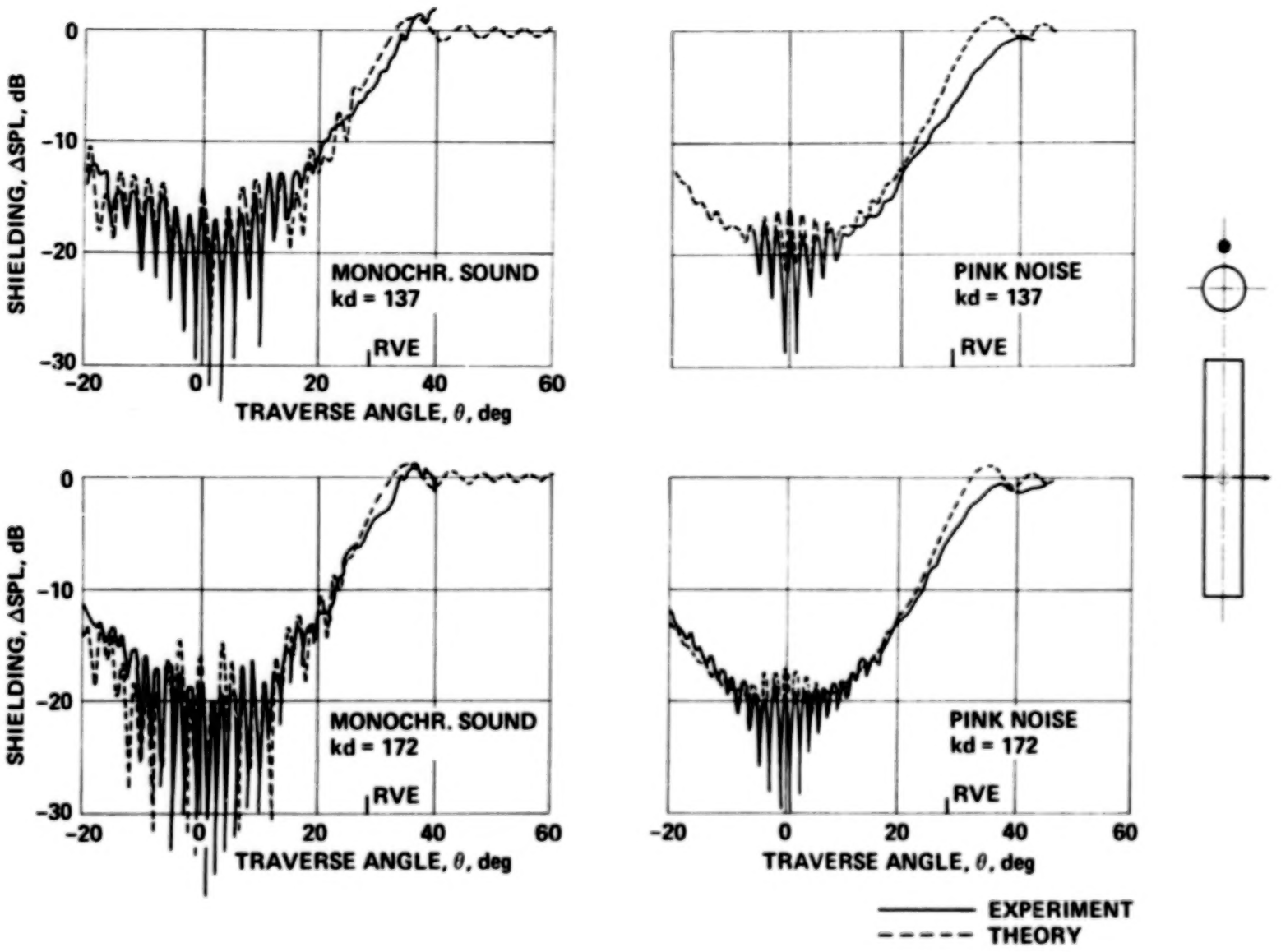

Figure 26.– Concluded.

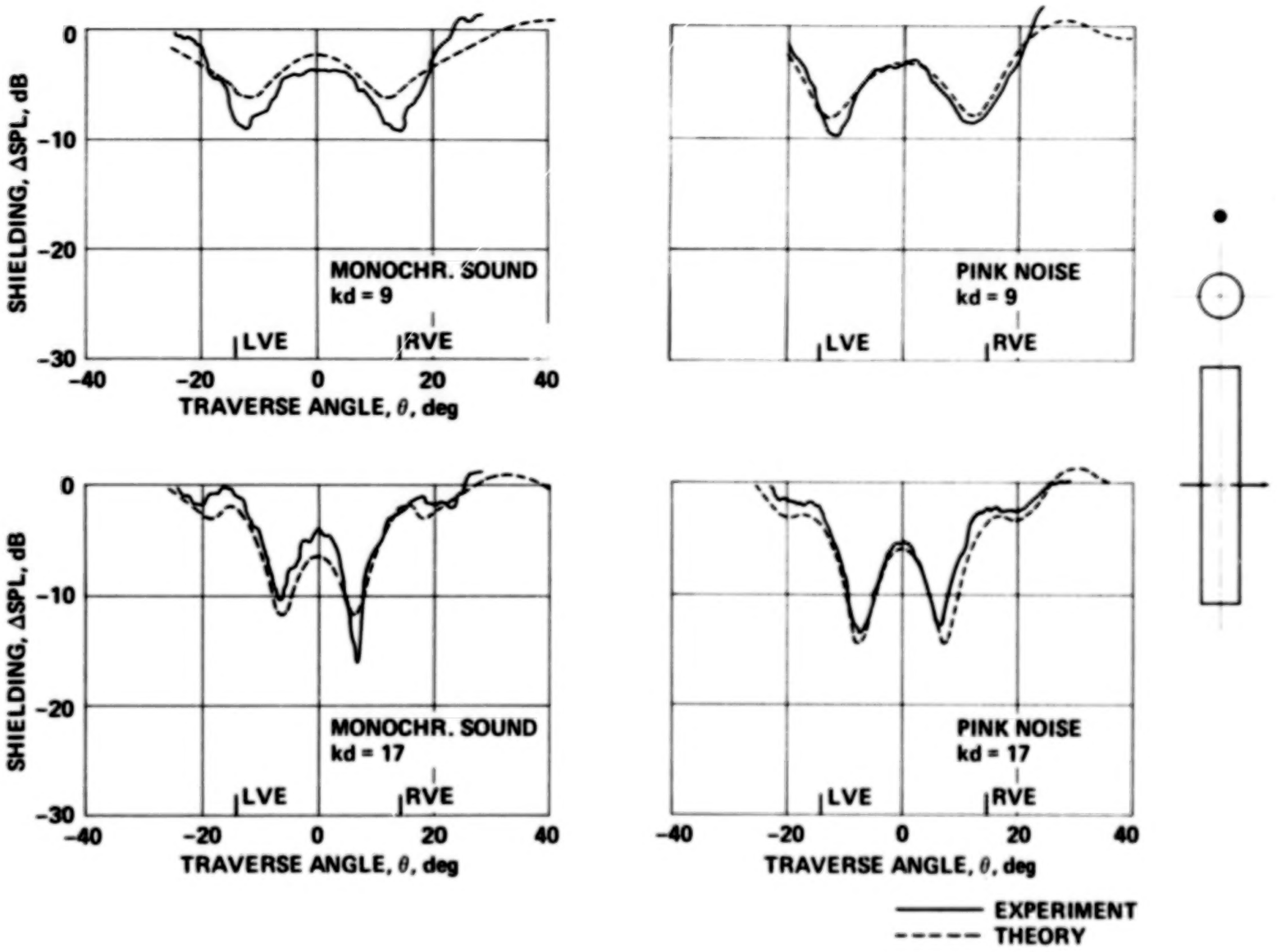

Figure 27.– Comparison of experimental shielding with theoretical shielding for circular cylinder – Series C2.

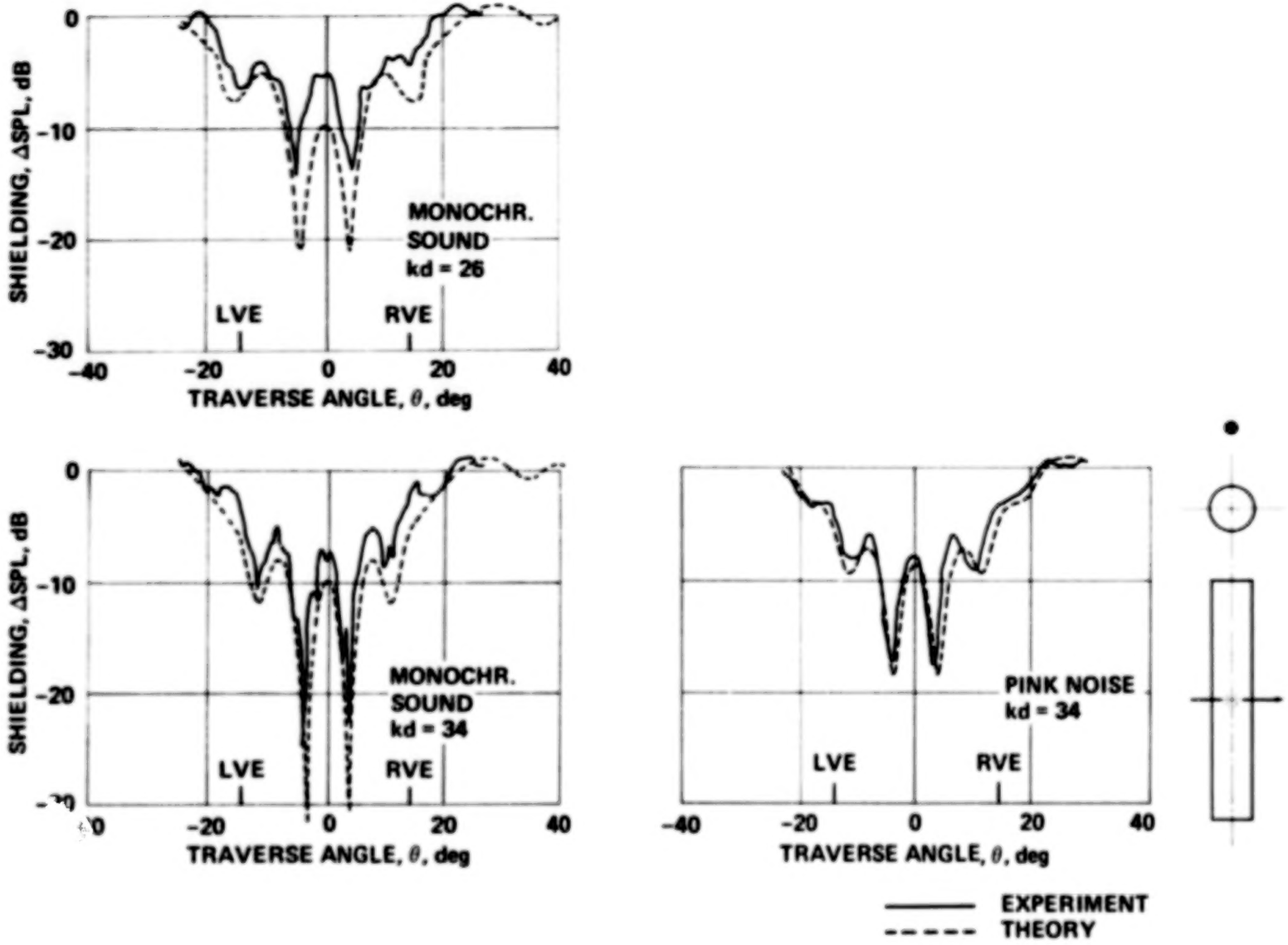

Figure 27.– Continued.

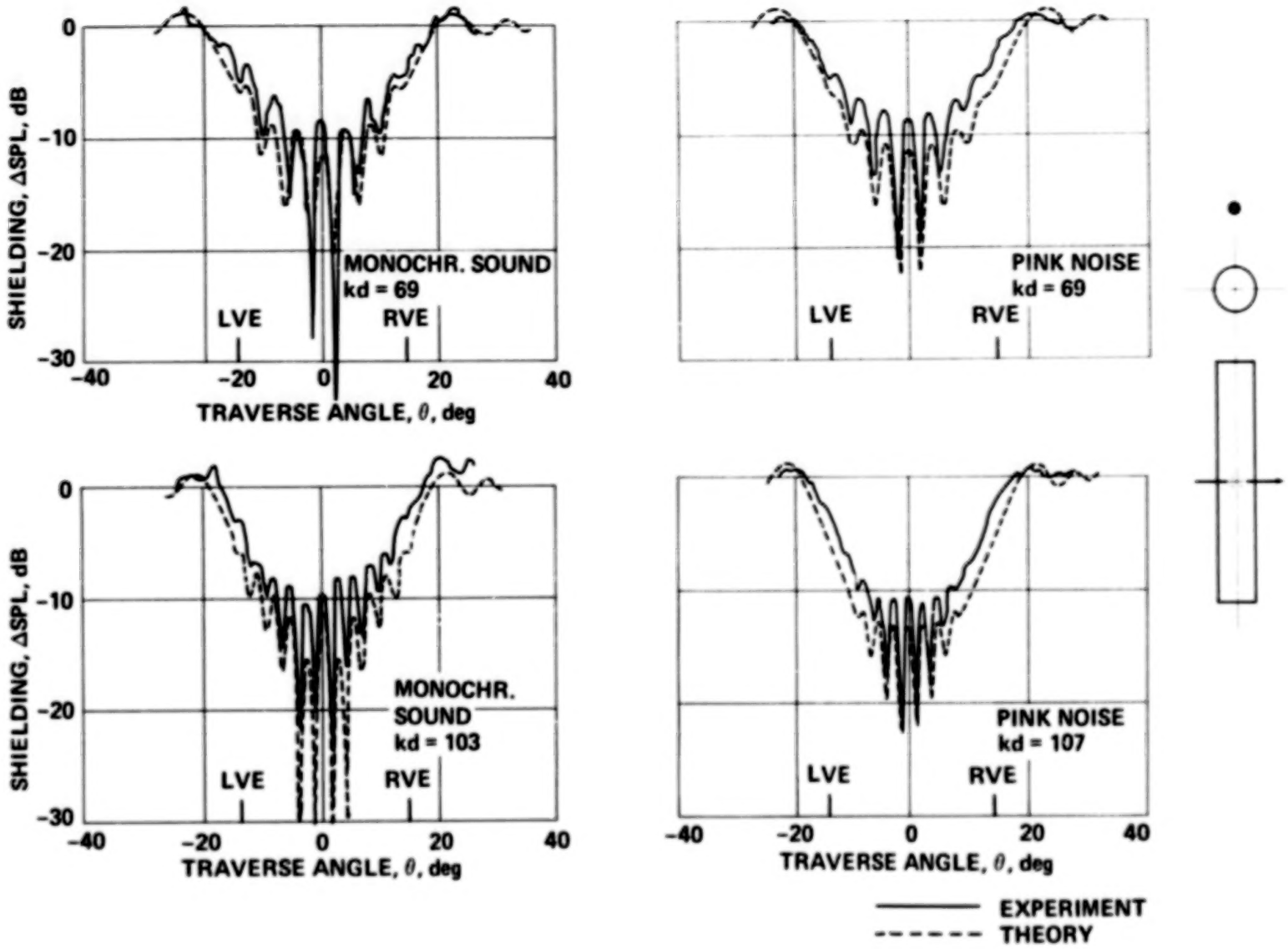

Figure 27.– Continued.

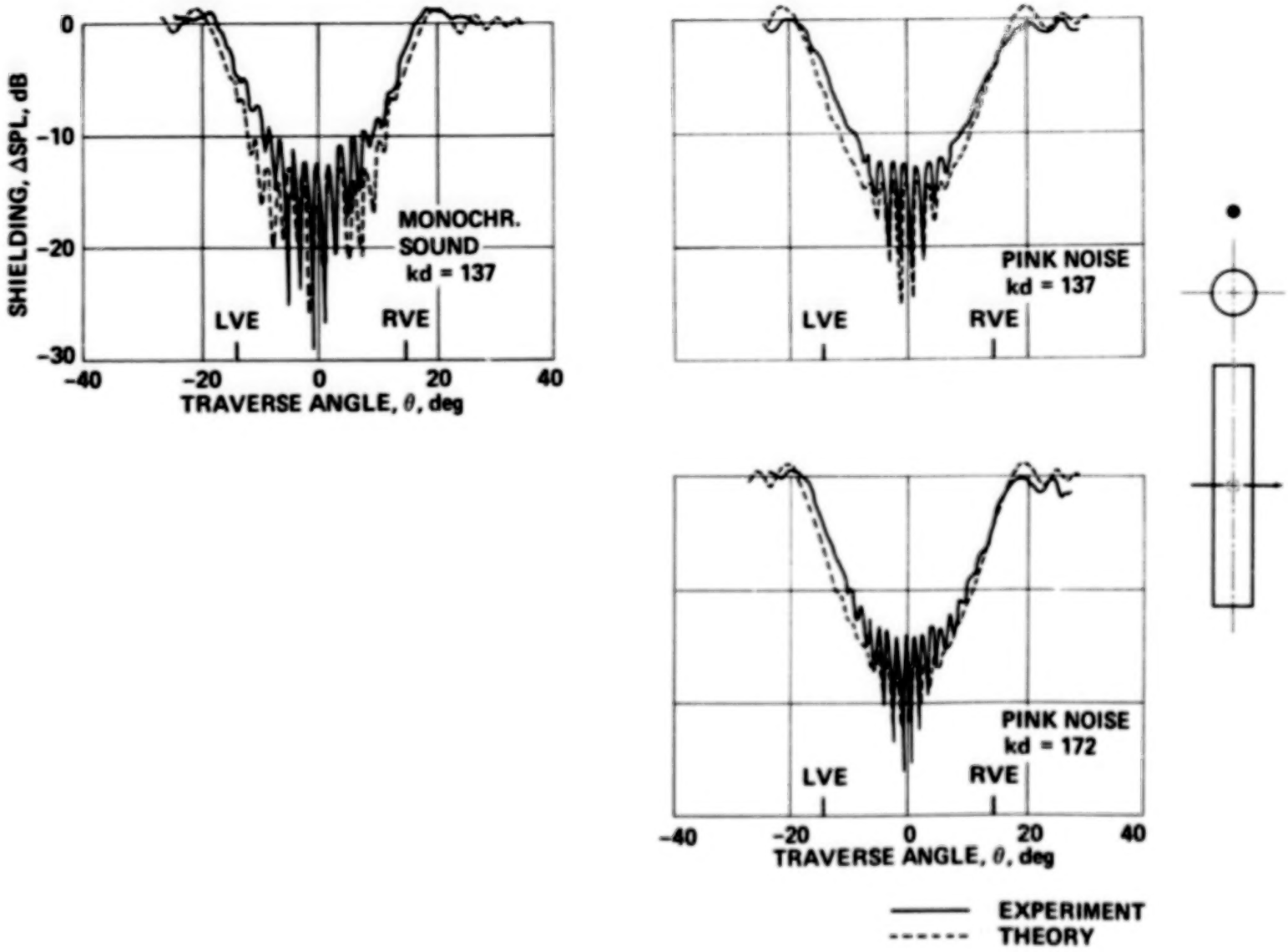

Figure 27.– Concluded.

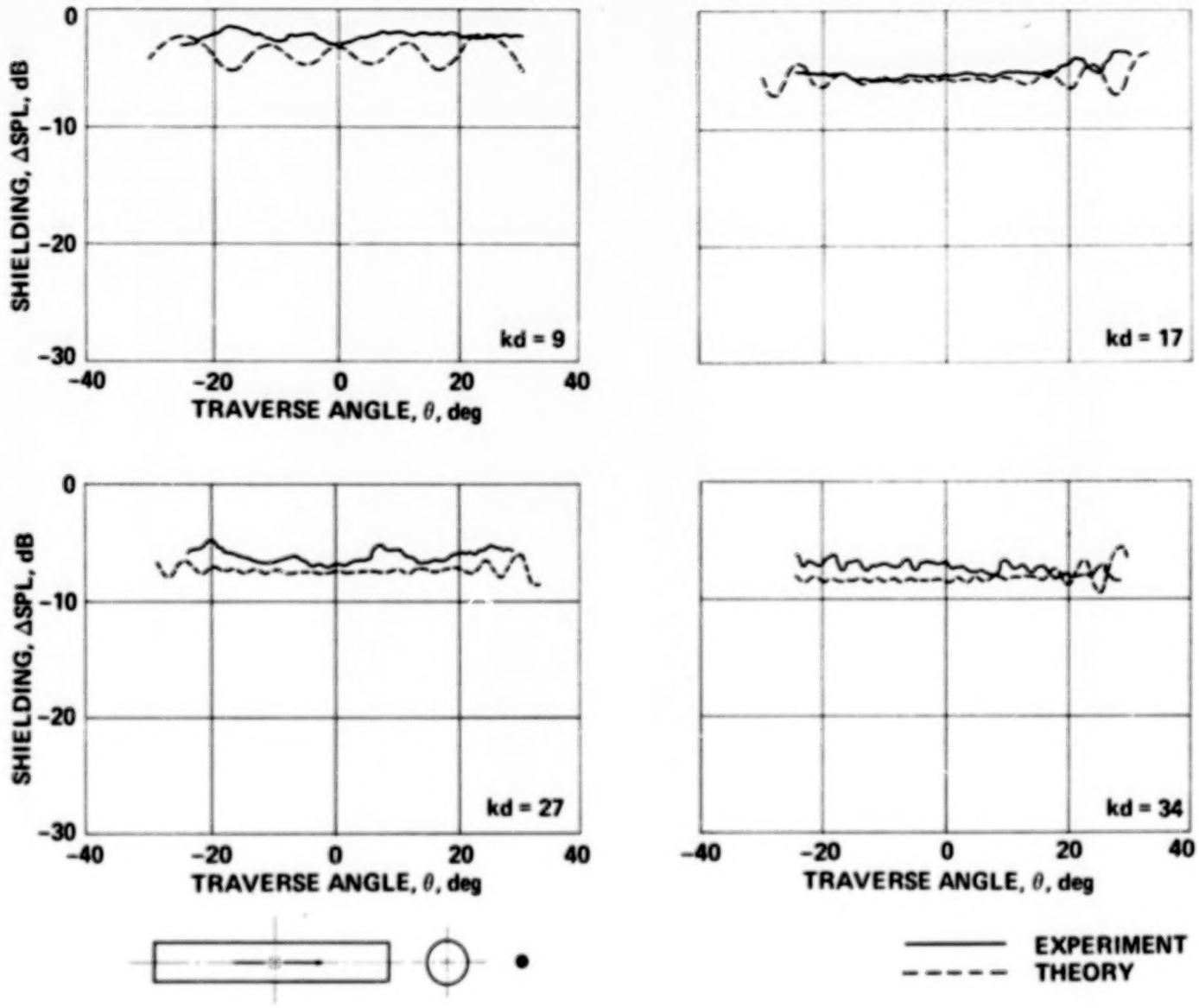

Figure 28.– Comparison of experimental shielding with theoretical shielding for circular cylinder – Series CH1, pink noise.

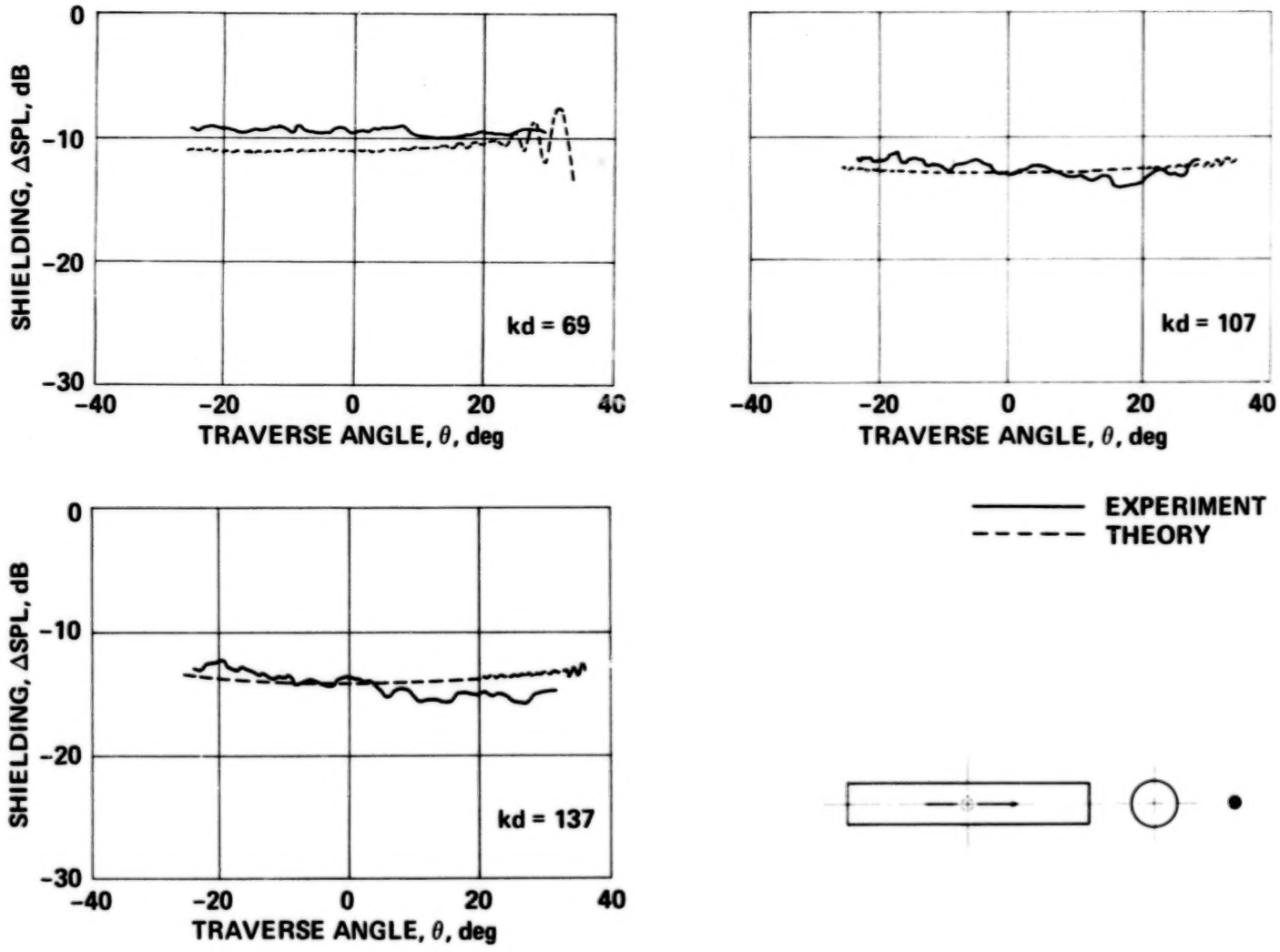

Figure 28.– Concluded.

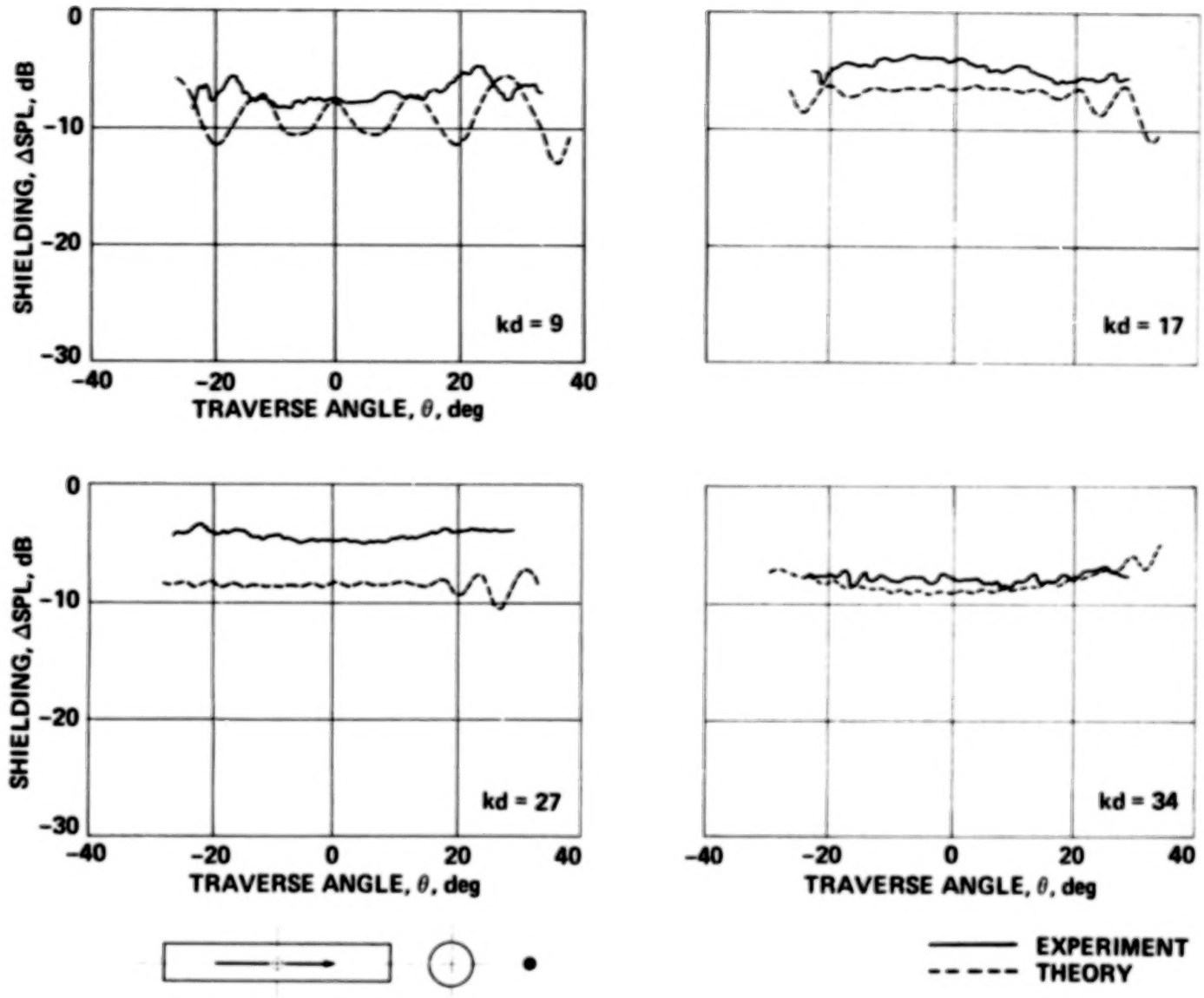

Figure 29.– Comparison of experimental shielding with theoretical shielding for circular cylinder – Series CH3, pink noise.

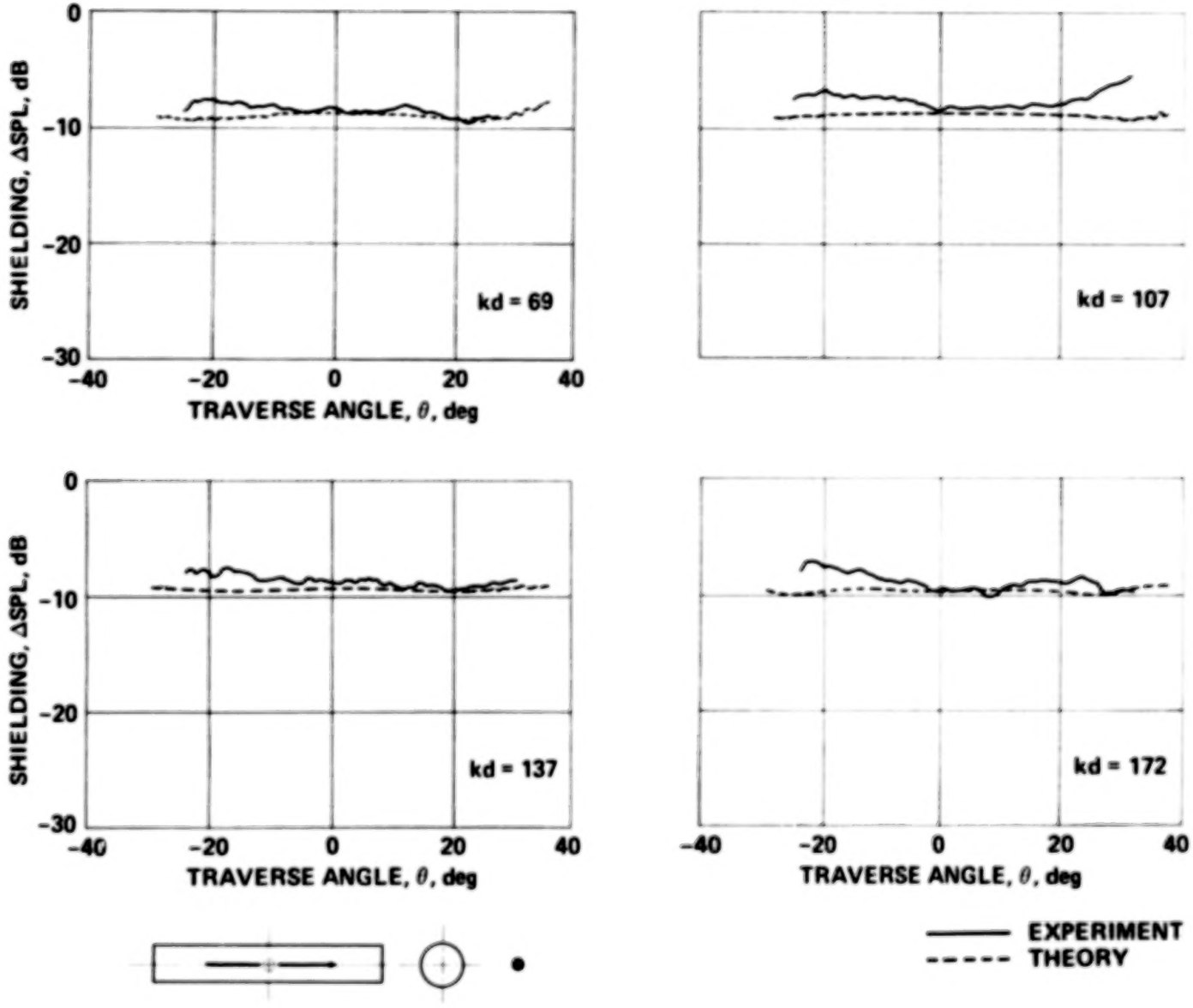

Figure 29.– Concluded.

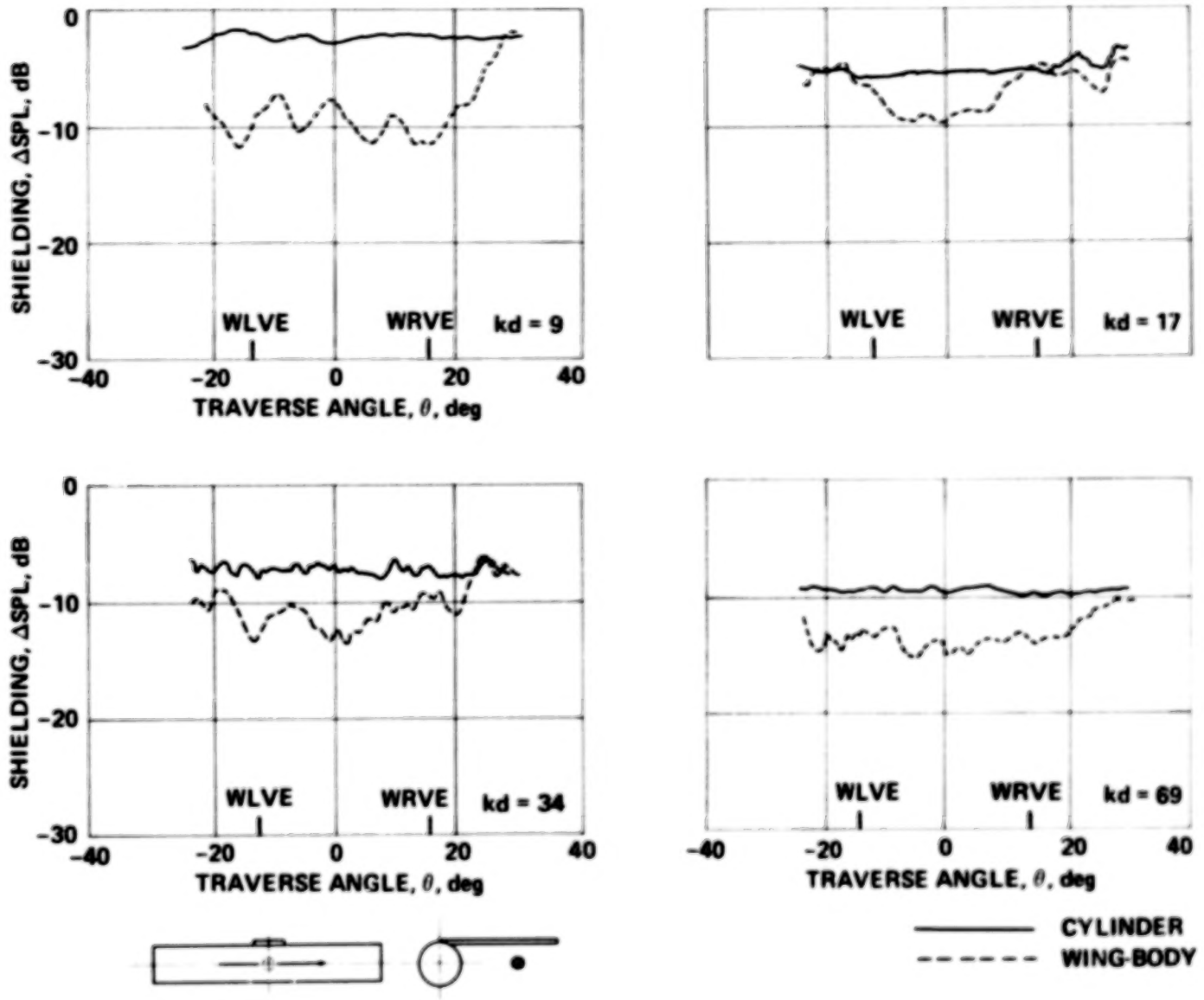

Figure 30.– Comparison of measured cylindrical shielding with measured wing-body shielding – Series CH2, pink noise.

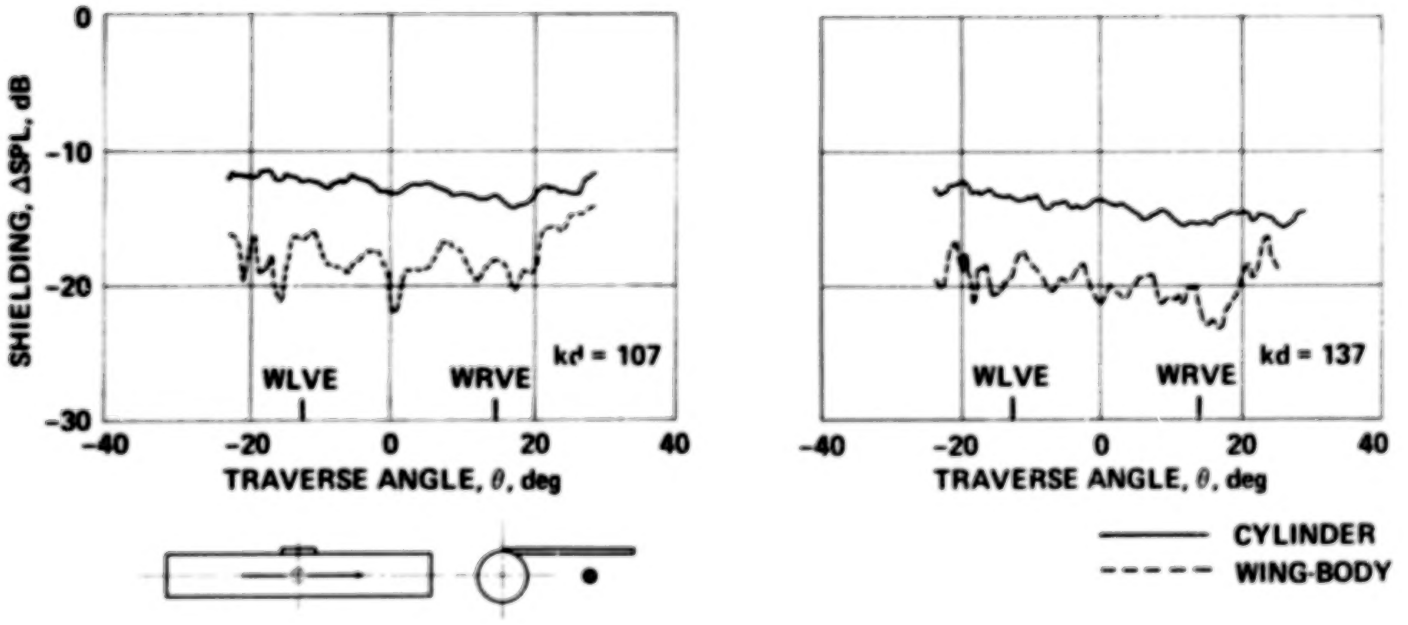

Figure 30.– Concluded.

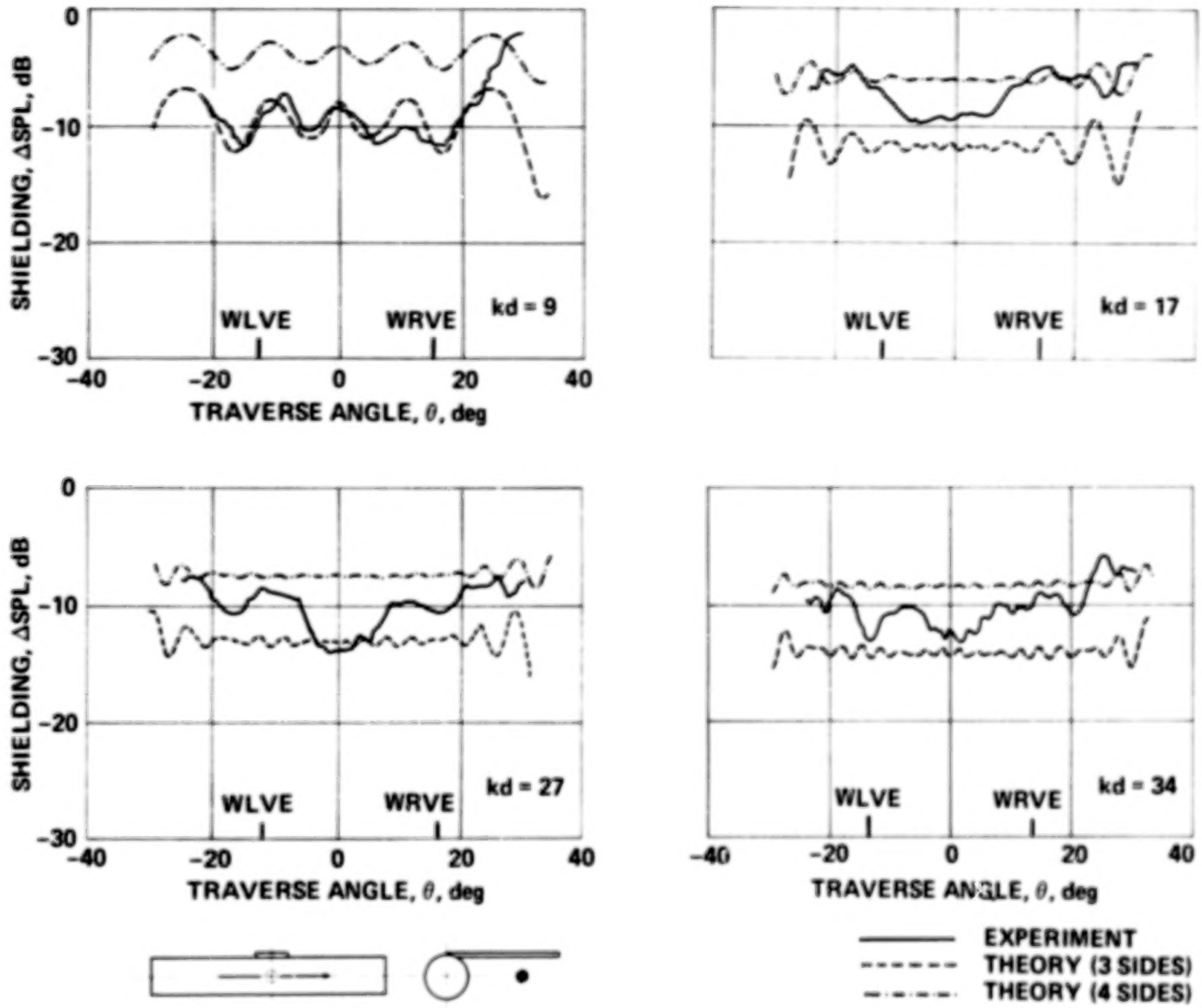

Figure 31.– Comparison of measured wing-body shielding with various approximations – Series CH2, pink noise.

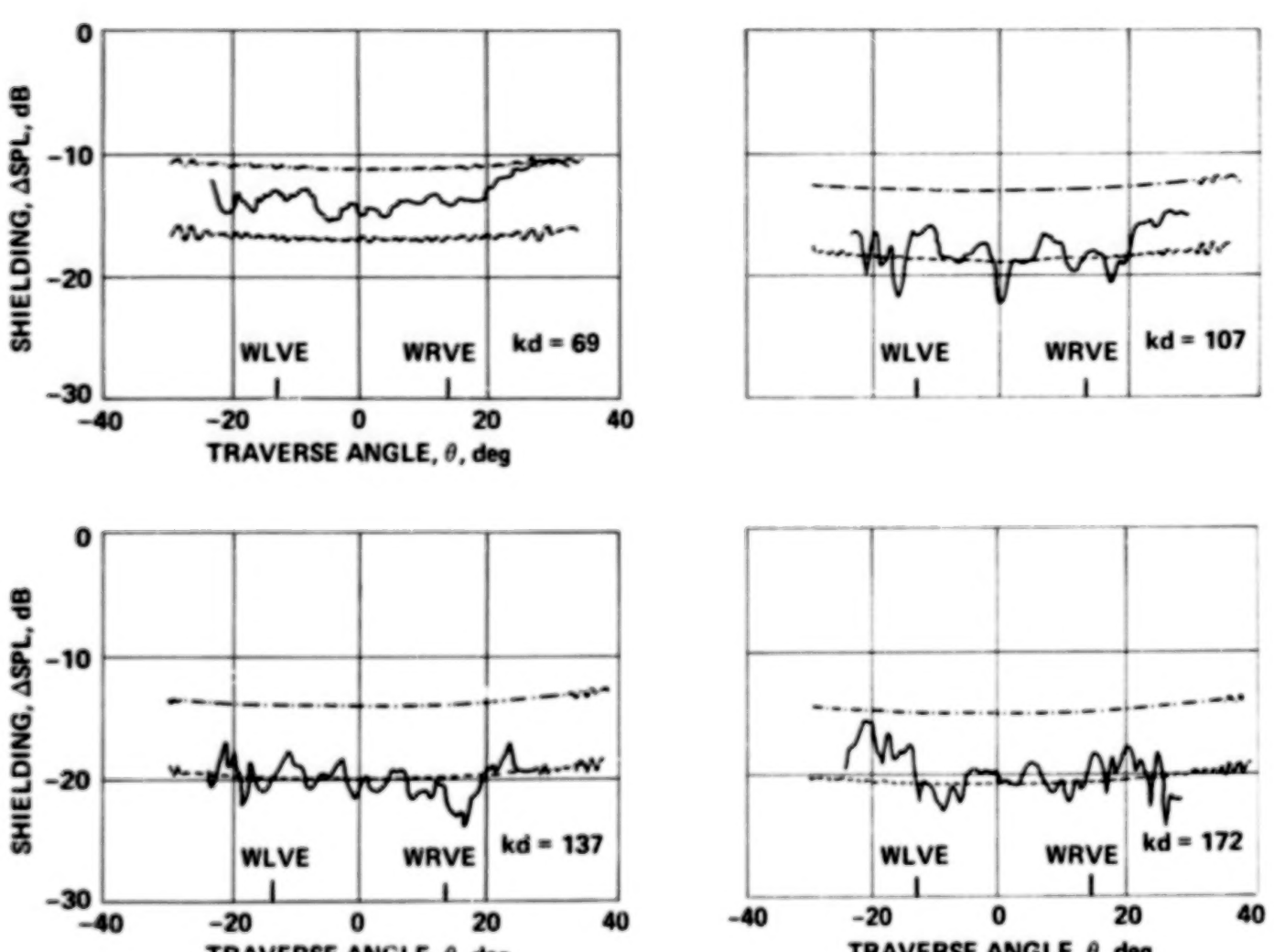

Figure 31.– Concluded.

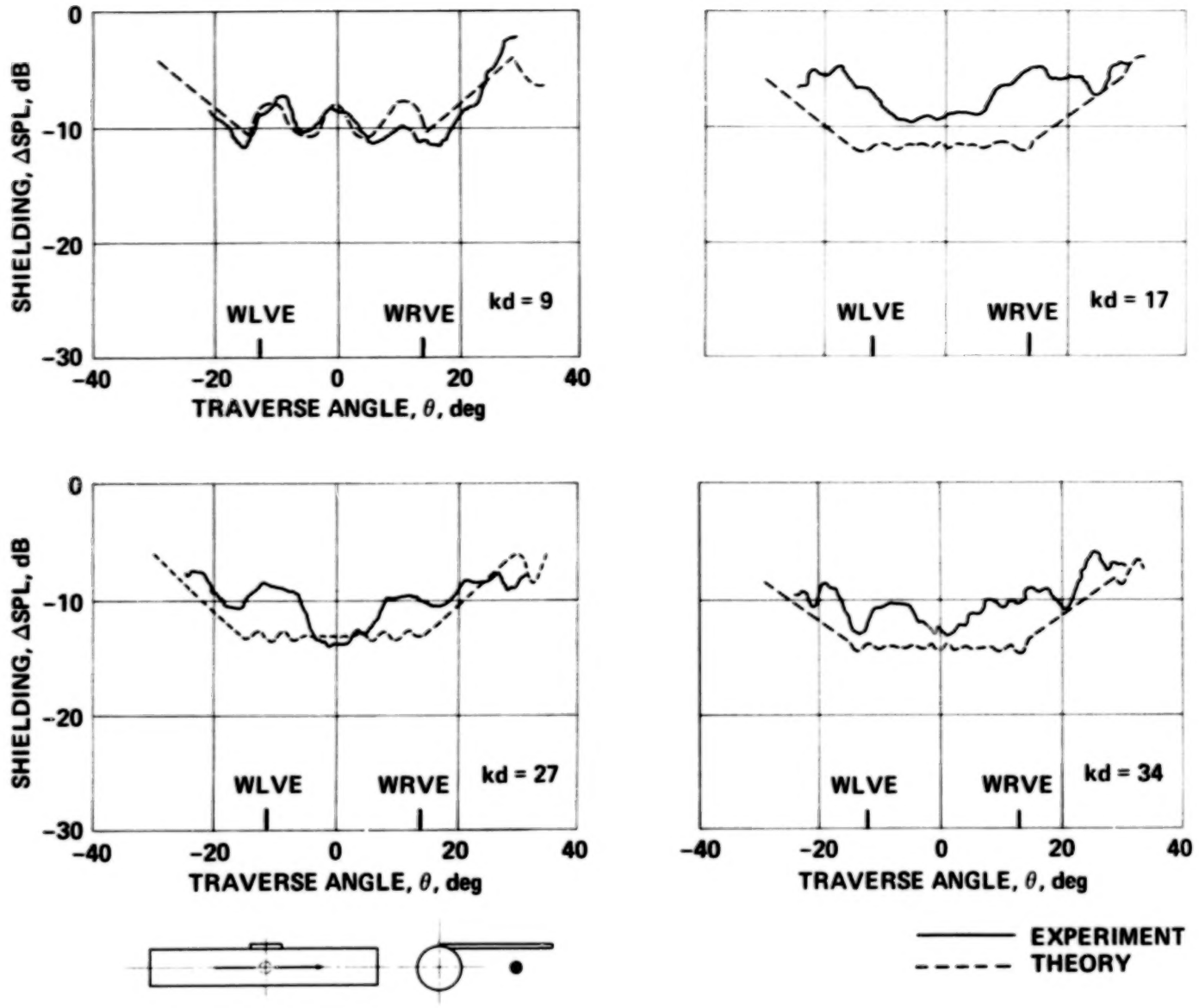

Figure 32.– Comparison of experimental shielding with theoretical shielding for wing-body combination – Series CH2, pink noise.

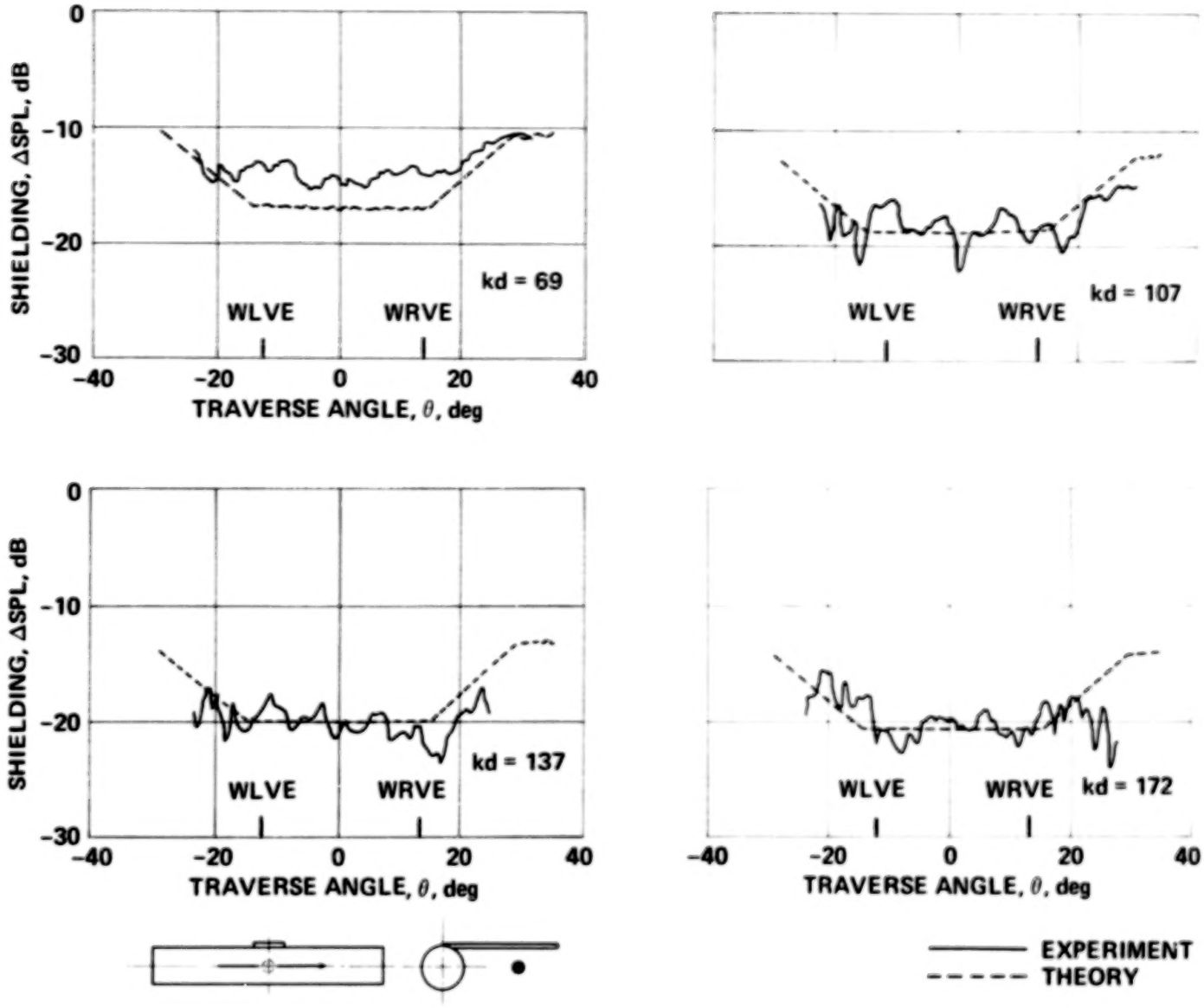

Figure 32.– Concluded.

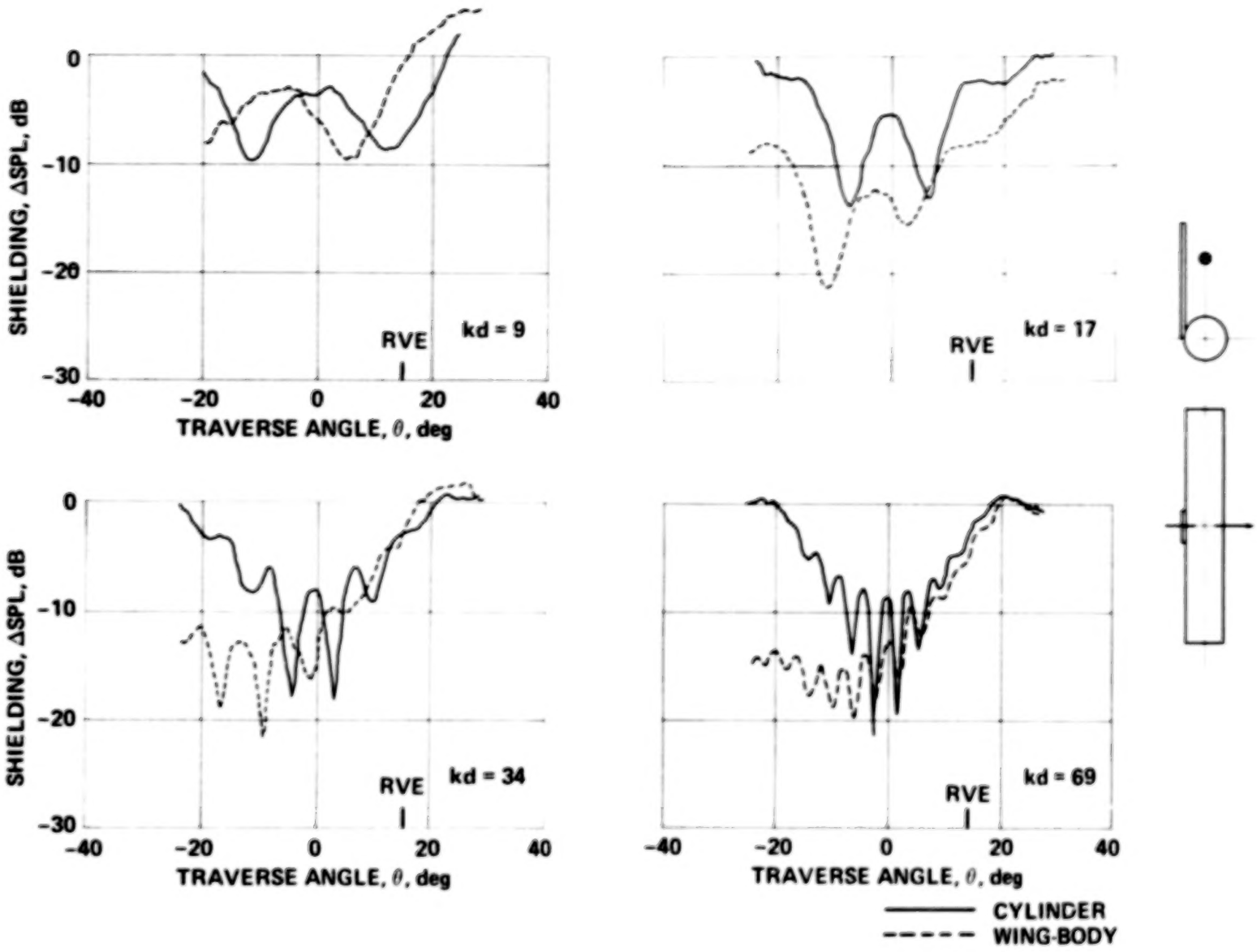

Figure 33.– Comparison of measured cylindrical shielding with measured wing-body shielding – Series C3, pink noise.

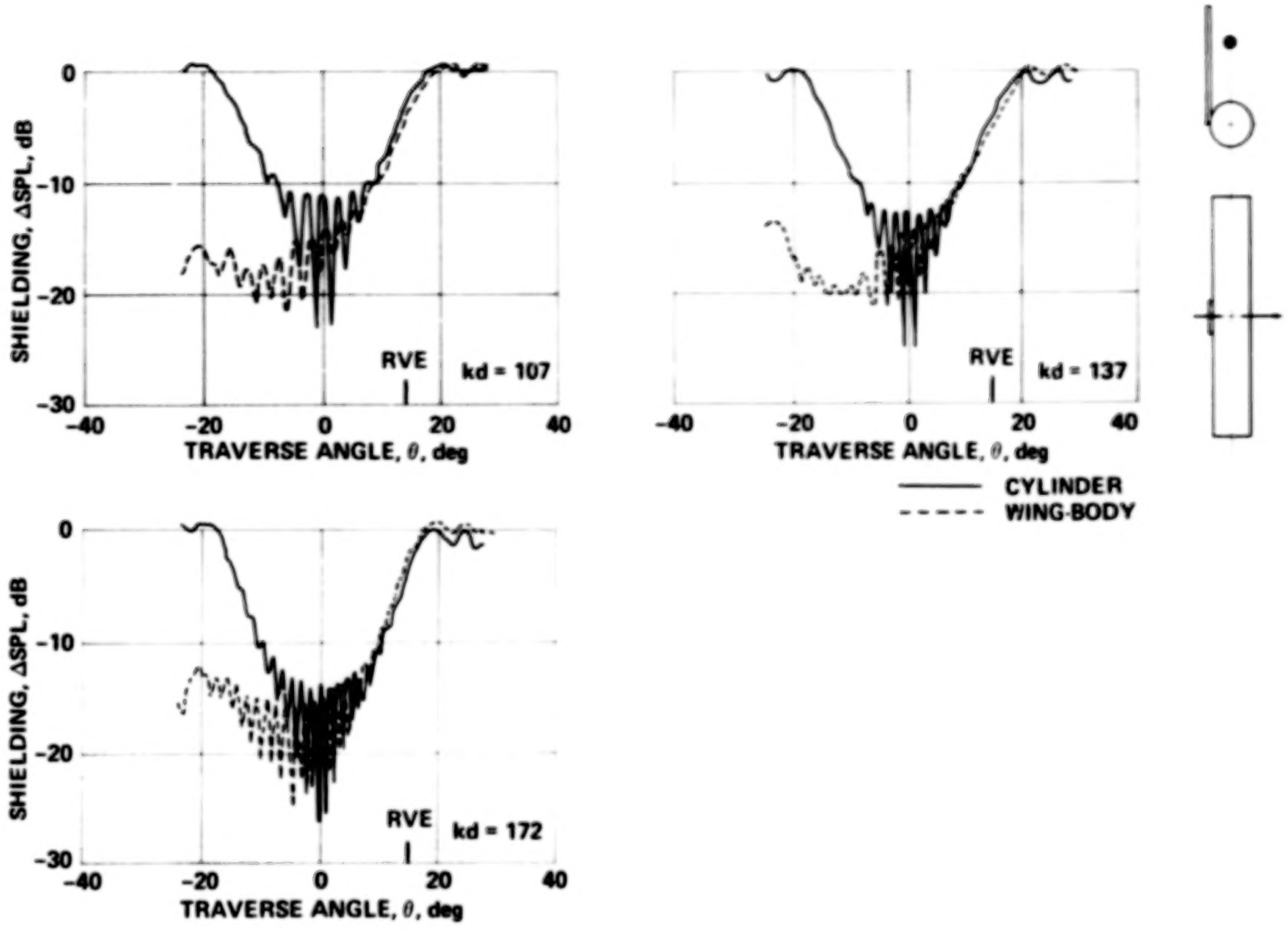

Figure 33.– Concluded.

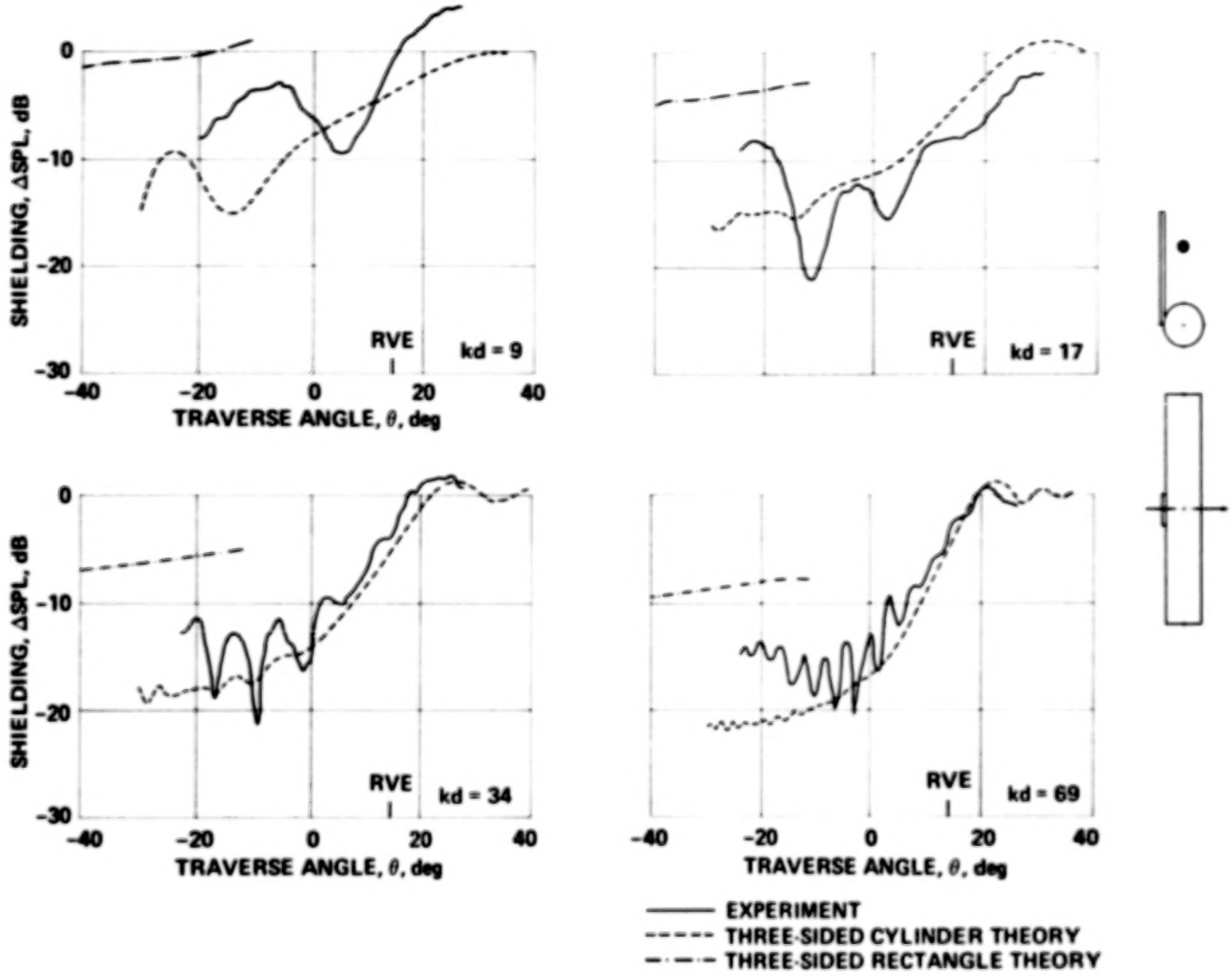

Figure 34.– Comparison of measured wing-body shielding with various approximations – Series C3, pink noise.

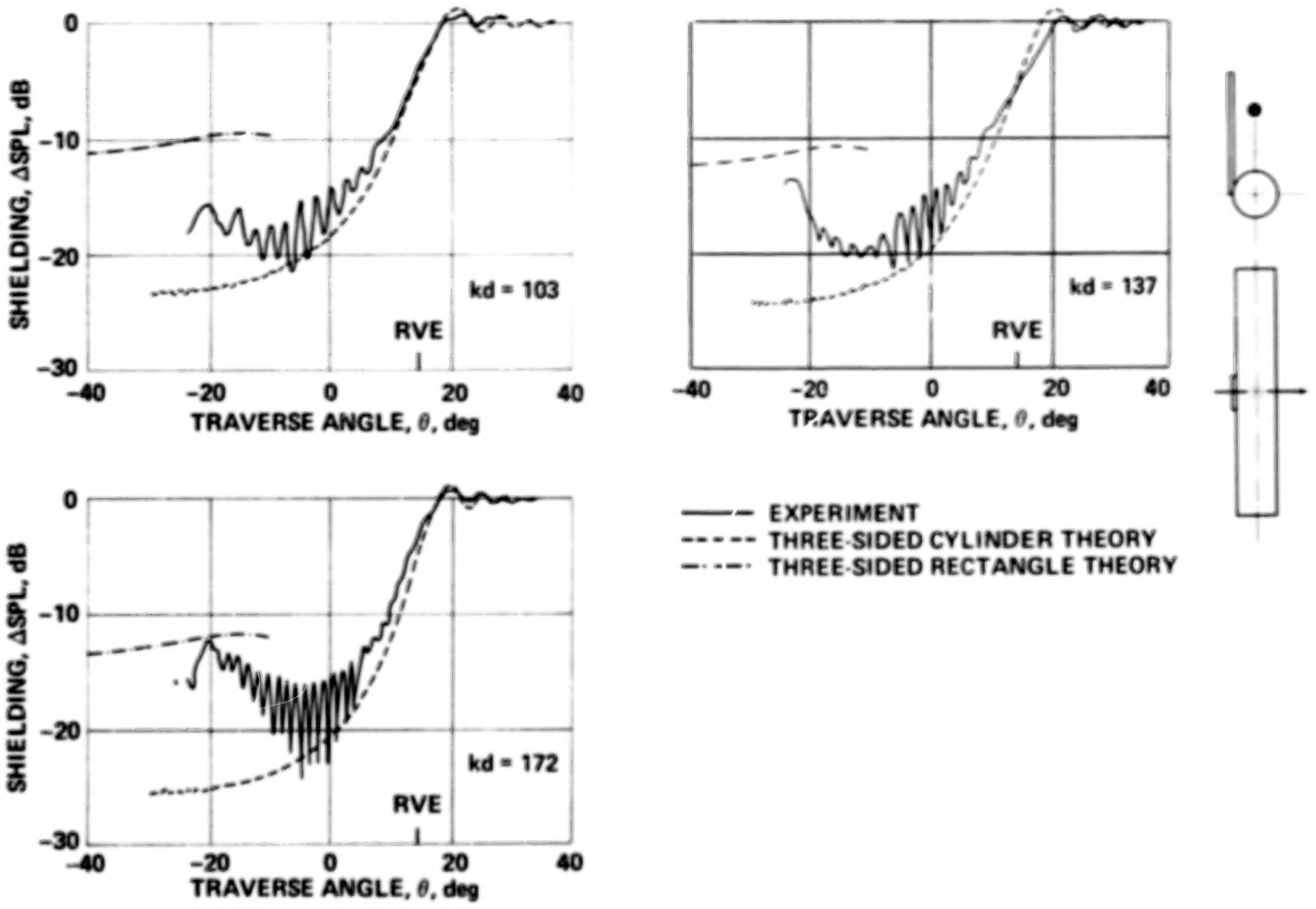

Figure 34.– Concluded.

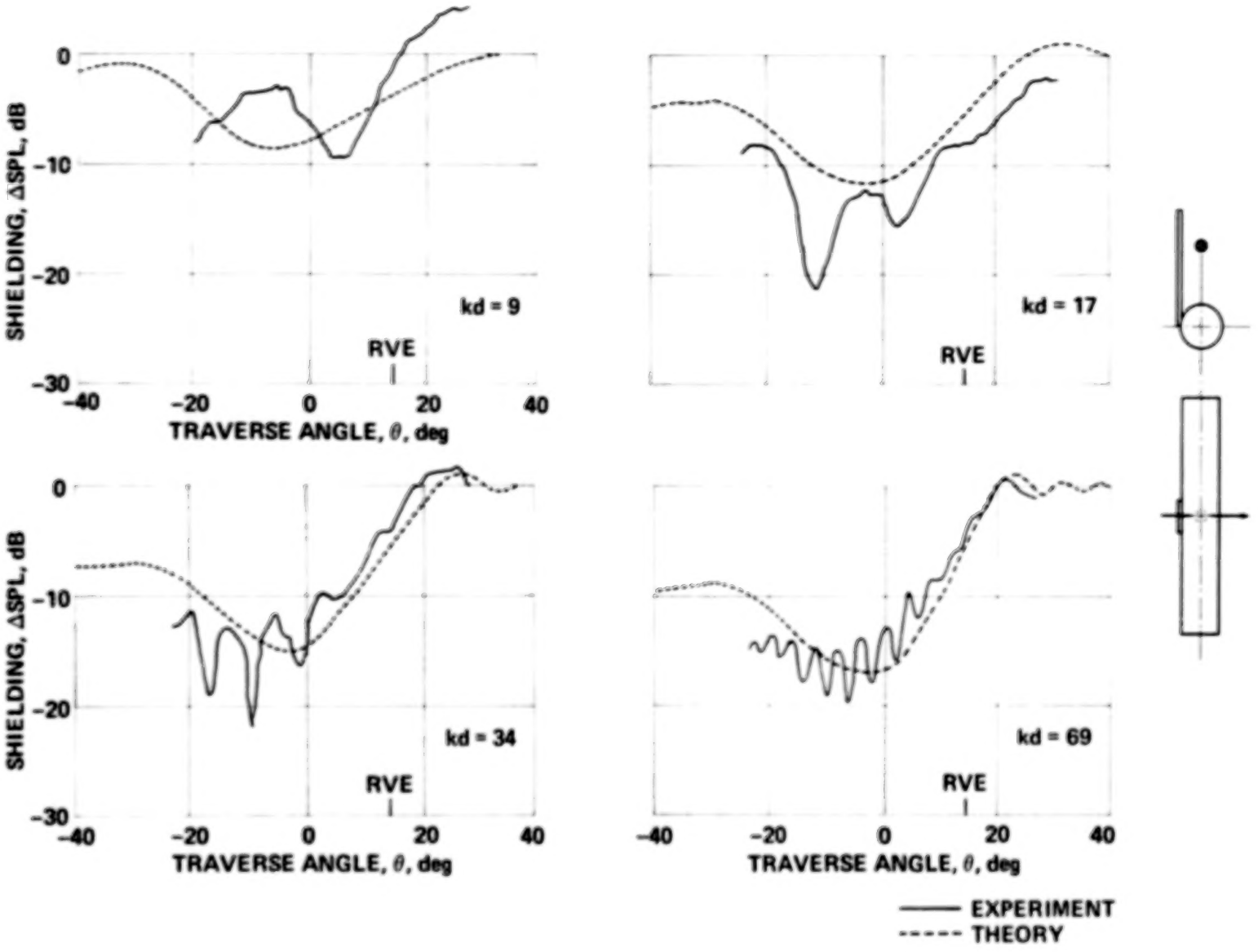

Figure 35.– Comparison of experimental shielding with theoretical shielding for wing-body combination – Series C3, pink noise.

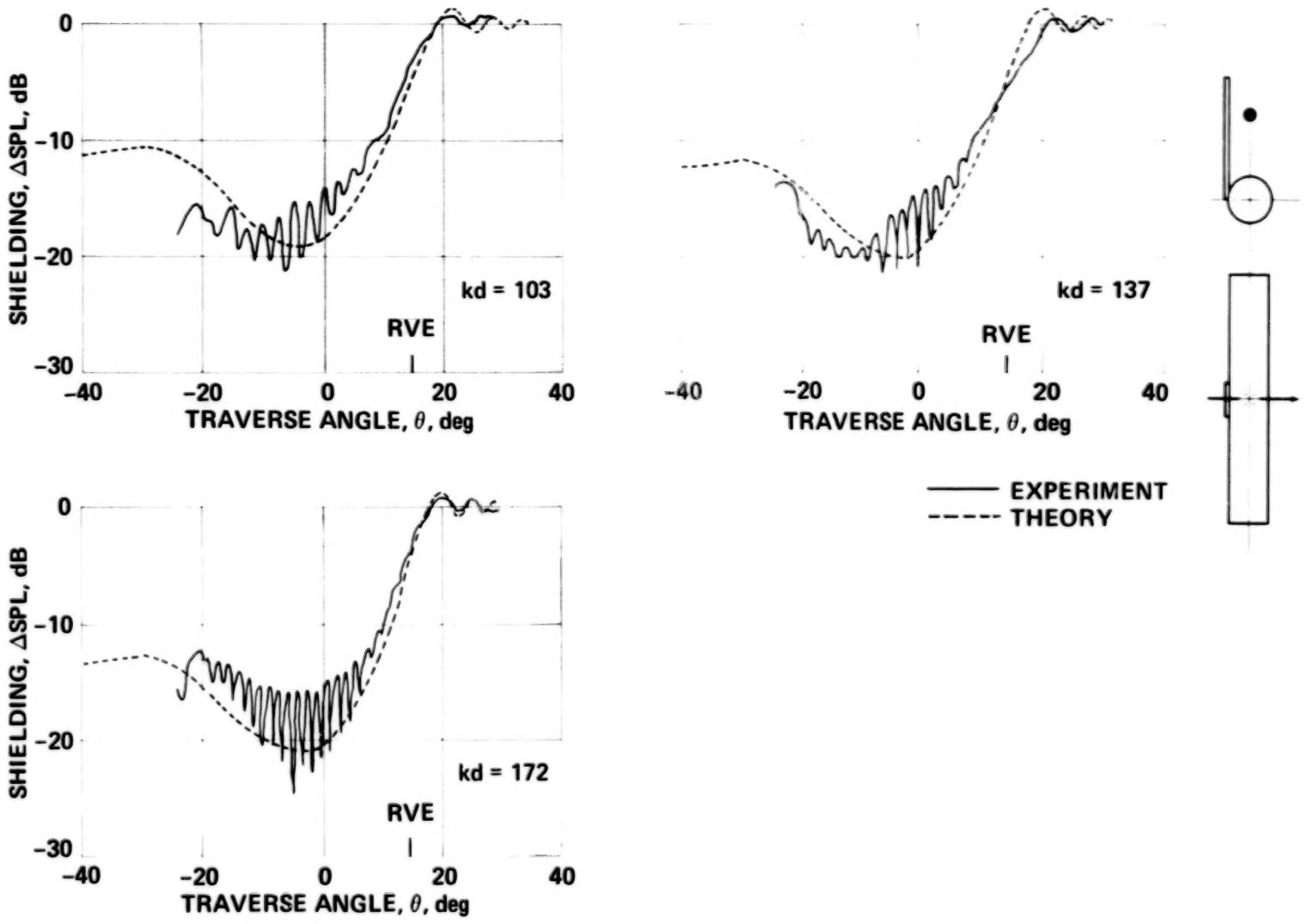

Figure 35.– Concluded.

1. Report No.	2. Government Accession No.	3. Recipient's Catalog No.
NASA TP-1004		

4. Title and Subtitle	5. Report Date
EVALUATION OF APPROXIMATE METHODS FOR THE PREDICTION OF NOISE SHIELDING BY AIRFRAME COMPONENTS	January 1980
	6. Performing Organization Code
7. Author(s)	8. Performing Organization Report No.
Warren F. Ahtye and Geraldine McCulley	A-6961
	10. Work Unit No.
9. Performing Organization Name and Address	505-06-23
Ames Research Center, Moffett Field, Calif. 94035 and Informatics, Inc., Palo Alto, Calif. 94303	11. Contract or Grant No.
	13. Type of Report and Period Covered
12. Sponsoring Agency Name and Address	Technical Paper
National Aeronautics and Space Administration Washington, D.C. 20546	14. Sponsoring Agency Code

15. Supplementary Notes

16. Abstract

The present investigation was conducted to evaluate some approximate methods for the prediction of shielding of monochromatic sound and broadband noise by aircraft components. The approach was to make anechoic-chamber measurements of the shielding of a point source by various simple geometric shapes, and to then compare the measured values with those calculated by the superposition of asymptotic closed-form solutions for the shielding by a semi-infinite plane barrier.

The shields used in the measurements consisted of rectangular plates, a circular cylinder, and a rectangular plate attached to the cylinder to simulate a wing-body combination. The normalized frequency, defined as a product of the acoustic wave number and either the plate width or cylinder diameter, ranged from 4.6 to 114.

Microphone traverses in front of the rectangular plates and cylinders generally showed a series of diffraction bands that matched those predicted by the approximate methods, except for differences in the magnitudes of the attenuation minima which can be attributed to experimental inaccuracies.

The shielding of wing-body combinations was predicted by modifications of the approximations used for rectangular and cylindrical shielding. Although the approximations failed to predict diffraction patterns in certain regions, they did predict the average level of wing-body shielding with an average deviation of less than 3 dB.

17. Key Words (Suggested by Author(s))	18. Distribution Statement
Noise shielding Noise barrier	Unlimited STAR Category – 07

19. Security Classif. (of this report)	20. Security Classif. (of this page)	21. No. of Pages	22. Price*
Unclassified	Unclassified	103	$6.50

*For sale by the National Technical Information Service, Springfield, Virginia 22161

NASA-Langley, 1980